2015

Fracture control of small diameter gas pipelines

Youyou Wu
University of Wollongong

UNIVERSITY OF WOLLONGONG

FRACTURE CONTROL OF SMALL DIAMETER GAS PIPELINES

This thesis is presented as part of the requirements for the award of the Degree

DOCTOR OF PHILOSOPHY

of the

University of Wollongong

by

YOUYOU WU

B.Tech. (Hons.) National University of Singapore, 2011

Dip.Eng. Ngee Ann Polytechnic, Singapore, 2007

Faculty of Engineering and Information Sciences

School of Mechanical, Materials and Mechatronic

August 2015

DECLARATION

I, Youyou Wu, declare that this thesis, submitted in fulfilment of the requirements for award of Doctor of Philosophy, in the school of Mechanical, Materials and Mechatronics Engineering, University of Wollongong, Australia, is wholly my own work unless otherwise referenced or acknowledged. The document has not been submitted for qualifications at any other academic institution.

Youyou Wu

August, 2015

ACKNOWLEDGEMENTS

This work was funded by the Energy Pipelines Cooperative Research Centre (EPCRC), supported through the Australian Government Cooperative Research Centre Program. The funding and in-kind support from the Australian Pipelines & Gas Association Research and Standards Committee (APGA RSC) is gratefully acknowledged. In-kind supports from JFE Steel Corporation and BlueScope Steel are appreciated.

First and foremost, I would like to express my great appreciation to my supervisor, Associate Professor Cheng Lu for constant guidance and strong support, and my co-supervisors, Dr Guillaume Michal and Professor Huijun Li for inspiring discussions and encouragement.

My sincere gratitude goes to co-supervisor / industry advisor Mr Leigh Fletcher, without whom the journey of PhD wouldn't have begun. The sharing, encouragement and guidance from Leigh have made this a fantastic journey in Wollongong.

I would like to express my warm thanks to: Dr John Piper, Professor Frank Barbaro, Dr Lenka Kuzmikova and Dr Ajit Godbole for review and provision of valuable advice for my work. I am grateful for the assistance on the experimental works from: Dr Zhixiong Zhu, Dr Jintao Li and Dr Jian Han. The guidance on numerical methods from Dr Hailiang Yu is appreciated.

Khoa Vo, Bradley Davis and Peichun Xiao, are thanked for all the good days and bad days that we went through together that made my PhD life in Wollongong memorable. Special thanks to my friends Dr Lihong Su and Dr Haina Lu for the supports over all these years. In addition, thank to my guitar teacher Mr Behzad Mesgaran, for teaching me how to play and enjoy a guitar.

Last but not least, a special thanks to my parents, my brother Fan and sister-in-law Xunyi, for the unconditional supports that sustained me thus far!

PUBLICATIONS

Y. Wu, C. Lu, G. Michal, L. Fletcher, P. John, and F. Barbaro, "Drop weight tear tests on small-diameter linepipe," in *6th International Pipeline Technology Conference* Ostend, Belgium, 2013, pp no. S04-02.

Y. Wu, H. Yu, C. Lu, K. Tieu, G. Ajiit, and G. Michal, "Transition of ductile and brittle fracture during DWTT by FEM," in *13th International Conference on Fracture*, Beijing, China, 2013.

Y. Wu and L. Fletcher. (2013, 30 August) "A cautionary tale on propagating brittle fracture in pipelines", Pipeline International.
Available:http://pipelinesinternational.com/news/a_cautionary_tale_on_propagating_brittle_fracture_in_pipelines/83225

L. Fletcher and **Y. Wu**, (2014, September) "2 + 2 = 5, fudge factors in pipeline fracture control, the CRC program, AS2885, and succession planning in the Australian pipeline industry", Pipelines International.
Available: http://pipelinesinternational.com/news/a_fairy_tale_outcome/89045

Y. Wu, B. Davis, C. Lu, G. Michal, L. Fletcher, P. Venton, *et al.*, "Specimen thickness effect on Charpy absorbed energy in line-pipe steels," Special issue on Characterization and assessment of fracture behaviour of modern pipeline, *Engineering Fracture Mechanics*, 2015. (***IF 1.67*** **Accepted*)***

ABSTRACT

Pipelines are the main arteries of the oil and gas transportation systems. The failure of a gas pipeline could result in casualties of catastrophic numbers and untold dollar amounts of property damage. The capacity of a pipeline to arrest a running crack is one of the fundamental properties required to ensure a safe operation. The ability to arrest a running crack is one of the key features in the safe design of pipeline systems. Therefore, it is necessary to test the mechanical properties of line pipe steels to ensure they are sufficient to prevent long running fractures in the pipeline.

The approaches to brittle and ductile fracture control for gas pipeline were developed in the 1960s and 1970s, and laboratory tests to characterise the fracture behaviour of line pipe steel were proposed accordingly. In the current design codes, the crack arrest properties of a pipeline should meet two requirements: crack propagation has to occur in a ductile manner, and enough energy should be dissipated during propagation so as to exceed the driving force. While the first criterion is assessed by conducting the Battelle drop weight tear test (DWTT) at design temperature, the latter requirement is converted into a lower bound for impact absorbed energy (arrest toughness) measured by the Charpy test.

DWTT is a mandatory requirement for pipe with diameters greater than or equal to 500 mm in the widely used standard API RP5L3. However, the absence of a DWTT requirement for small-diameter pipe (<DN500mm) may lead to a brittle fracture in practice, because it has been proven that small-diameter pipelines were not immune to brittle fracture. In addition, it has also been more and more difficult to meet the ‘no buckling’ requirement for DWTT in the standard for modern high-toughness line pipe steels.

As for ductile fracture control, the determination of the material toughness value required for arresting ductile fracture propagation has been based on the Battelle two curve model (BTCM), in which the relationship between Charpy absorbed energy

and the Charpy specimen thickness plays an important role. While the Charpy energy/thickness relationship was found to be linear when BTCM was developed during the 1960s, the material properties of line pipe steels manufactured nowadays have been significantly improved. The Charpy/thickness relationship is no longer linear and this has been identified as one of the main factors causing the inaccurate prediction of arrest toughness by BTCM in higher-toughness steels.

The current research focuses on two problems: 1) How to improve brittle fracture propagation control for small diameter gas pipelines by investigating the difficulties or dilemmas encountered with DWTT; 2) How to improve the arrest toughness prediction for ductile fracture control of small diameter gas pipelines by investigating the Charpy specimen thickness effect on absorbed energy. Both experimental and numerical works are carried out to solve the current dilemma. Based on the investigation outcomes, recommendations on the improvement of current pipeline fracture control approaches are made to ensure a safe operation of the small diameter gas pipelines.

The findings demonstrate that the Charpy test is no longer suitable for transition temperature prediction, especially in small-diameter, thin-walled pipes, where various sub-size Charpy specimens could create more uncertainties. DWTT is essential for predicting the transition temperatures of small-diameter line pipes. Flattened DWTT specimens with reinforcement plates successfully minimise buckling and deliver more accurate transition temperature predictions compared to the results of full-scale tests. A new method to determine the FPTT by starting the DWTT from lower shelf is also proposed which needs to be further validated. As for ductile propagation control, the linear CVN absorbed energy/thickness relationship is replaced by an exponential relationship to improve the BTCM predictions for high-toughness line pipe steels.

TABLE OF CONTENTS

LIST OF TABLES

LIST OF FIGURES

ABERRATIONS AND SYMBOLS

Aberrations

API	American Petroleum Institute
AS	Australian standards
ASME	American Society of Mechanical Engineers
ASTM	American Society for Testing and Materials
BFCM	Bulk fracture Charpy machine
BS	British Standards
BTCM	Battelle two-curve model
CSA	Canadian Standards Association
CSM	Centro Sviluppo Materiali
CT	Compact Tension
CTOA	Crack tip opening angle
CVN	Charpy V-notch
CR	Conventional Rolling
DBTT	Ductile-brittle transition temperature
DN	Diameter nominal
DNV	Det Norske Veritas
DWTT	Drop weight tear test
El	Elongation
EN	European Standards

EPCRC	Energy Pipeline Cooperative Research Centre
FEM	finite element method
FPTT	Fracture propagation transition temperature
FPZ	fracture process zone
GTN	Gurson–Tvergaard–Needleman
HFERW	high frequency electric resistance welding
HPC	high performance computer
HSLA	high strength low alloy
IGEM	Institution of Gas Engineers & Managers
ISO	International Organization for Standardization
JFMS	Japanese ferrite/martensite dual-phase steel
LAF	Local approach to fracture
MCVN	miniature Charpy V-notch
OD	outside diameter
PZCF	plastic zone correction factor
QT	quench and temper
SA	shear area
SEB	single edge bending
SMYS	specified minimum yield strength
T-L	transverse-longitudinal
TMCP	thermomechanical controlled processing
T-S	transverse-short

USE	upper shelf energy
YS	yield strength
TS	tensile strength
Y/T	yield to tensile ratio

Symbols

A	notch depth
A-A	cross-sectional area of fracture plane
A_{kv}	response of Charpy impact test
A_1	upper shelf response
A_2	lower shelf response
B	Charpy V-notch specimen thickness
b	ligament length
C	constant
C_v	Charpy V-notch absorbed energy
CVN_{BTCM}	full-size Charpy arrest energy calculated with the BTCM
CVN_{Leis}	corrected full-size Charpy arrest energy from Leis's model
E	elastic modulus
(E/A)_BTCM	Charpy specific energy calculated with Battelle two-curve model
(E/A)_(Corrected-Charpy)^W1977	Charpy specific energy calculated with Wilkowski correction model published at year 1977

(E/A)_(Corrected-Charpy)^W2000	Charpy specific energy calculated with Wilkowski correction model published at year 2000
FPV_{CVN}	fracture process volume of Charpy V-Notch specimen
$FPVLINE_{MCVN}$	fracture process volume of miniaturized Charpy V-Notch specimen
G_c	crack resistance force
h	fracture path at Charpy specimen
h_n	represent h at the notch tip
h_t	represents h at the top or striker impact point of the specimen
J_{IC}	J-integral
K	stress concentration factor
K_{IC}	critical stress intensity factor
K_t	elastic stress concentration factor
KV_B	Absorbed energy from non-standard Charpy V-notch specimen with thickness B
L	span
L_d	lateral displacement
L_d/T	lateral displacement to thickness ratio
P_a	arrest pressure
P_d	dynamic gas pressure
R	specific toughness
USE_{CVN}	upper shelf energy from Charpy V-notch specimen
USE^f	upper shelf energy from full-size Charpy V-notch specimen

USE_{MCVN}	upper shelf energy from miniaturized Charpy V- notch specimen
USE_p	absorbed energy for a specimen fatigue pre-cracked to half the width
$(USE_p)_n^S$	normalised absorbed energy for a sub-size specimen fatigue pre-cracked to half the width
USE^s	upper shelf energy from sub-size Charpy V-notch
V	fracture velocity
W	width
$\dot{e}_{kk}^p$	macroscopic plastic strain rate tensor
f	void volume fraction
$\dot{f}$	void volume fraction rate
$\dot{f}_{growth}$	void volume fraction growth rate
$\dot{f}_{nucl}$	void volume fraction nucleation rate
f_0	initial void volume fraction
f_c	critical void volume fraction
f_n	void volume fraction of the void-nucleating particles
f_u^*	ultimate void volume fraction
f_f	void volume fraction at final failure
r	outside radius
σ'	stress after applying the strain rate effect
σ	true stress
σ_f	flow stress

σ_f	critical fracture stress
σ_{yy}	normal stress
σ_w	Weibull stress
σ_c	average macroscopic Cauchy stress
$\bar{\sigma}$	yield tress
σ_m	mean normal part of average macroscopic Cauchy stress
σ_e	effective part of average macroscopic Cauchy stress
$\dot{\varepsilon}^p$	plastic strain rate
ε_n	mean void nucleation strain
s_n	standard deviation
$\dot{\varepsilon}$	strain rate
$\dot{\varepsilon}_o$	initial strain rate
t	wall thickness
t_c	critical thickness
t	test response corresponding temperature
t_0	transition temperature
k, n	material-dependent constants
q_1 , q_2	material parameters introduced by Tvergaard
T_0	maximum temperature of lower shelf region
ΔT	temperature change over the narrow transition zone
Δt	transition range
l	Length of the unbroken ligament of Charpy V-notch specimen

CHAPTER 1

INTRODUCTION

1.1. General background

The growth in worldwide demand for energy and the resulting expansion of the oil and gas industry have led to the increasing use of pipelines to transport hydrocarbons [1]. The newly constructed pipelines, particularly those carrying gases, tend to operate at higher pressures, and carry richer mixtures, and are constructed of steels that are stronger and tougher than those in the past [2, 3].

There are more than 33,000km of high-pressure steel pipelines in Australia as showed in Figure 1.1, of which more than 25,000 kilometres are used for natural gas transmission. The diameters of the transmission gas pipeline are usually less than 18” and material grades ranged from API 5L grade X42 to grade X70.

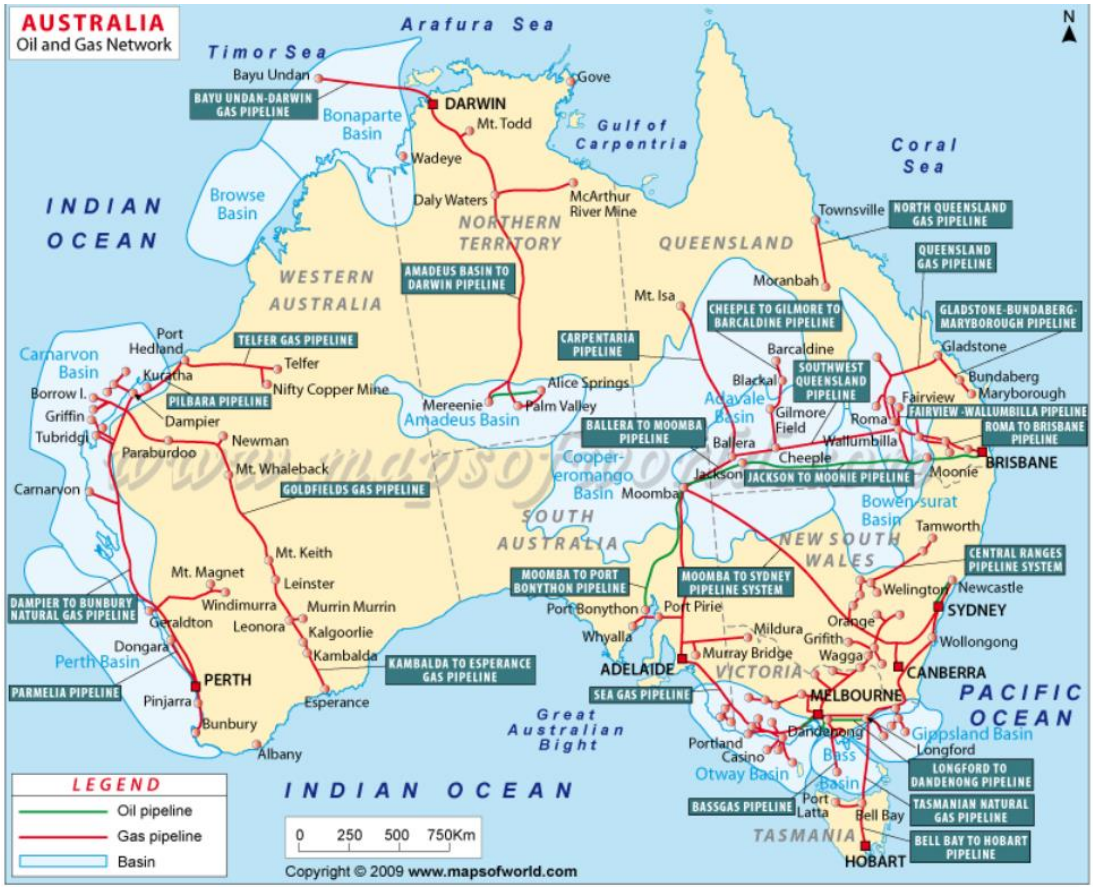

Figure 1.1 Oil and gas pipelines network of Australia [4].

The failure of a gas pipeline could result in a numerous casualties and untold dollar amounts in property damage. An important catastrophic event occurred with the explosion of a major underground high-pressure natural gas pipeline in Ghislenghien, Belgium, on July 30, 2004 [5]. Twenty-four people died and more than 122 people were injured. The material damage estimation was over 100million Euros. Although Australia has a good record in preventing failure of gas pipelines [6], it is generally acknowledged that some degree of mechanical damage during pipeline construction and third-party damage during pipeline operation is unavoidable [7]. Therefore, the risk is very real and it is vital to continue every effort to maximise pipeline safety.

To prevent the failure of gas pipelines, suitable physical measures can be put into place during the design of pipeline. The prevention of fracture initiation is the first step in pipeline fracture control, particularly for pipelines potentially subjected to ground movement hazards or mechanical damage due to external interference. The

next line of defence is the prompt arrest of propagating fractures.

A number of fracture propagation control models have been developed, most of which are based on data gathered from full scale tests conducted in the 1960s and 1970s. Since the 1980s, however, line pipe steels have become cleaner due to reductions in sulphur content and inclusion shape control. At the same time steel toughness increased greatly with grain refinement in thermomechanical controlled processing (TMCP). As such, improving fracture control models applicable for modern 'clean' steel pipelines has attracted significant interest in recent decades.

Fracture propagates in pipeline in either a brittle or ductile manner. Fracture propagation control is achieved by ensuring that (a) the fracture will propagate in the pipe in a ductile manner at and above the pipeline design minimum temperature and (b) the toughness of the line pipe steel is sufficiently high to arrest a propagating ductile fracture within a statistically acceptable number of pipe lengths.

1.1.1. Brittle fracture control

The drop weight tear test (DWTT) is the key technique for determining the fracture propagation transition temperature (FPTT) [8]. If the pipeline design minimum temperature is above the FPTT, the pipeline will not fail by brittle fracture.

The fundamental gap being addressed in the current research is the control of brittle fracture on small-diameter pipes. Most of the recent research works on DWTT have been performed on large-diameter, thick-walled pipes and have focused on the effects of specimen/experimental conditions on transition temperature. Unfortunately, although brittle fracture has been observed on small diameter pipelines (diameters of 90, 200 and 406 mm) [9], the amount of existing research experience with small-diameter, thin-walled pipes is very limited. This is particularly relevant for the Australian pipeline industry as the Australian pipeline network is dominated by relatively small-diameter, thin-walled pipe sections.

The more severe curvature of small diameter pipe makes flattening and DWTT specimen preparation difficult, and the associated deformation can affect the test results. DWTT in accordance with API RP5L3 [10] is an optional requirement for API 5LPSL 2 welded pipe for diameters greater than or equal to DN500 mm, which states that the specimen needs to be completely broken in one impact. The test must be repeated if buckling occurs. However, there is no quantitative definition and allowable extent given for "buckling". It was observed that the occurrence of buckling significantly increased in modern line pipe steels, especially for small-diameter thin-walled line pipes. The 'no buckling' requirement is more and more difficult to meet using the standard DWTT specimen. Due to the absence of the DWTT requirements in the line pipe standards for smaller diameter pipeline, it is difficult for a purchaser to obtain pipes that meet the requirement for brittle fracture control except by special order. This can give rise to difficulties with short pipelines where the quantity of pipes is small.

1.1.2. Ductile fracture control

The determination of the material toughness value required for arresting ductile fracture propagation has historically been based on the Battelle two-curve model (BTCM) [11]. The BTCM provides the minimum required value of the Charpy V-notch (CVN) absorbed energy (arrest toughness) as a function of pipe geometry, pipe grade, applied hoop stress, gas composition, pressure and temperature.

Measuring the CVN energy levels involves extracting a specimen from the pipe sample, which can prove to be challenging for small wall thicknesses or inconveniently shaped components. For instance, a standard specimen with cross-sectional dimensions of 10 mm x 10 mm and a length of 55 mm cannot be extracted from the material used for small wall thicknesses or components with complex shapes [12]. In such cases, it is usual to extract a reduced-thickness specimen. The specified 'sub-size' specimen thicknesses are 7.5 mm (3/4 of the standard size), 6.7 mm (2/3), and 5 mm (1/2). Of those thicknesses, 6.7 mm is the most commonly used

sub-size dimension in the pipeline industry and also the sub-size was used to calibrate the original BTCM in 1970s, because of the relatively small wall thickness of the line pipes in use at that time.

The relationship between the CVN absorbed energy and the CVN specimen thickness plays an important role in pipeline fracture control models. It is particularly relevant to the Australian pipeline industry, as the Australian pipeline transmission network is dominated by relatively small-diameter and thin-walled pipelines [13]. The CVN energy/specimen thickness relationship is assumed to be linear in the BTCM. The crack velocity is expressed by the function of CVN absorbed energy based on the results of traditional steel with low toughness below 95J, therefore, absorbed energy is one of the factors could lead to the deviation of the velocity of the observed fracture from the velocity predicted by the BTCM. However, some experimental results have shown that the linear relationship is only suitable for 'dirty' line pipe steels (i.e. steels containing a high level of impurities such as phosphorus and sulphur), while the absorbed CVN energy in 'clean' line pipe steels varies nonlinearly with specimen thickness [14]. The relevant questions regarding small-diameter pipes include 1) Why is the CVN energy/specimen thickness relationship different in clean and dirty steels? and 2) What is the relationship that should be used in pipeline ductile fracture control?

In order to explore the concerns of the Australian pipeline industry, the Energy Pipeline Cooperative Research Centre (EPCRC) granted the University of Wollongong two projects in 2012:

1) RP6.1.03: Review of ductile fracture control in AS2885.1
2) RP6.1.04: Investigations of drop weight tear test (DWTT) for smaller diameter pipeline

The research conducted in these two EPCRC projects forms the present thesis.

1.2. Research objectives

The present research aims to improve the fracture control approaches used for small-diameter pipelines. The research objectives are:

1) To investigate the buckling phenomenon in DWTT for small-diameter pipeline
2) To improve DWTT to eliminate the buckling effect
3) To improve brittle fracture control of small-diameter pipelines
4) To study experimentally the CVN energy/specimen thickness relationship
5) To implement a proper CVN energy/specimen thickness relationship in pipeline ductile fracture control
6) To develop a numerical model to simulate fracture behaviours in DWTT and CVN tests
7) To utilise the numerical model to gain a deeper understanding of the CVN energy/specimen thickness relationship

1.3. Thesis overview

Chapter 2 provides an exploration of the literatures relating to the size effect in brittle and ductile fracture control. The review includes topics on performing DWTT on small-diameter pipe, the thickness effect on CVN absorbed energy, and numerical evaluation for steel fracture behaviour analysis.

Chapter 3 presents the methods and equipment used in this study. The test methods adopted are tensile test, DWTT, and CVN test. The finite element method (FEM) simulations are performed using a commercial software ANSYS/LS-DYNA and a high-performance computer.

Chapter 4 focuses on the DWTT on small-diameter pipes. Both gull-wing- and flattened-type DWTT specimens are tested for X42 and X70 line pipes. The effects of buckling on the DWTT results are discussed.

Chapter 5 presents collaborative works on full-scale West Jefferson tests between EPCRC and JFE Steel Corporation. The full-scale test results are used to validate the transition curves determined from gull-wing DWTT, flattened DWTT with reinforcement plates, and CVN specimens.

Chapter 6 investigates experimentally the relationship between the CVN energy and the CVN specimen thickness. An exponential CVN energy/thickness relationship has been found to exist for high toughness line pipe steel. The FEM simulations are performed to gain a deeper understanding of the CVN energy/thickness relationship. The power relationship is then applied to the BTCM to improve the prediction of arrest toughness for ductile fracture control.

Chapter 7 compares the transition curves determined by DWTT and CVN tests with various specimen thicknesses for different pipe dimensions and grades. Correlations of DWTT transition temperatures and CVN transition temperatures are compared with existing model.

Chapter 8 draws the primary conclusions of the research work conducted in this thesis and makes recommendations for the standards and for future work.

CHAPTER 2

LITERATURE REVIEW OF GAS PIPELINE FRACTURE CONTROL

In this chapter, a substantial amount of information is reviewed regarding topics considered essential for a better understanding of fracture control of small-diameter gas pipelines.

2.1. Fracture propagation in gas pipeline

A possible consequence of a rupture in a gas or high-vapour-pressure liquid pipeline is fracture propagation. As the fracture propagates throughout the pipeline, the fluid escapes through the fracture, resulting in pressure decay (gas decompression) inside the pipe. As the fluid escapes, a decompression wave travels down the pipeline (away from the opening) at a certain velocity, called the gas decompression wave velocity. A competition between two velocities-the fracture propagation velocity and the gas decompression wave velocity-controls the fracture propagation length.

If the gas decompression wave velocity is less than or equal to the fracture propagation velocity, the hoop stress at the tip of the fracture remains the same. In this case, the fracture continues to run. If the gas decompression wave velocity is greater than the fracture propagation velocity, the hoop stress at the tip of the fracture decreases progressively as gas escapes and the internal pressure drops, and

the fracture propagation velocity is reduced. When the fracture propagation velocity decreases to zero, the running fracture is 'arrested'. The facture propagation velocity depends on the pipe temperature relative to the fracture propagation transition temperature (FPTT) or ductile-to-brittle transition temperature (DBTT) of the line pipe steel.

For pipelines with operating temperatures below the DBTT, the fracture propagates in a brittle mode. Typically, the brittle fracture propagation velocity ranges from approximately 450 m/s to 900 m/s, which is far above the decompression wave velocity in lean natural gas under normal operating conditions [15]. This means that there is no pressure reduction ahead of the brittle fracture, and consequently, the brittle fracture can run for a very long distance while ever this situation prevails.

When the pipeline operates at a temperature above the DBTT, the fracture behaves in a ductile mode. The ductile fracture propagation velocity depends on steel strength and toughness and on the hoop stress at the fracture tip. For higher hoop stresses, the ductile fracture velocity ranges from about 90 m/s to about 360 m/s, which is generally lower than the natural gas decompression wave velocity if the pressure , and temperature remain the constant [15]. This means that the ductile fracture begins to slow down as gas escapes, the pressure falls, and the hoop stress acting on the fracture tip falls correspondingly. If the ductile fracture propagation velocity is always less than the gas decompression wave velocity, the fracture will arrest due to loss of driving force. However, if the ductile fracture propagation velocity is higher than the gas decompression wave velocity the ductile fracture will run for a long distance because the driving force is maintained.

2.2. Brittle fracture control

2.2.1. Brittle fracture control approach

Brittle fracture in steel pipes propagates axially at fracture velocities ranging from approximately 450 m/s to 900 m/s typically in a sinusoidal pattern, with one or many fractures propagating simultaneously [16]. An example of sinusoidal brittle fracture is shown in Figure 2.1. Maxey [17] suggested that the fracture velocity range of 450 m/s to 900 m/s is similar to the range of velocities of propagating elastic stress waves associated with flexural vibration of a cylinder. Deflection of the pipe in the vicinity of the crack tip or preceding the crack tip is less noticeable. The fracture appears to be mostly elastic with the average crack driving force being equal to the nominal stress in the pipe wall. Theoretically, the crack would appear to be directed by the influence of stress waves in the pipe which modify the nominal stress field and the principal stress orientation thus producing the sinusoidal fracture pattern. Shannon *et. al* [18] explained that the sinusoidal path is due to the interaction between the circumferential and longitudinal elastic stress waves coupled with the effect of asymmetric pressure loading on the edge of a cracked pipe. The asymmetry that produced in the radial deformation of a cracked pipe will lead to a twisting moment of the pipe due to the discharging gas. The twisting moment will induce shear stress in addition to the biaxial stress emerging from the longitudinal and bending stresses associated with the bulging.

Figure 2.2 Sinusoidal brittle fracture [17]

With reductions in temperature, fractures of line pipe steels change from ductile to brittle, that is from shear to cleavage in terms of a micro-mechanism and fibrous to crystalline in terms of appearance [19]. This change can be characterised by a fracture propagation transition temperature (FPTT) that depends on material properties of the steel. To ensure the pipe is not fractured in a brittle manner, the FPTT of the full-scale pipe should be below the minimum operating temperature [9].

2.2.2. Full-scale West Jefferson test

Figure 2.2 shows a schematic of West Jefferson tests (named after a small town in Ohio where the tests were first performed) which were used to investigate the fracture patterns and behaviours of pipe [20]. This test is essentially hydraulic, being nearly completely filled with water or brine depending on the test temperature. A small gas pocket is left near the top of the pipe. Pressuring is performed with gaseous nitrogen and a fracture is initiated in a milled V-notch placed longitudinally in the pipe wall. Test temperature is obtained by circulating water or brine past a heat exchanger external to the pipe.

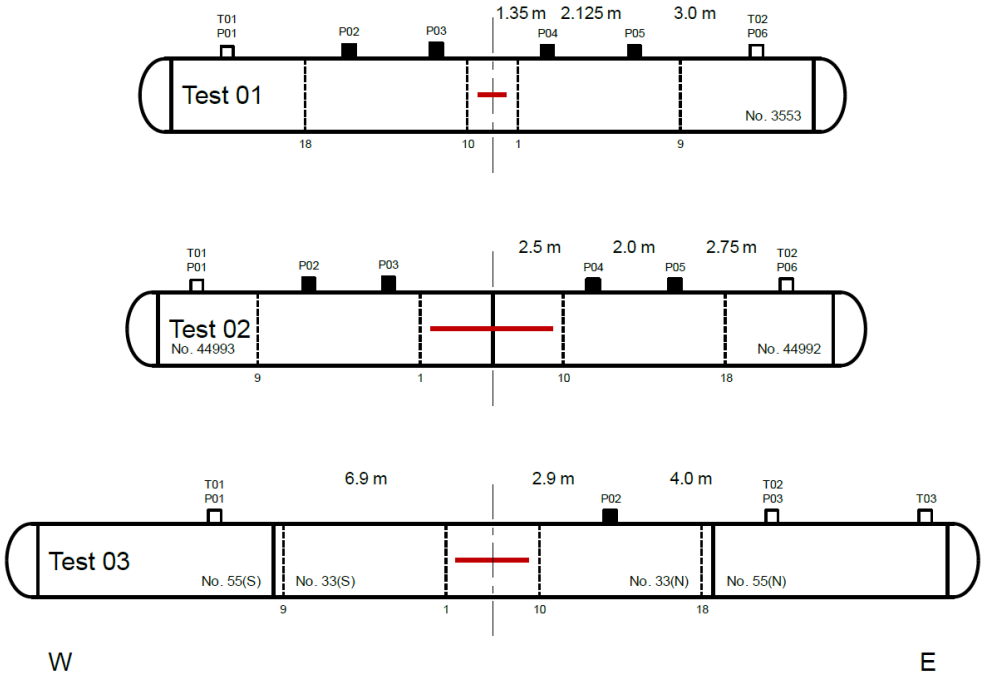

Figure 2.3 Schematic of West Jefferson tests [20]

The full-scale transition temperature of a pipe can be determined by West Jefferson tests conducted at various temperatures. Figure 2.3 shows, schematically, the measured fracture propagation speed against the temperature. The abrupt transition shown in this figure is typical. Above this full-scale transition temperature, the fracture will be of the shear type and relatively slow speed. Below the transition temperature, the fracture is of the cleavage type with relatively high propagation velocity. In the transition range, the fracture might be mixed shear and cleavage, with a velocity somewhere in the range between the upper and lower plateaus.

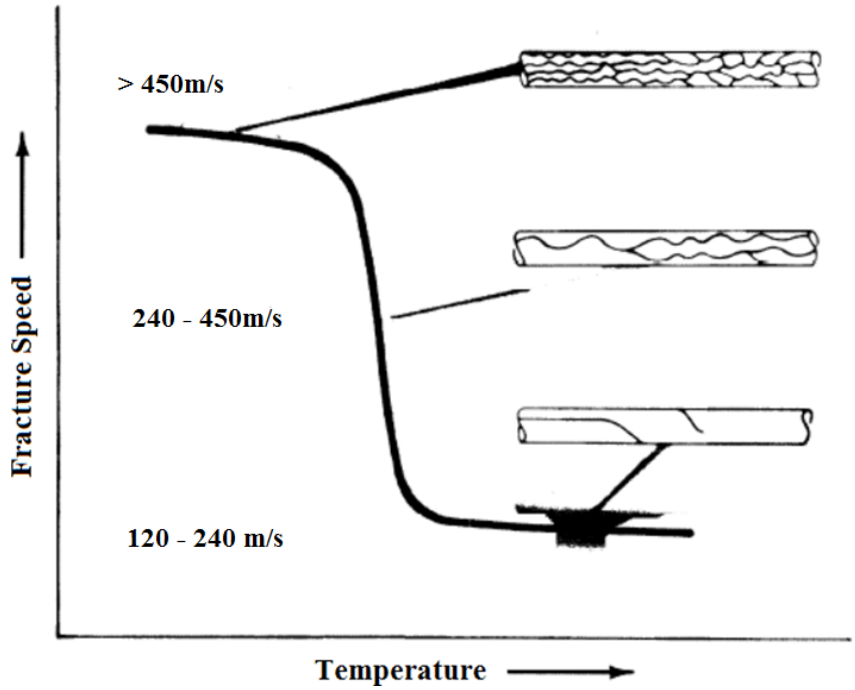

Figure 2.4 Fracture propagation speed against temperature in full scale tests [21]

2.2.3. Drop weight tear test (DWTT)

Full-scale tests are expensive and time-consuming. Lab-scale tests, validated by full-scale test results, are generally used to determine the FPTT in practice. The DWTT, a key lab-scale testing technique for determining FPTT, was developed by Battelle Memorial Institute in 1962 during the course of the American Gas Association NG-18 Research Program [22] to overcome some limitations of the Pellini drop-weight test which was developed by the US Naval Research Laboratory. The DWTT was subsequently standardised in API RP 5L3 [10]. As shown in Figure 2.4, the DWTT specimen is a rectangular bar with a length of 305 mm, a width of 76 mm, and full pipe thickness (up to at least 19 mm). The specimen has a shallow pressed notch made by a sharp indenter with a 45° included angle, resulting in a notch depth of 5 mm and a tip radius of 0.0127–0.0254 mm [10].

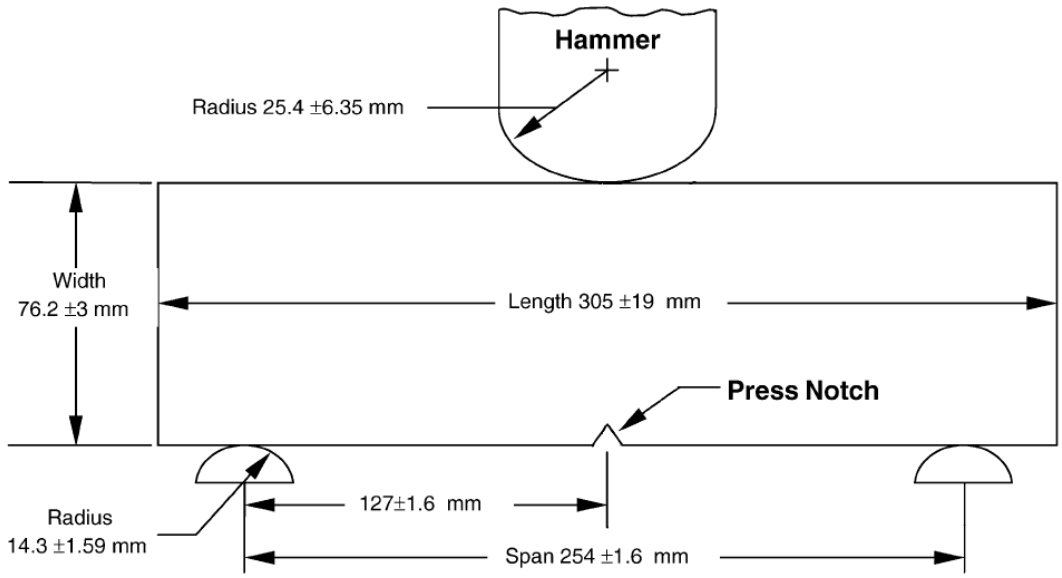

Figure 2.5 Drop weight tear test (DWTT) specimen [23]

A gull-wing DWTT specimen can be used for pipes with a D/t (diameter to wall thickness ratio) less than 40 [10]. In this preparation method, the support and load points of the test specimen are aligned by bending it into a 'gull-wing' shape, while the central part (25–50 mm) of the specimen is not flattened, as shown in Figure 2.5, to avoid the problems caused by work hardening.

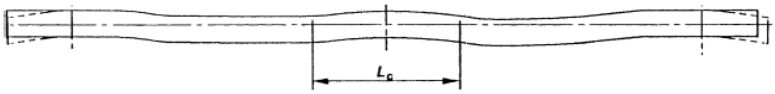

Figure 2.6 Gull-winged drop weight tear test (DWTT) specimen [23]

During the DWTT the specimen is impacted with three-point bending by a dropped hammer in the drop tower (or by the less commonly used pendulum method). The percentage of shear area (SA) can be determined from the appearance of the fracture surface, ignoring a length equal to the thickness of the specimen at each end. In order to determine the FPTT, a series of specimens are broken at various temperatures and the shear area percentage is measured for each temperature.

Figure 2.6 compares the shear area percentages of propagating fractures in pipes with those of DWTT specimens at various temperatures. It can be seen that two curves are in good agreement. Historically, it has been recommended that the temperature corresponding to the DWTT 85% shear area percentage represents the full-scale FPTT [16] [24], as demonstrated in Figure 2.7.

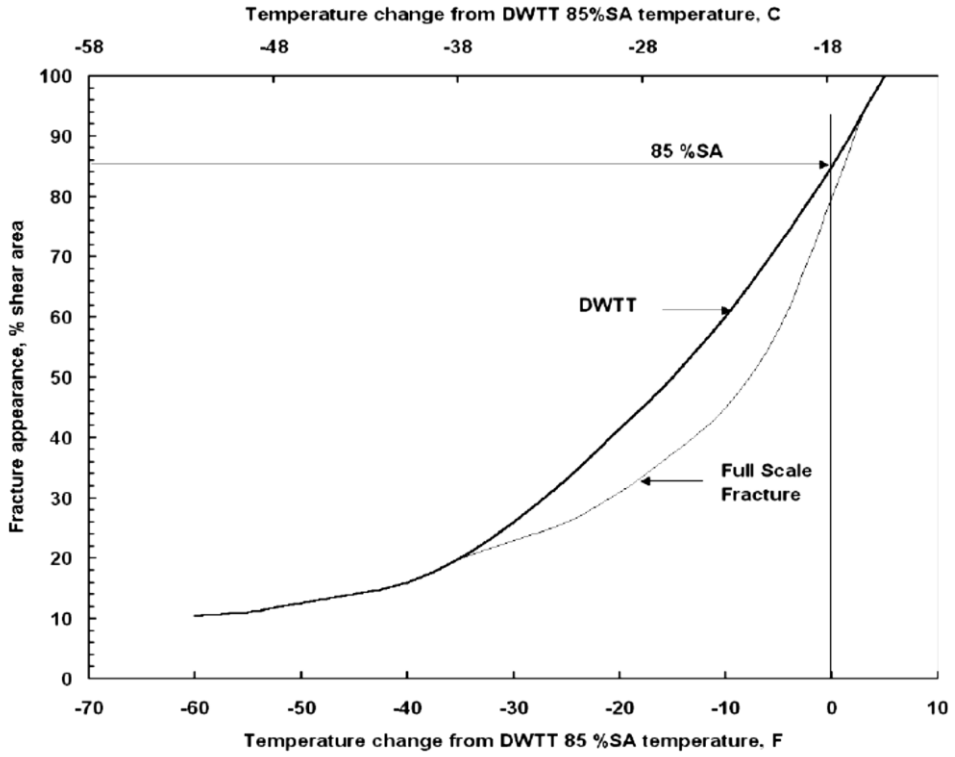

Figure 2.7 Average full-scale pipe fracture appearance versus temperature relative to the DWTT 85% shear area transition temperature [16]

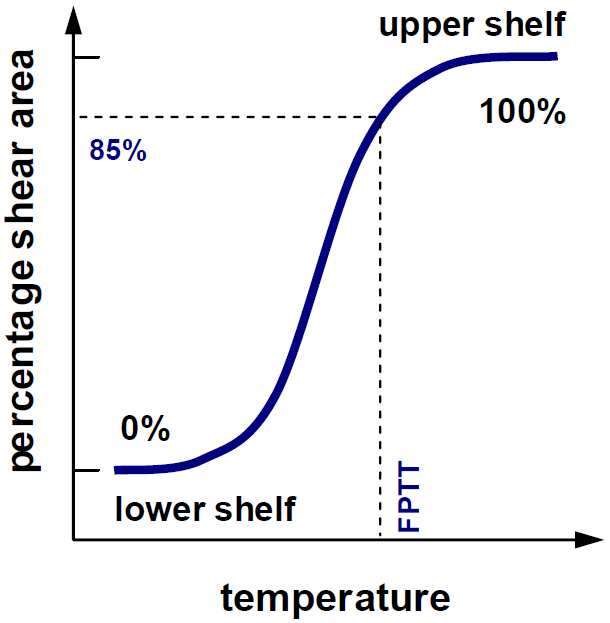

Figure 2.8 Schematic of shear area percentage vs. temperature curve [22]

2.2.4. Validation of DWTT for high toughness steels

The DWTT 85% criterion has been widely used in the standards to determine full-scale FPTT. This criterion was developed by comparing the DWTT results and the full-scale test results of low-toughness line pipe steels. It has also been validated recently for high-toughness line pipe steels [25].

A European Pipeline Research Group (EPRG) study on thick-walled X65 pipe illustrated in Figure 2.8, shows the differences in transition curve between CVN, DWTT and West Jefferson tests. Compared to the DWTT and West Jefferson tests, the Charpy transition curves are not conservative. In addition, the attained Charpy transition curves at the centre and surface of the plate exhibit large variations. It is recommended that the full thickness DWTT is satisfactory enough to predict the propagation behaviour of brittle fracture of high-grade line pipe at least up to X80, and probably, X100 [25].

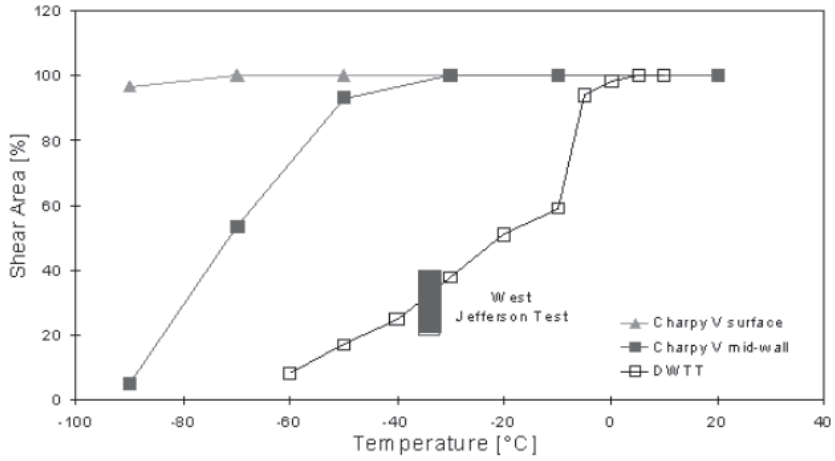

Figure 2.9 Transition curve results from tests on 27.5 mm wall DN900 X65 line pipe [25]

In order to validate the DWTT for predicting full-scale behaviour in X100 line pipes, a series of West Jefferson full-scale tests were conducted on two pipe geometries (DN1400 x 19.1mm and DN900 x 16.0mm) at temperatures below 0°C. Figure 2.9 and 2.10 illustrate comparisons of the achieved transition curves from DWTT, CVN and West Jefferson (WJ) tests. The figures demonstrate that DWTT conservatively predicted transition temperature compared to full scale WJ tests[26].

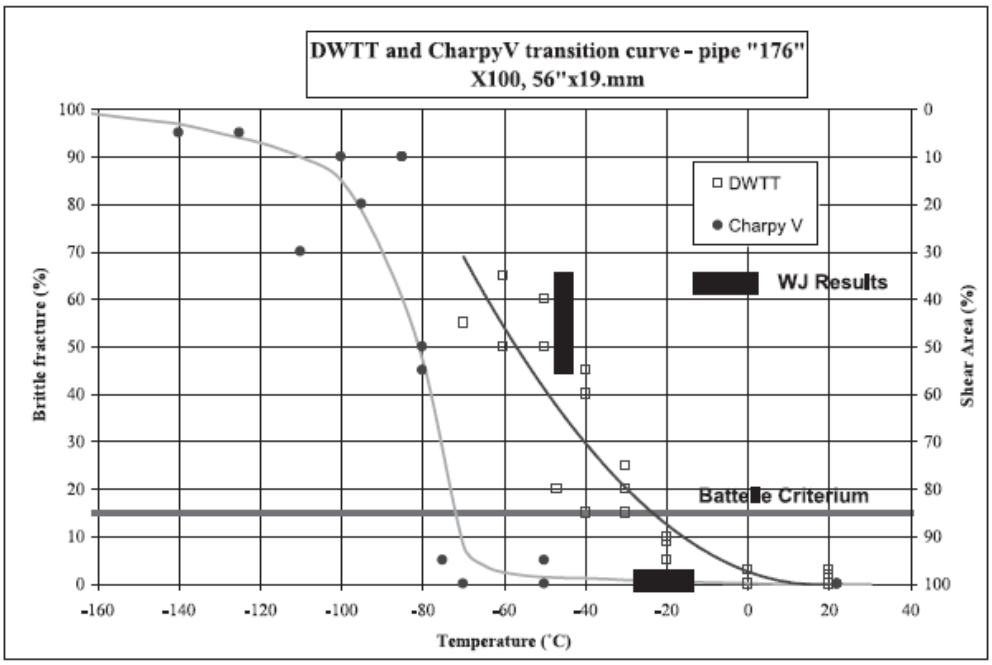

Figure 2.10 Comparison between CVN, DWTT and West Jefferson test results (X100, DN1400 x 19.1 mm) [26]

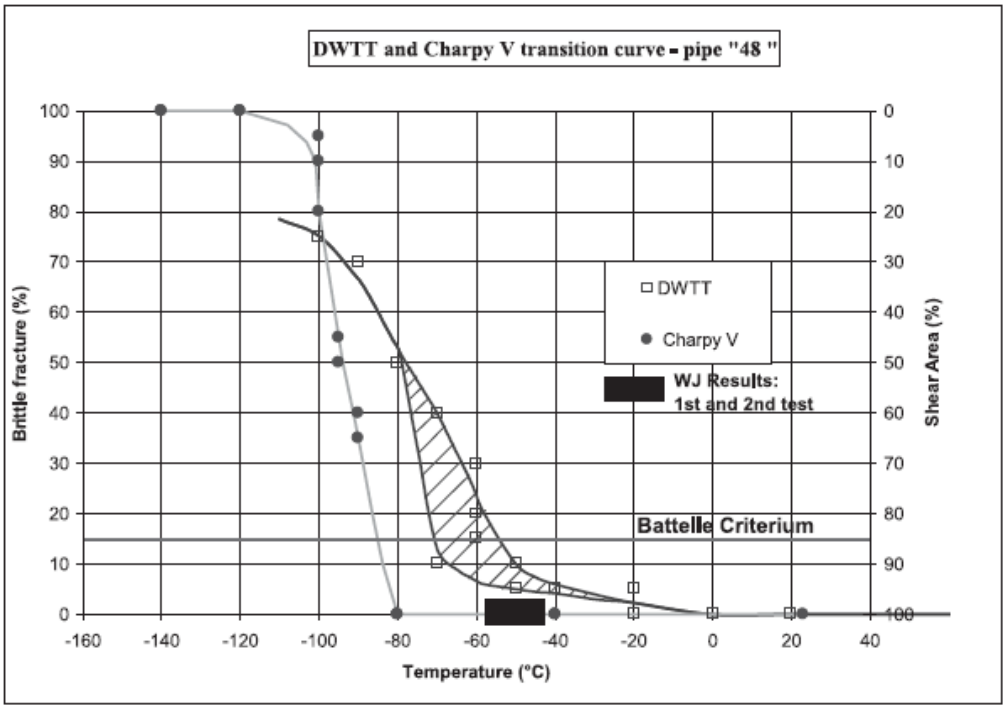

Figure 2.11 Comparison between CVN, DWTT and West Jefferson test results (X100, DN900 x 16.0 mm) [26]

A comparison of the results from X100 experiments with data of high-grade steels up to X80 collected from a previous study, shown in Figure 2.11, confirms the validity of the DWTT 85% shear area criterion and DWTT capability to conservatively predict the transition temperature of X100 pipe material.

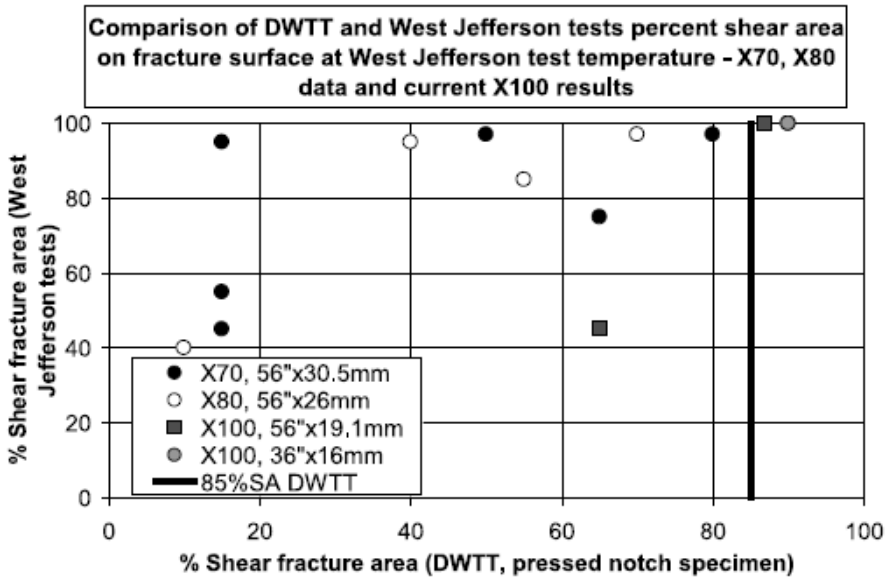

Figure 2.12 Comparison between DWTT and West Jefferson test percent shear area at West Jefferson test temperature for high grade steels [26]

The transition curves obtained from 2/3 thickness CVN, DWTT, and full-scale tests are illustrated in Figure 2.12. The results are for a DN750 with 9.52mm wall thickness and X52 semi-killed line pipe[16].The DWTT transition curve correlated well with the full-scale test in both the shape of the transition curve and transition temperature, while the $CVN_{2/3}$ transition curve only agreed in shear area above 80–85%. Again, these results demonstrated that DWTT is more reliable than CVN for predicting fracture behaviour in a full-scale test.

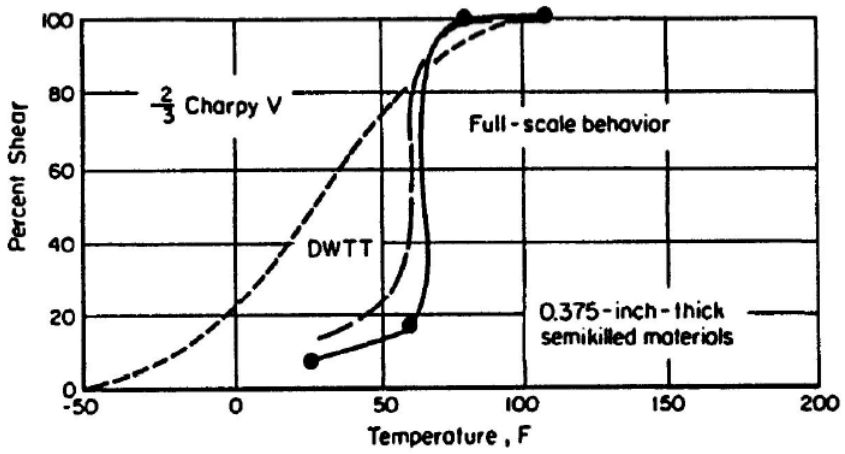

Figure 2.13 Fracture appearance measured in 2/3 CVN, DWTT and full-scale tests on DN750 x 9.5 mm, X52 semi-killed line pipe steel [16]

2.2.5. Alternative to DWTT 85% criterion

CVN is the most common alternatives to DWTT suggested for brittle fracture control. Similar to the DWTT, CVN tests can be performed to determine the transition temperature. However, there were studies showing that CVN and crack arrestor do not work for brittle fracture control.

Cosham *et al.* [22] presented cases of 355 mm and 457 mm welded pipes, where high CVN impact energy and shear area percentage (SA%) coexisted with a low DWTT SA%, and thus there was a risk of brittle fracture even though the Charpy results appeared to be good. This illustrated the importance of performing DWTTs on all pipe sizes. CVN impact energy and shear area criterion were not a sufficient criterion.

Several years ago, within Australasia, a short DN350 gas pipeline was required, and the quantity of pipe was insufficient to warrant a special order. Therefore, it was necessary to use pipe from a stockist. Prudently, the designer chose to conduct DWTTs on PSL2 pipe (a designation in API 5L that has specified fracture toughness properties) available from stockists. The pipe was DN350 12.7mm wall thickness certified PSL2 and had Charpy values of 90, 112, and 130J at 0°C. These values would lead one to expect adequate resistance to brittle fracture. However, when the DWTTs were performed, the results were 0% shear at -10°C and 10% and 90% shear at the design minimum temperature of 0°C. The DWTT pieces after fracture are shown in Figure 2.13.

Figure 2.14 Brittle DWTT performance of DN350 12.7 mm wall thickness API X42 PSL2 pipe with an average Charpy energy value over 100 J at 0°C [27]

This pipe, which appeared to be fit for purpose based on its certification as PSL2 and excellent Charpy properties, did not comply with AS2885.1 and constituted a serious risk of propagating brittle fracture. On this basis it could not be used, and other means had to be sought to control brittle fracture in that pipeline.

At the time, a suggestion was made that the material could have been safely used if some crack arresters had been incorporated. As illustrated in Figure 2.14, practical designs of crack arresters do not work for brittle fracture where there is negligible plastic deformation and no significant crack opening that can be contained and prevented by the crack arresters. Furthermore, since the pipeline was to be located in a high consequence area, it was required to meet the no-rupture and limited release rate provisions of AS2885.1, which would also have ruled out the use of a design where brittle fracture control was based on the use of crack arresters.

Figure 2.15 Multiple longitudinal brittle fractures in a section of pipeline entirely encased in reinforced concrete [28]

The advantages of the DWTT-based approach compared with the CVN-based approach are summarised as follows:

- The fracture appearance of DWTT specimens reflects the actual pipe behaviour more accurately as the longer ligament of DWTT specimens allows a larger plastic zone, and because the DWTT specimen is the same thickness as the pipe, and therefore, the level of constraint is the same [29].

- The longer ligament of the DWTT specimen reduces the influence of the increasing proportion of crack initiation energy in total energy absorption of tougher materials. This influence could be further reduced or even removed by modifying the notch of the DWTT specimen. Experiments conducted by Demofonti et al. [30] indicated that the amount of crack initiation energy for a standard press-notch DWTT specimen was considerable, while a chevron-notch DWTT specimen displayed less crack initiation energy. In a pre-cracked DWTT specimen, the crack-initiation energy was almost eliminated, as a result of the pre-crack.

- As the DWTT specimen thickness is the same as the pipe thickness, the difficulties associated with the nonlinear wall thickness effect on absorbed energy can also be eliminated.

2.2.6. DWTT requirement in specifications

ANSI/API Specification 5L [31] and ISO 3183:2012 [32] (the most widely used standard worldwide):

DWTT is a optional requirement for PSL 2 welded pipe for diameters greater than or equal to 508 mm, along with the CVN testing of the pipe body. For DWTT of the pipe body, the average shear fracture area shall be above or equal to 85%, based upon the test temperature specified in the purchase order. For welded pipe with a diameter less than 508 mm, only CVN testing of the pipe body is required. Where DWTT is required, it is performed in accordance with API RP5L3 [10], which states that the specimen needs to be completely broken in one impact. The test must be repeated if buckling occurs. However, there is no quantitative definition and allowable extent given for "buckling". The high toughness of modern line pipe steels significantly increases the occurrence of buckling, and the 'no buckling' acceptance criterion is no longer practical.

Australian pipeline standard AS2885.1:2012 [33]**:**

Australian pipeline standard AS2885.1 specifies that fracture appearance testing for control of brittle fracture shall be performed using DWTT on diameters of 300 mm and above in accordance with AS1330 [23] or an alternative standard for the same test method. An alternative method for assessing the fracture appearance of ferritic steels with a thickness greater than 19 mm is allowed in standard AS1330. In that case, the standard indicates that excessive plastic deformation at the impact point leads to conservative results, a point which may or may not be true. The direction and magnitude of temperature shift between the transition curves of specimens with and without plastic deformation are not known for modern line pine steels, and it is necessary to carry out experiments for clarification. Moreover, the quantitative definition of 'excessive' is not given, and there is no replacement required for specimens with excessive plastic deformation. It is noted that API and ISO DWTT standards use the term 'buckling' instead of 'plastic deformation', and 'plastic deformation' is considered more specific.

ASME B31.8: 2014 (USA) [34]:

ASME B31.8 requires DWTT for diameters greater than or equal to 400 mm when the pipeline operates at a hoop stress of 40–80% of specified minimum yield strength (SMYS), and for smaller diameters when the pipeline operates at a hoop stress of 72–80% SMYS.

CSA Z245.1: 2012 (Canada) [35]:

CSA Z245 requires that fracture appearance testing be conducted using DWTT for pipe diameters greater than 457 mm and CVN testing as a substitution for pipe diameters equal or smaller than 457 mm.

BS EN 10208-2: 2009 (UK) [36]:

The standard specifies that DWTT is to be conducted on pipes with diameters greater than 500 mm, wall thicknesses greater than 8 mm, and specified yield strengths greater than 360 MPa.

DNV-OS-F101: 2012 for submarine pipeline system [37]:

DWTT is required for line pipe diameters greater than 400 mm, wall thicknesses greater than 8 mm, and specified yield strengths greater than 360 MPa in the DNV-OS-F101 2012 version. The diameter limit was reduced from 500 mm to 400 mm in the 2010 version due to industry comments.

IGEM/TD/1 Edition 5 (Institution of Gas Engineers and Managers, UK) [38]

A full wall DWTT is required for line pipe diameters exceeding 323.9 mm to assess resistance to brittle fracture. For smaller diameter pipes, extraction of a sample for DWTT is said not to be possible and fracture appearance using the Charpy test should be substituted.

GBE/LX1, LX4 and LX5 (internal specifications of British Gas)

British Gas internal specifications require a minimum shear area in a DWTT for all line pipes with diameters greater than 323.9 mm for submerged arc-welded, seamless, and electric-welded pipe. A minimum shear area in a CVN test is required

at a lower test temperature for smaller diameter seamless and electric-welded line pipe. The specification covers wall thicknesses up to 12.7 mm for diameters smaller than or equal to DN300 [22].

The FPTT is the only parameter that controls brittle fracture propagation in all the standards. The CVN transition temperature is required as a substitution for DWTT in some standards (API 5L, CSA Z245.1, etc.). However, guidance on the method of correlation from the CVN transition temperature to the DWTT transition temperature is missing in these standards. The DWTT transition temperature may be higher than the CVN transition temperature, which means that the CVN transition temperature would not prevent brittle fracture propagation in pipelines.

Except for AS2885, all of the specifications require DWTT to be performed and evaluated according to API RP 5L3 [39] . While it is required that AS1330 [23] is to be followed in AS2885. AS1330 requirements are in agreement with API RP 5L, except that no replacement is required for specimen exhibiting buckling.

2.2.7. Difficulties of performing DWTT on small diameter pipes

In 1969, the limit of 508 mm was introduced for practical reasons in the API/ISO standard, according to Cosham *et al.* [22]: 'In small diameter thin walled line pipe it is difficult to extract and gull wing a satisfactory drop weight tear test specimen'.

A number of difficulties attached to DWTT on small pipe diameters have been mentioned in the literatures:

- The extreme curvature makes flattening and DWTT specimen preparation problematic, and the associated deformation might affect the test results. In gull-wing preparation, the support and load points of the test specimen are aligned by careful bending into a 'gull-wing' shape, while the central part (25–50 mm) of the specimen is not flattened. This process is possible, but it is inconvenient for production testing and it is not well standardised [40].

- A report on the applicability of DWTT on seamless pipes with diameter down to 300mm was presented by Schmidt [41]. Extensive lateral deformation and inverse fracture were observed, leading to invalid results and a failure to obtain the FPTT. Unbroken specimens (Figure 2.15) with no crack initiation were observed in some cases.

Figure 2.16 'No-Break' specimen extracted from a seamless smaller-diameter pipe [41]

API RP 5L3 requirements for a valid DWTT are summarised as follows [39] :

- Specimens shall be completely broken in one impact;
- Specimen is not allowed to buckle. If buckling occurs replacement is necessary;
- Specimen is required to exhibit cleavage fracture from the notch tip with exception of specimens that exhibit ductile fracture on the complete fracture surface.

2.3. Ductile fracture control

2.3.1. Battelle two-curve model (BTCM)

The calculation of the magnitude of the material toughness required to arrest ductile fracture propagation in natural gas pipelines in Australia has traditionally been based on the 'short-form' equations produced from curve fitting BTCM results. This

method considers the minimum CVN absorbed energy as the criterion for the arrest of the propagating ductile fracture. The estimated CVN energy for fracture arrest is a function of pipe geometry, grade, applied hoop stress, gas composition, and temperature.

BTCM involves the superposition of two independently determined curves—the gas decompression wave speed characteristic and the fracture propagation speed characteristic—each as a function of local gas pressure.

Figure 2.16 shows, schematically, one gas decompression wave speed curve and three fracture propagation speed curves (Curves 1~3) [42]. The three fracture curves represent three cases with different material toughness (Charpy absorbed energy). As the toughness increases the fracture curve moves up.

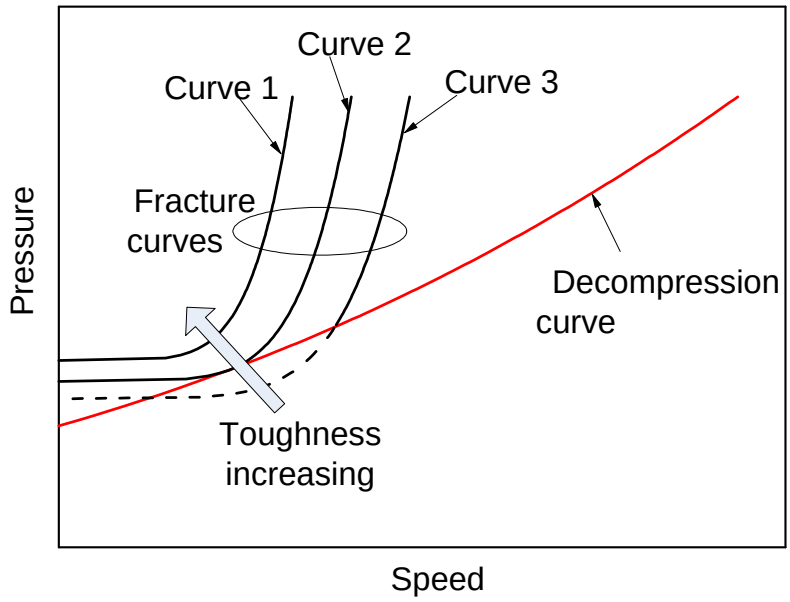

Figure 2.17 Schematic of the BTCM [42]

It can be seen in Figure 2.16 that initially (at high pressure) the decompression wave speed exceeds the fracture propagation speed. As the gas decompression proceeds, both the gas decompression speed and the fracture propagation speed decrease. A fracture curve such as Curve 1 does not intersect the gas decompression curve at any point. This indicates that the fracture propagation speed is always slower than the gas

decompression wave speed, leading to continuous decrease of the fracture propagation speed down to zero. In this case, the fracture is arrested.

A fracture propagation curve such as Curve 3 intersects the decompression curve at a certain pressure level. Note that Curve 3 intersects the decompression curve at two points. Only the upper intersection point (at the higher pressure) is considered relevant in the BTCM. Above this pressure the fracture speed is lower than the decompression speed at the same pressure. As in the case of Curve 1, the fracture propagation speed continues to drop initially until it reaches the pressure corresponding to the intersection point. It is assumed in the BTCM that at the intersection point, the fracture and the gas decompression wave propagate at the same speed. This means that the gas pressure at the tip of the fracture no longer decreases, and both the fracture and the gas decompression wave continue to move at the same speed, resulting in an extended fracture propagation length.

The boundary between the arrest and propagation of a running fracture is represented by a tangency between the gas decompression curve and the fracture curve (Curve 2). The minimum toughness required to arrest the running fracture, defined as 'arrest toughness', is the value corresponding to this condition.

In the BTCM, the expression used to calculate fracture velocity is

$$V = C\frac{\sigma_f}{\sqrt{R}}\left(\frac{P_d}{P_a} - 1\right)^m \tag{2.1}$$

where V is the fracture velocity, P_d is the dynamic gas pressure, P_a is the arrest pressure, R is the specific toughness, σ_f is the flow stress, and m and C are constants.

The arrest pressure is defined as:

$$P_a = \frac{2\sigma_f t}{3.33\pi r} arccos\left(e^{-\left(\frac{\pi RE}{24\sqrt{rt}{\sigma_f}^2}\right)}\right) \tag{2.2}$$

where t is the wall thickness, r is the outside radius of the pipe and E is the elastic modulus.

Using the CVN absorbed energy, the specific toughness R in Eqn. (2.1) can be calculated as

$$R = \frac{C_v}{A} \tag{2.3}$$

where C_v is the CVN absorbed energy and A is the cross sectional area under the notch of the CVN specimen.

Measuring the CVN energy levels can prove to be challenging for thin walls or small diameter pipes. For instance, a standard specimen with cross-sectional dimensions of 10 mm x 10 mm and a length of 55 mm cannot be extracted from the material used for thin walls or components with complex shape [12]. In such cases, it is usual to extract a specimen with a reduced thickness. The commonly specified 'sub-size' specimen thicknesses are 7.5 mm (3/4 of the standard size), 5 mm (1/2), and 2.5 mm (1/4). Specimens 6.7 mm (2/3) and 3.3 mm (1/3) in thickness can also be used; 6.7 mm is the most commonly used sub-size in the pipeline industry. The relationship between the Charpy absorbed energy at the upper shelf region (upper shelf energy (USE)) value and the Charpy specimen size is particularly relevant to the Australian pipeline industry, as the pipeline transmission network is dominated by relatively small-diameter, thin-walled pipelines [13].

The currently used relationship between the energy absorbed in the pipe body and the Charpy toughness value in the BTCM is not clear, particularly regarding to thickness effects. AS2885.1 [33] allows a non-linear relationship to be established and used in converting energy from one size to another. However, it was demonstrated by Maxey [43] that these nonlinear effects were not taken into account in the development of the BTCM.

2.3.2. Ductile fracture control models for high toughness steels

The Battelle fracture model was calibrated against low-strength, low-toughness steels in the 1960s and 1970s. It is known to provide non-conservative results when

used in the BTCM for steels with CVN energy above 95 J [21]. This limitation was partially overcome with the introduction of correction models developed by Leis, Wilkowski, and Centro Centro Sviluppo Materiali (CSM).

Leis developed an equation to correct the arrest toughness for toughnesses greater than 95 J predicted by the BTCM [21]. The Leis correction model is:

$$CVN_{Leis} = CVN_{BTCM} \quad for \quad CVN_{BTCM} < 95\,J \tag{2.4}$$

$$CVN_{Leis} = CVN_{BTCM} + 0.002 \times CVN_{BTCM}^{2.04} - 21.18 \quad for \; CVN_{BTCM} \geq 95\,J \tag{2.5}$$

where CVN_{Leis} is the corrected full-size Charpy arrest energy and CVN_{BTCM} is the full-size Charpy arrest energy calculated with the BTCM.

Wilkowski *et al.* developed correction models based on the relationship between Charpy specific energy and pressed-notch DWTT specific energy. The Wilkowski 1977 correction model [23] is:

$$(\mathrm{E/A})^{\mathrm{W1977}}_{\mathrm{Corrected-Charpy}} = \frac{\left(\frac{3(\mathrm{E/A})_{\mathrm{BTCM}} + 1800}{175}\right)^{1/0.385} - 300}{3} \tag{2.6}$$

However, the Wilkowski 1977 equation did not adequately reflect later full-scale data and was adjusted in the Wilkowski 2000 equation [24]:

$$(E/A)^{W2000}_{Corrected-Charpy} = \frac{\frac{\left(\frac{3(E/A)_{BTCM} + 1800}{175}\right)^{1/0.385}}{1.3} - 300}{3} \tag{2.7}$$

CSM compared the experimental results of full-scale fracture propagation tests on large-diameter (greater than 36”), high-pressure X80 pipes with BTCM predictions [25]. It was found that a multiplying factor of 1.43 applied to the predicted value is sufficient for X80 pipes to ensure that no propagation points appear below the propagation/arrest boundary.

There are several published reviews from Cosham *et al.* [44], Zhu *et al.* [45, 46], Wilkowski *et al.* [47], and Wolodko *et al.* [48] on various correction methods that were developed to improve the prediction for higher toughness steels. All of the correction methods thus far were developed based on empirical adjustments. But it does not seem that this approach can continue to be successfully applied to higher and higher-toughness steels with CVN values well above 200J and reaching up to 400J, and none of these approaches have considered the effect of Charpy specimen thickness. Takahashi *et al* [49] pointed out that the effect of thickness on fracture toughness was one of the factors that cause the observed crack velocity to deviate from the predicted crack velocity in the BTCM. , None of existing fracture control correction methods has considered the effect of Charpy specimen thickness

2.3.3. Charpy specimen thickness effect on upper shelf energy

2.3.3.1. USE normalisation models

Corwin *et al.* [50] investigated the influence of specimen size on the USE of 12Cr-1MoVW ferritic steel. Their paper was one of the earliest papers to adopted the power relationship between CVN absorbed energy and CVN specimen thickness. Two types of impact specimens were examined. Full-size specimens were used according to ASTM specification E23 [51], with dimensions of 10 mm x 10 mm x 55 mm length, containing a 2mm-deep, 45° V-notch with a 0.25mm root radius. Sub-size specimens were 5 mm x 5 mm x 25.4 mm length, containing a 0.76mm deep, 30° V-notch with a 0.05–0.08mm root radius. All specimens were of the L-T orientation.

In order to normalise the impact energies of the specimens, their values were divided by the nominal fracture area (*Bb)* and the nominal fracture volume $(Bb)^{1.5}$. This yielded an improved correlation between the full- and sub-size specimen datasets. Here, *B* is the specimen width and *b* is the length of the ligament. Bb equals 80 mm^2

and 21 mm^2 for full- and sub-size specimens, respectively. $(Bb)^{1.5}$ equals 720 mm^3 and 98 mm^3 for full- and sub-size specimens, respectively.

Figure 2.17 shows the influence of area and volumetric normalisation on the impact energy for full- and sub-size specimens of 12Cr-1MoVW steel. The best correspondence between the full- and sub-size data sets was observed for USEs normalised with respect to nominal fracture volume. However, agreement was still only fair, with the energy per unit volume being consistently greater for the sub-size specimens. Figure 2.17 indicates that the volume-normalised USE for the sub-size specimens exceeds that of the full-size specimen by about 10%. Normalisation on an area basis produced no agreement between the different specimen sizes.

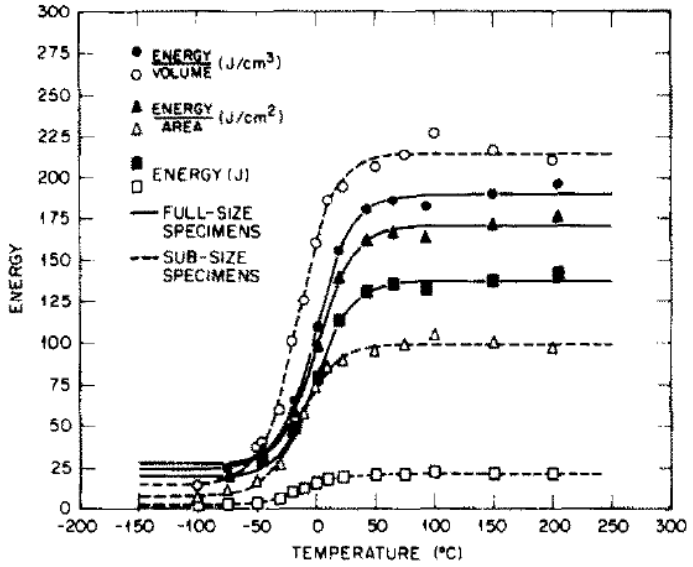

Figure 2.18 Effect of area and volumetric normalisation on impact energy for full- and sub-size specimens of 12Cr-1MoVW steels [52]

The sub-size sample geometries used in Corwin *et al*' were different from those specified in the current ISO and ASTM standards. They reduced not only the thickness, but also the ligament length and the span. The normalisation by $(Bb)^{1.5}$ was more accurate than the normalisation by *Bb*. If the ligament length (*b*) remained constant, the results indicated that the 1.5 power relationship can describe the effect of specimen thickness on the USE better than the linear relationship can. Bb was used to represent the fracture area, while $(Bb)^{1.5}$ was used to represent the

deformation volume before fracture. The result indicated that the deformation volume plays an important role in fracture initiation and fracture propagation. It should be noted that this relationship originated from the thought that the CVN absorbed energy was related to the volumetric deformation, rather than resulting from experimental curve fitting.

The normalisation factor presented in Equation (2.8) was derived in a study carried out by Louden *et al.* [53], The normalisation factor incorporates all specimen dimensions as well as the notch geometry:

$$B(W-A)^2/LK \tag{2.8}$$

where *K. L, B, W,* and *A* are the stress concentration factor, span, thickness, width, and notch depth, respectively. The stress concentration factor was a function of the ligament size *(W–A)* and the radius of the notch root. The normalised USE was the ratio of the measured USE to the normalisation factor.

The insight underlying this combination of parameters can be observed by examining their individual effect on the USE. For example, the strain rate at the notch and the USE decrease when span length L increases. A high value of *K* can cause brittle fracture which leads to decreased USE. Finally, the product $B(W–A)^2$ is an approximation of the volume of plastic deformation at the crack tip. As this volume decreases, the value of USE is also reduced.

This normalisation factor was applied to data obtained from various materials. Figure 2.18 shows a graph of normalised USE against full size USE. The normalised USE was divided by the average of the normalised values of full-, half-, and one-third-size specimens obtained for each material. The normalised energies for the full-, half-, and one-third sizes would be equal, and the points in Figure 2.18(a) fall on the horizontal line with the ordinate equal to 1 if the normalisation factor was indeed valid. It is clear in Figure 2.18(a) that the normalisation using formula ($B(W–A)^2$) was more accurate (within ±10%) for materials with relatively low USE values (i.e. for full-size USE values less than 150 J).

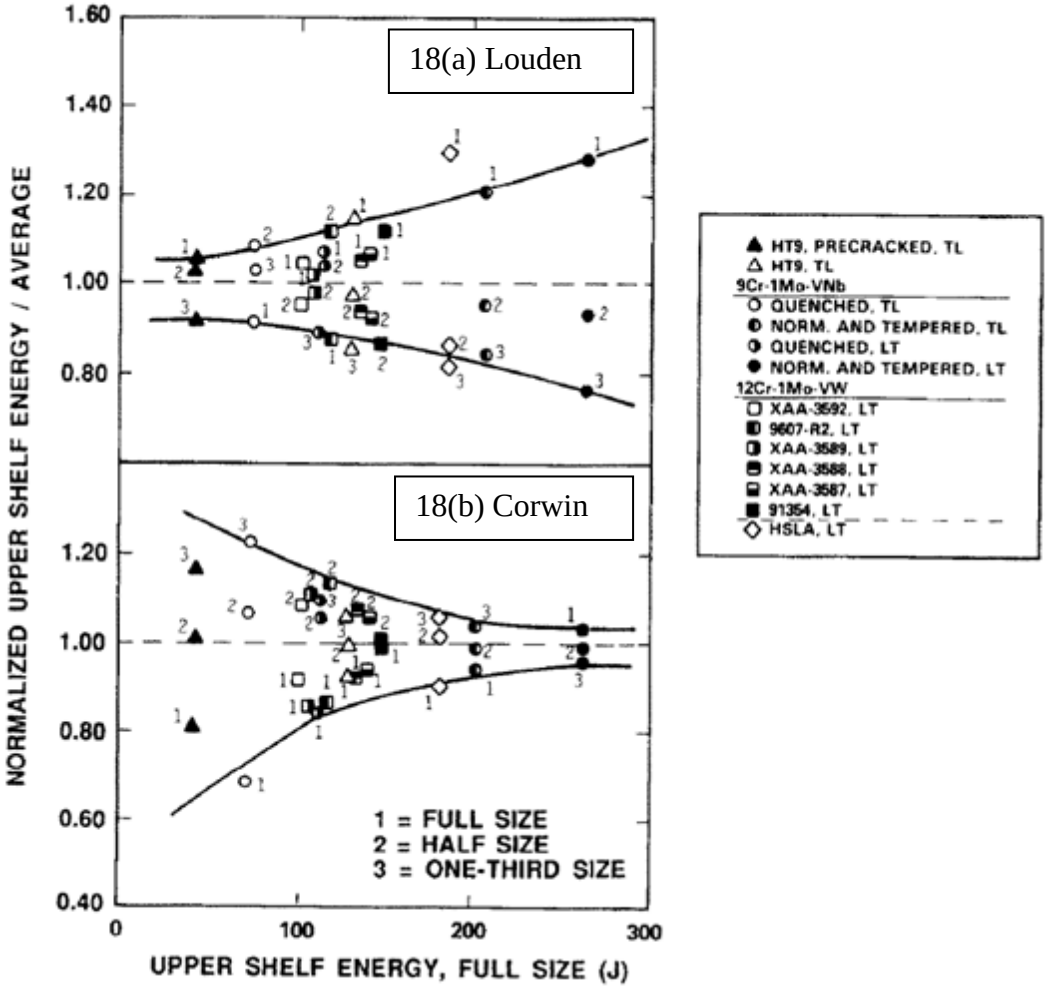

Figure 2.19 Comparison of normalised USEs of various materials [53]

Corwin *et al*. [50] used $(B(W–A))^{1.5}$ as a normalisation factor, which is related to the extent of plastic deformation below the notch root. The normalisation approach of using $(B(W–A))^{1.5}$, gave good results with relatively high toughness (roughly above 150 J). Figure 2.18(b) shows that when used to analyse the same USE data field, Corwin's normalisation factor failed to correlate the materials exhibiting low USEs. Corwin's model would be expected to work best under conditions where notch geometry is relatively unimportant; i.e. in alloys with a greater degree of ductility (less notch sensitivity) and whose fracture energies are affected by the influence of substantial work hardening. At lower levels of ductility, the influence of work hardening is relatively small compared to stress concentration considerations, and the proposed model is more successful.

Note that in Figures 2.18(a) and 2.18(b) there is a persistent bias with respect to the placement of the normalised data as a function of specimen size, and that the sense of this bias is reversed in the two correlations. This also implies that the full dependence on size effects has not been incorporated in either model. It should be noted, however, that the bias in both models is minimised in the range of fracture energies where each correlation is most successful.

Four ferritic steels with different Charpy impact properties were investigated by Kurishita *et al*. [54]. Japanese ferrite/martensite dual-phase steels (JFMS), in both un-irradiated and irradiated conditions, were used along with two other high-strength ferritic steels that have lower USE and ductile–brittle transition temperature values than the un-irradiated and irradiated JFMS. The longitudinal axes of the full-size and sub-size Charpy specimens were parallel to the rolling direction. That study used four different miniaturized specimen geometries: 3.3×3.3×23.6 mm, 2.0×2.0×20 mm, 1.5×1.5×20 mm, and 1.0×1.0×20 mm. These specimens also had three to four different notch dimensions selected from options: 0.51 mm, 0.40 mm, 0.6mm, 0.3 mm, 0.45mm and 0.2 mm.

To correlate the USE of the miniaturised and full-size specimens, the measured USEs were categorised by various geometric factors and then compared. The best correlation, which was still not satisfactory, was obtained when Bb^2 or $(Bb)^{1.5}$ was used as a normalising factor, where B was the specimen thickness, and b was the ligament size. These volumetric parameters are known to be related to the extent of plastic deformation below the notch after general yield. Figure 2.17 shows the influence of the notch dimensions on the USE normalised by $(Bb)^{1.5}$ for all the sub-size and full-size specimens of un-irradiated JFMS that were considered in this work. Here, the effect of the notch geometry was expressed by applying the elastic stress concentration factor, K_t.

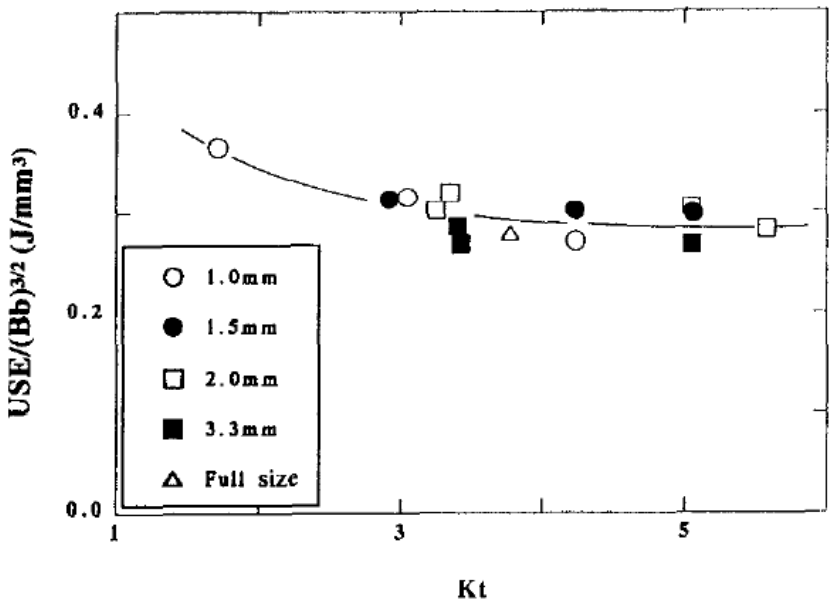

Figure 2.20 Normalised USE values plotted against the elastic stress concentration factor, K, for full-size and sub-size Charpy specimens of un-irradiated JFMS [54]

It was found that except for one data point (corresponding to a 1mm specimen with a very large notch root radius of 0.25 mm), all data points of un-irradiated JFMS exhibited a normalised USE consistent to within ±15%, regardless of the stress concentration factor, K_t [54]. This means that the observed dependence of USE on notch depth resulted only from the dependence of USE on ligament size: the notch geometry apparently had only a negligible effect on USE. The higher normalised USE of the 1mm specimen indicated that the normalisation parameter Bb^2 or $(Bb)^{1.5}$ underestimated the fracture volume and that the actual fracture volume was greater.

On the other hand, it was also found that for the irradiated JFMS and other un-irradiated high-strength ferritic steels, the normalised USE of full-size specimens was always lower than that of sub-size specimens, and the ratio of the full-size to normalised sub-size USE decreased with the decreasing USE (un-normalised) of full-size specimens [54]. This finding indicated that for full-size specimens of these ferritic steels, the normalisation parameter Bb^2 or $(Bb)^{1.5}$ overestimated the fracture volume, and the actual fracture volume should be smaller. These results suggested that the observed difference in the effect of specimen size on the USE of the different alloy and irradiation conditions occurred due to a greater reduction in

specimen volume associated with fracture for full-size specimens than predicted using volumetric parameters Bb^2 or $(Bb)^{1.5}$.

To demonstrate this concept, the ratio of the normalised USE of full-size specimens to that of sub-size (one-third-size) specimens, α, was calculated for all the ferritic steels reported to date in the literature, including the un-irradiated and irradiated JFMS considered in this work. Figure 2.20 plots α against the un-normalised full-size USE. A linear relationship was observed between α and the un-normalised USE of the full-size specimens. Therefore, the relationship between the un-normalised USE of full-size specimens and the normalised USE of sub-size specimens was also linear, as shown in Figure 2.21.

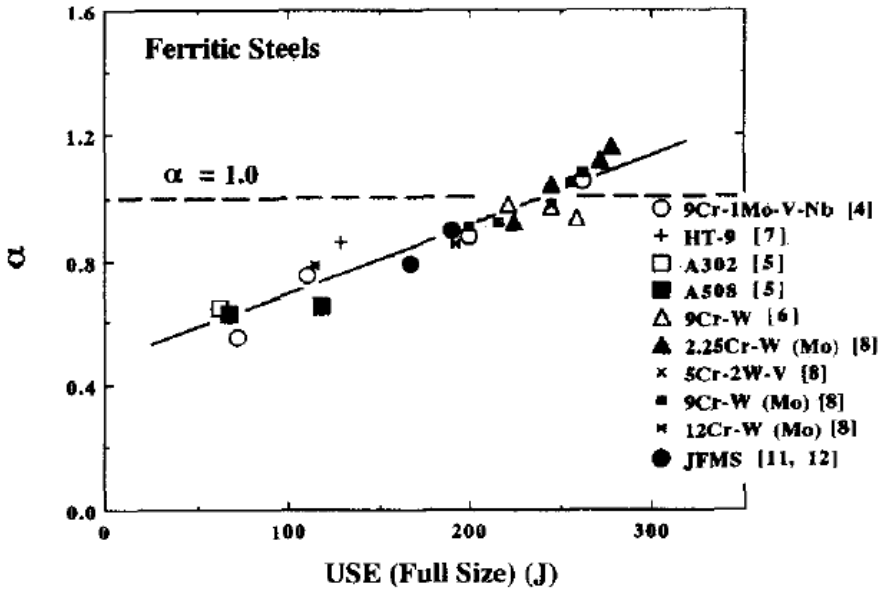

Figure 2.21 Plot of the ratio, α, USE/$(Bb)^{1.5}$ of full size specimens to that for 1/3 size specimens against the unnormalised USE of full size specimens in ferrite steels [54]

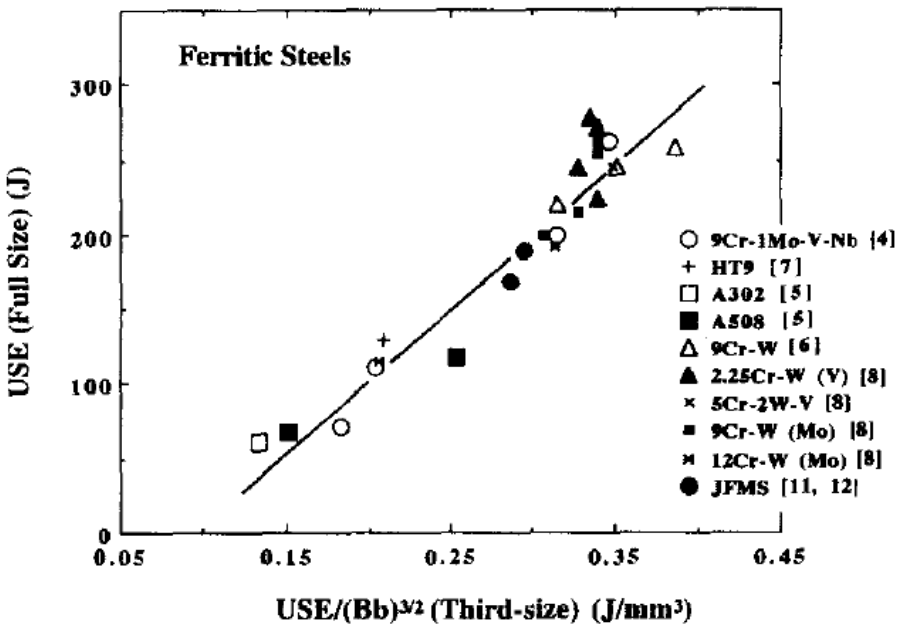

Figure 2.22 Plot of the USE of ferritic steels. Values of full size specimens are plotted against the USE/(Bb)$^{1.5}$ of third size specimens [54]

Accordingly, it was concluded that the effect of specimen size on USE can be implied in terms of the specimen volume associated with the fracture. In addition, the observed linear relationship between the un-normalised USE of full-size specimens and the normalised USE of sub-size specimens can be applied to determine the USE of full-size specimens from the USE of sub-size specimens.

The study from Kurishita *et al*. used non-standard sub-size specimen geometry. All dimensions (thickness, ligament length, and span) were reduced in the sub-size specimens. The normalised USE by $(Bb)^{1.5}$ was not consistent, which might be due to the changes in span and/or ligament length. The effects of span and ligament length do not need to be considered in pipeline CVN tests.

Abe *et al.* [55] studied the effect of specimen size on USE using full-size, half-size, and one-third-size V-notch specimens of 9Cr-W steels. The absorbed energy of full-size, half-size, and one-third-size specimens of 9Cr-2W steel are plotted as a function of test temperature in Figure 2.22. Specimen size has been shown to be a serious influence on absorbed energy. Specifically, the measured USE values were 245.2 J, 34.3 J, and 9.8 J for the full-size, half-size, and one-third-size specimens,

respectively. The USE of the one-third-size sample was only 1/25 of the full-size USE.

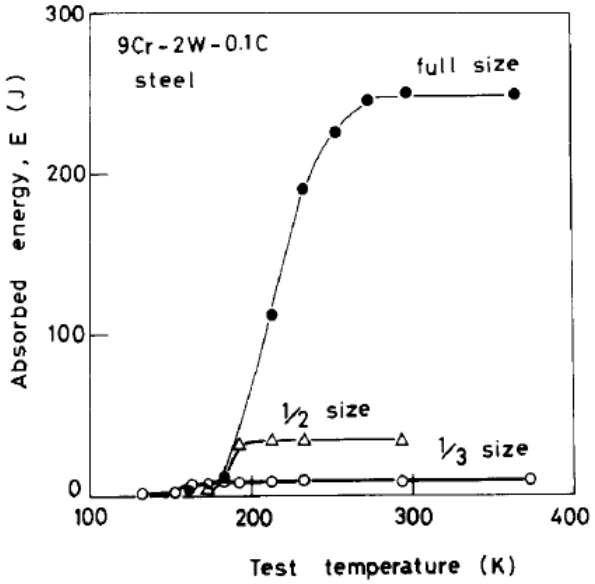

Figure 2.23 Absorbed energy of full-size, half-size, and one-third-size specimens of 9Cr-2W steel as a function of test temperature [55]

The best correlation of the USE of full-size and sub-size specimens was obtained by normalising the absorbed energy by nominal fracture area *Bb* and nominal fracture volume $(Bb)^{1.5}$, where *B* is the specimen width and *b* is the ligament size. Figures 2.23 and 2.24 show the datasets of the area and volume normalisation, respectively, for 9Cr-2W steel. No agreement in USE between the different specimen sizes was observed when using the area normalisation shown in Figure 23. The area normalised USE given by US*E/(Bb)* for the one-third-size specimens was about 10^6 J/m^2, which was significantly lower than that of the full-size specimens (3.1 x 10^6 J/m^2). Conversely, excellent agreement was attained through volume normalisation, as can be seen in Figure 2.24. The volume normalised USEs, given by US$E/(Bb)^{1.5}$, were about 3.5 x 10^8 J/m^3, 3.5 x 10^8J/m^3, and 3.4 x 10^8J/m^3 for the full size, half-size, and one-third-size specimens, respectively. Excellent agreement was also obtained when volume normalisation was applied to the dataset for 9Cr-1W and 9Cr-4W steels.

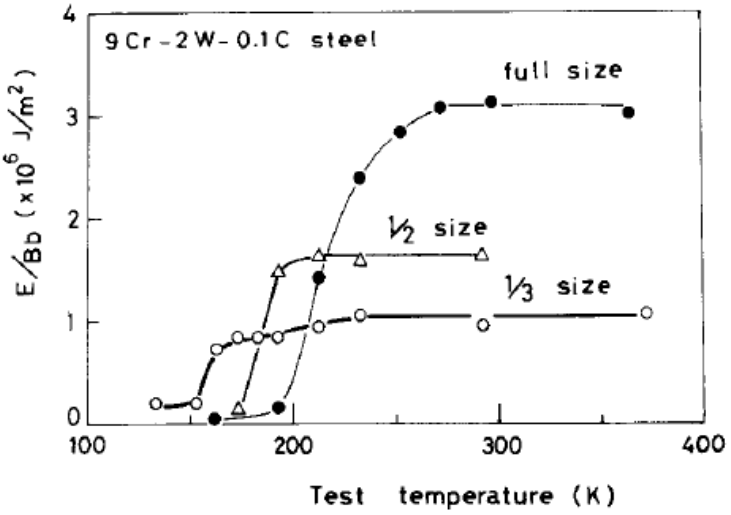

Figure 2.24 Area normalisation of the absorbed energy curves for the three different specimen sizes of 9Cr-2W steel [55]

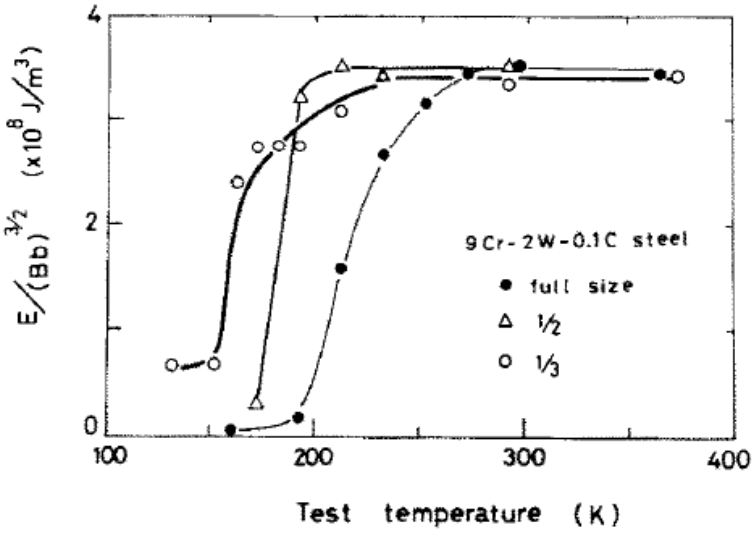

Figure 2.25 Volume normalisation of the absorbed energy curves for the three different sizes of 9Cr-2W steel [55]

The USE of the material studied by Abe *et al*' was high (245.2 J for the full-size specimen). The 1.5 power relationship predicted an excellent correlation in USE data between the full-size and sub-size specimens.

2.3.3.2. USE normalisation models with pre-crack effect

The methodology proposed by Kumar *et al.* [56] was applicable to pressure vessel weld materials in both un-irradiated and irradiated states with USEs in the intermediate region (100 J < USE < 200 J). The methodology used partitioning of the USE into two components: USE_p and ΔUSE (= USE – USE_p). USE_p is the absorbed energy for a specimen fatigue pre-cracked to half the width. The predicted value of the USE of full-size specimens was the sum of two terms [56]. The first term consists of the product of the normalised ΔUSE of the sub-size specimen and the full-size normalisation factor for ΔUSE, and the second term consists of the product of the normalised USE_p of the sub-size specimen and the fracture volume of the pre-cracked full-size specimen. The datasets collected for the full-size USE based on half-size and one-third-size showed that the predicted values were within approximately 10% of the measured values for both un-irradiated and irradiated materials.

The predicted value of full-size USE based on sub-size data was calculated by the following equation [56]:

$$USE^f = (\Delta USE)_n^s \times NF^f + (USE_p)_n^s \times NF_p^f \tag{2.8}$$

Superscripts f and s represent full- and sub-size specimens, respectively, and subscript n represents the normalised value [56]. In addition,

$$(\Delta USE)_n^s = (\Delta USE)^s / NF^s \tag{2.9}$$

$$(USE_p)_n^s = (USE_p)^s / FV_p^s \tag{2.10}$$

$$NF = Bb^2 / K_t L \tag{2.11}$$

$$FV_p = Bb_p^2 \tag{2.12}$$

$$K_t' = K_t Q \tag{2.13}$$

$$Q = 1 + \pi/2 - \theta/2 \tag{2.14}$$

$$K_t = \frac{2(b/R+1) - f(b/R+1)^{1/2}}{4(b/R+1)/g - 3f} \tag{2.15}$$

where

$$f = \frac{2(b/R+1)(b/R)^{1/2}}{(b/R+1)arctan(b/R)^{1/2} + (b/R)^{1/2}} \tag{2.16}$$

$$g = \frac{4(b/R)^{1/2}}{3\left((b/R)^{1/2}+(b/R-1)arctan(b/R)^{1/2}\right)} \quad (2.17)$$

and b_p is the ligament length below the pre-crack.

A similar methodology was proposed by Schubert *et al*. [57] to correlate the USE of full-size and sub-size Charpy specimens of a nuclear reactor pressure vessel plate material. The normalisation of USE was conducted with a normalisation factor involving the elastic stress concentration factor, the dimensions of the Charpy specimen, and the plastic constraint at the notch root. It was discovered that the normalised USE values did not change with specimen size.

Full-size and sub-size USEs were correlated more accurately by the advanced normalisation equation as follows:

$$(N) = Bb^2/K_t'L \quad (2.18)$$

where B is the specimen thickness, b is the specimen thickness under notch (ligament), K_t' is the modified stress concentration factor = K_tQ and L is the specimen span [57].

2.3.3.3. Fracture process zone model

A fracture process zone (FPZ) model was developed by Manahan [58] to correlate impact energies between sub-size and full-size specimens. It was proposed that a fracture process volume normalisation can be applied directly to the sub-size specimen data if the stress fields in the miniature and conventional specimens are similar.

It has been found that the energy required to initiate the crack (approximated as the pre-maximum load energy) at the root of the notch was about one-third of the total

energy in both the CVN and miniaturized (MCVN) specimens if the stress field in the MCVN specimen matches closely that of the conventional specimen. This initiation energy proportionality did not depend on the ductility of the material. Thus, the pre-maximum load energy was proportional to the total energy absorbed by the specimen, and FEM results of the plastic zone size prior to crack initiation can be used to correct the fracture volume to account for differing ductility. This discovery is crucial, as it precludes the need for performing FEM simulation of crack growth. Since the ratio of the maximum load to the yield load is proportional to the plastic zone size prior to crack initiation, this ratio can be used to adjust the calculation of the fracture process volume. This approach is appealing because the characteristic loads can be measured using an instrumented striker, as discussed below.

When the stress fields are similar, the ratio of the CVN USE to the fracture process volume (FPV) is proportional to the similar ratio for the MCVN specimens. In particular:

$$\frac{USE_{CVN}}{FPV_{CVN}} \propto \frac{USE_{MCVN}}{FPVLINE_{MCVN}} \tag{2.19}$$

The constant of proportionality, which is a function of ductility, represents the degree to which the MCVN stress field simulates the CVN stress field. Therefore, Eqn (2.19) may be written as follows:

$$\frac{USE_{CVN}}{FPV_{CVN}} = (PZCF)\frac{USE_{MCVN}}{FPVLINE_{MCVN}} \tag{2.20}$$

where PZCF is the plastic zone correction factor.

Grubb and Manahan [59] applied the FPZ model to investigate the toughness of nickel alloy 22 as a function of temperature and specimen thickness. A comparison of the experimental results with predictions of the FPZ model and Wallin's model is shown in Figure 2.22. For sub-size specimens, the USE increased according to the B^2b. The plastic zone correction factor of Eqn. (2.19) can be taken to be unity for this

material. This model fitted the data for sample thicknesses up to 8 mm very well as shown in Figure 2.25, but beyond 8 mm, appears to change linearly.

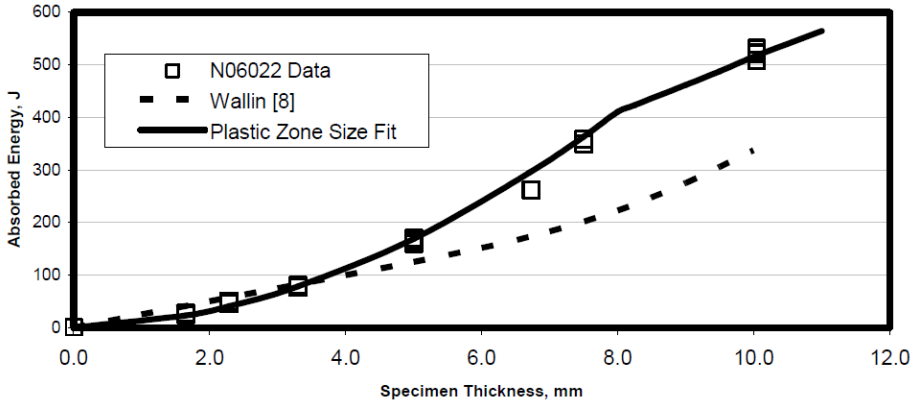

Figure 2.26 Impact energy vs. specimen thickness for N06022 [59]

The proposed FPZ model requires the load-time curve obtained from miniature CVN specimens by a modified instrumented CVN machine, and the model has not been validated for varying materials with a wide ductility range.

2.3.3.4. Hyperbolic-tangent model

Wallin investigated the effect of CVN specimen thickness on USE [60]. Eighty-eight datasets, including the standard 10mm-thick Charpy-V upper shelf data and data for various sub-size (*B* varying 2.5–9 mm) and/or over-size (*B*=20 mm) specimens were used in that study. Many materials had data that was obtained from different orientations (T-L, T-S, L-T, and L-S). Structural steels with yield stresses in the range of 244–975 MPa were mainly used. The database also contained results for three stainless steels, two Al–bronze alloys, and one Al specimen. The data was applicable to both ASTM and ISO impact strikers. The Charpy-V USEs covered a range from 20 to 300 J.

The energy per ligament area for the non-standard specimens ($KV_B/(bB)$) plotted against the standard specimen energy ($KV_{10}/0.8$) is shown in Figure 2.26. A linear relationship between $KV_B/(bB)$ and $KV_{10}/0.8$ can be observed for samples of roughly

KV_{10}/0.8<120 J/cm^2. When KV_{10}/0.8≥120J/cm^2, the sub-size CVN specimens absorbed less energy per area than the standard size CVN specimens.

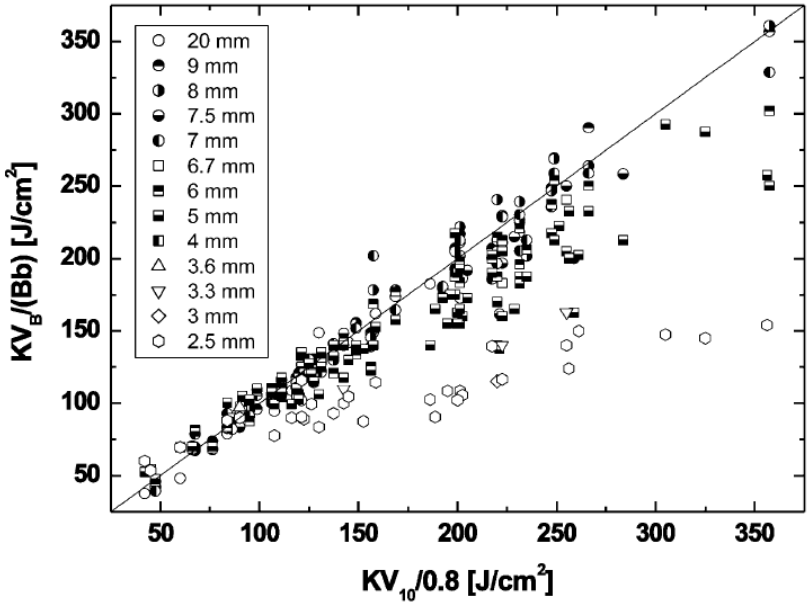

Figure 2.27 Database used in [60], comparing proportional sub-size impact energy with standard and over-size impact energy.

Figure 2.27 illustrates the reason for the above observation, as suggested in [14]. When a CVN specimen undergoes ductile tearing fracture, the fracture surface is made up of 'flat' fracture (middle part) and shear fracture (sides) regions. As the crack starts to grow, the shear regions (lips) begin to develop. Their size increases with crack growth and plateau towards a thickness that is dependent on the tearing resistance of the material. This shear lip development is largely independent of specimen thickness, which means that the proportion of shear lips on the fracture surface increases as the specimen size is reduced. The entire fracture surface shows shear fracture if the thickness is below a critical thickness. Since the energy absorbed in the fracture process is different for flat fracture and shear fracture, reducing the specimen thickness causes a transformation from a flat fracture description to a shear fracture description.

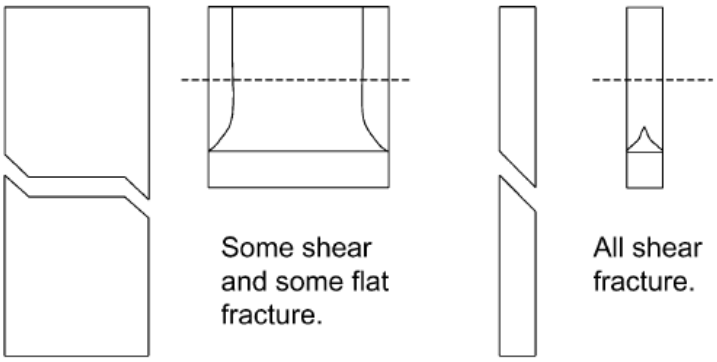

Figure 2.28 Schematic differences in fracture appearance of standard size and sub-size Charpy-V specimens [60]

The proportion of shear lips is controlled by two main parameters: specimen thickness and the material's ductile tearing resistance. It is suggested that KV_{10}/B is the logical parameter to describe the proportion of shear lips since tearing resistance can be correlated to the standard CVN USE. The yield strength of the material has only a very minor influence on development of the shear lip.

Figure 2.28 plots, the ratio of the energy per ligament area for the non-standard specimens and the standard specimen (KV_Bx10)/(KV_{10}xB), as a function of KV_{10}/B for all the data corresponding to steels. For small values of the parameter (KV_{10}/B), the proportional energy absorption of sub-size specimens is the same as that of full-size specimens. With increasing values of parameter KV_{10}/B, proportional energy absorption starts to decrease and seems to level out to a value close to half that of a full-size specimen.

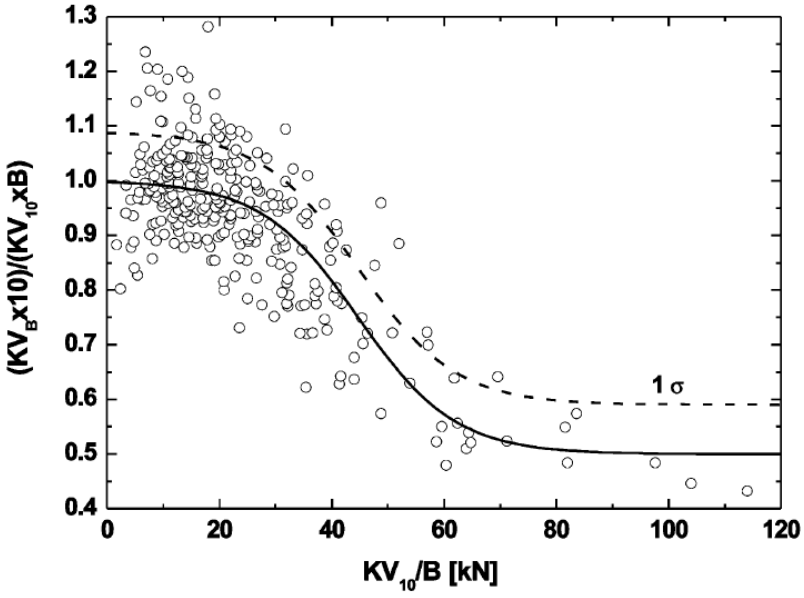

Figure 2.29 All results fitted with a hyperbolic-tangent equation (solid line). The dashed line corresponds to 1σ conservation [60]

All the data are fitted by a hyperbolic-tangent equation:

$$\frac{KV_B \times 10}{KV_{10} \times B} = 1 - \frac{0.5exp\left(\frac{2(KV_{10}/B - 44.7)}{17.3}\right)}{1 + exp\left(\frac{2(KV_{10}/B - 44.7)}{17.3}\right)} \tag{2.21}$$

Equation 2.21 is only valid for steels and 2.5 mm ≤ B ≤ 9 mm, and it needs to be inverted if it is used to predict full-size USE from a sub-size USE. This cannot be performed analytically in a closed form, but KV_{10} can be solved by the numerical method.

2.3.3.5. USE-B relationship in high toughness materials

An early work by Fergusson [61] on the dependence of toughness on sample geometry concluded that the USE was linearly related to sample thickness. However, later experiments conducted by Fergusson *et al.* [62] indicated otherwise. The USE in the ductile region decreased with reducing sample thickness, but the energy reduction was not solely related to thickness. It has been shown that a normalisation of the USE based on the fracture area did not generate equivalent

values for different thicknesses. Instead, the USE per unit fracture area tended to decrease with decreasing Charpy sample thickness [61].

Ferguson *et al.* conducted a series of longitudinal CVN impact tests on niobium-treated low-carbon steel plates using full-thickness, half-thickness, one-third-thickness and one-quarter-thickness specimens. Composite CVN samples were fabricated by riveting either one-third-thickness or one-quarter-thickness bars together to produce three-ply or four-ply laminated samples. The laminated samples were used to investigate the effect of splits (i.e. laminar defects or planes of low toughness in the microstructure).

The toughness data for a plate finish-rolled at 995°C is depicted in Figure 2.29. It was found that the ratios of the USE of the sub-size and conventional, full-size CVN samples were not equal to the ratios of cross-sectional areas. For instance, the USE at 93°C for the quarter thickness samples (24 J) was lower than one fourth of the USE for the full-size sample (183 J), as shown in Figure 2.29. However, it was also found that the USE of the composite samples was linearly related to the USE of their individual plies [61]. That is, the USE of the three-ply sample was approximately three times that of the one-third-thickness sample; the four-ply sample was four times that of the quarter thickness sample. Figure 2.29 also shows that the shapes of the curves for the laminated samples and their individual sub-size counterparts, e.g. four-ply and quarter thickness was similar. As the number of plies decreased, or the sub-size thickness increased, the slope of the transition region increased.

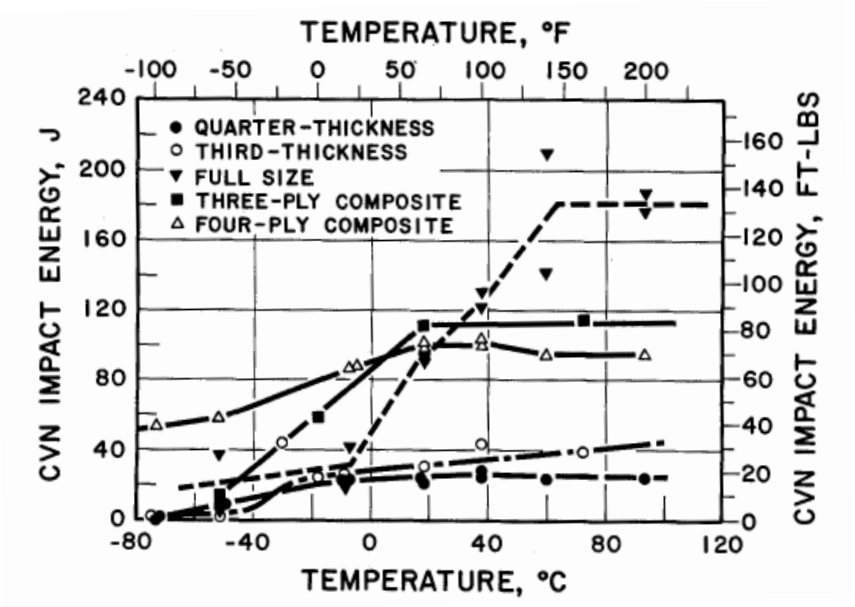

Figure 2.30 The effect of CVN sample thickness and laminated sample configuration on the impact energy of high-strength, low-alloy (HSLA) steel plate [61]

Figure 2.30 illustrates the relationship between the force needed to extend a crack and the thickness of the specimen **[61]**. This graph shows three fracture regions: (1) shear fracture, (2) mixed fracture (flat fracture plus shear lips), and (3) flat fracture. Below a critical thickness, the fracture is shear in nature and the toughness depends on the volume of material that undergoes deformation. As the thickness increases to the critical value, the volume of material that deforms prior to fracture increases, and the toughness as measured by crack resistance force G_c increases. For thicknesses greater than the critical thickness, strain localisation occurring at the crack tip reduces the effect of a volumetric deformation; the deformed zone in the plane of the fracture lips becomes predominant. In this regime, the toughness decreases with increasing thickness, as the stress state at the crack tip shifts from plane stress (shear fracture) to plane strain (flat fracture). For still larger thicknesses, plane strain dominates, and the crack resistance force converges to toughness level G_c.

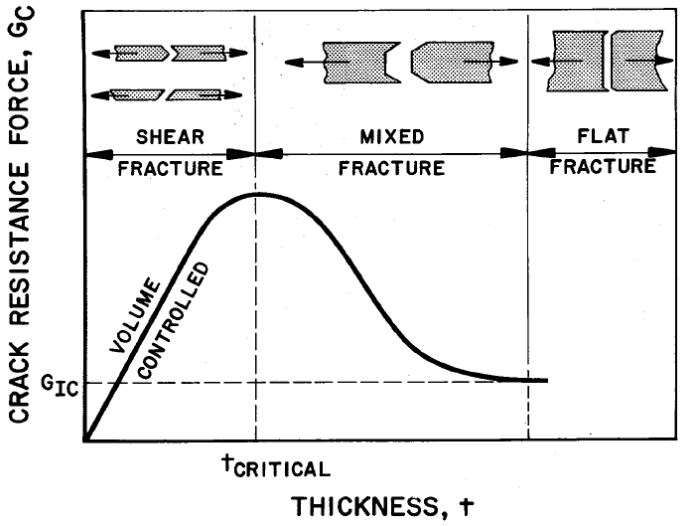

Figure 2.31 Schematic diagram showing the effect of sample thickness on toughness [61].

In the ductile region, the fracture mode can be changed from mixed mode to shear if the specimen thickness is reduced. Thus, the normalised impact energy (USE/cross-sectional area) can either fall or rise with a reduction in specimen thickness. Once the thickness is lower than the critical thickness (t_c), any further thickness reduction leads to further lowering of the normalised impact energy.

The USEs of the sub-size and full-size CVN specimens shown in Figure 2.29 were collected and plotted against the specimen thickness (Figure 2.31). It was found that the best-fit relationship was USE $= 7.99B^{1.36}$, which is closer to the 1.5 power relationship than the linear relationship. Here, B is the specimen thickness.

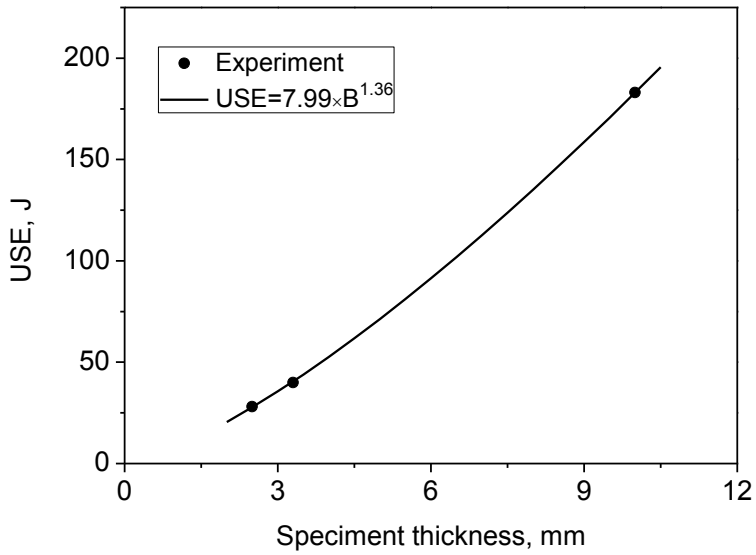

Figure 2.32 USE shown in Figure 2.29 as a function of specimen thickness

Towers carried out experimental work to assess the effect of specimen thickness on the results of CVN tests for metals behaving in a fully ductile manner [14].

The USE was obtained by using an ASTM E23-82 striker on BS 1501-281 and BS 1501-161 steels, 316 S16 stainless steel, BS 4360 Grade 50E structural steel and 5.5% nickel steel. The results are shown in Figure 2-32. The data obtained from tests conducted at room temperature with a BS 131: Part 2: 1972 striker on two Al-bronze specimens, 310 S24 stainless steel, and X56 line pipe steel, is shown in Figure 2.33. This figure also includes the results of tests on 316 S16 stainless steel, BS 4360 Grade 50E structural steel, and 5.5 % nickel steel.

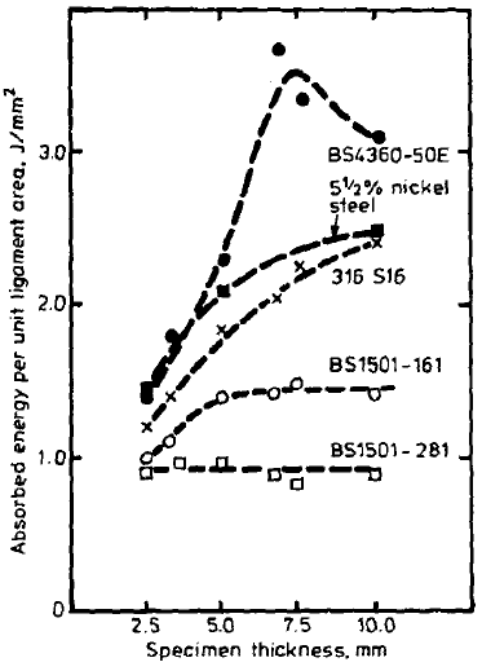

Figure 2.33 Effect of specimen thickness on mean USE per unit ligament area when using ASTM E23-82 striker [14]

The results for laminated test pieces on the BS 4360 Grade 50E steel were included in Figures 2.32 and 2.33 by adding the results from those test pieces to the results from specimens with thicknesses equal to the thickness of each ply in the laminate, (*e.g.* the absorbed energy per unit ligament area for a three-ply laminate is taken to be the average result of three tests on 3.3mm thickness specimens). Since the glue between the plies of the laminate is relatively weak compared with the steel sample in each ply, this procedure is considered to be appropriate.

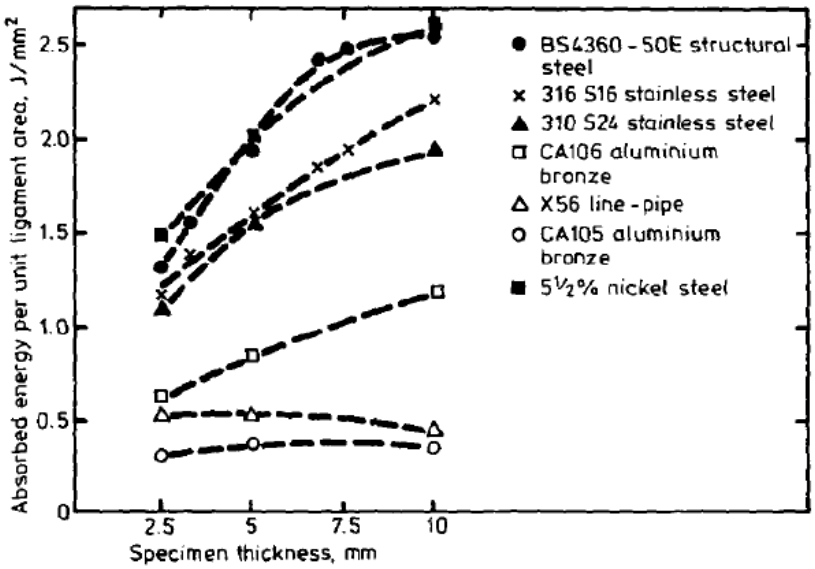

Figure 2.34 Effect of specimen thickness on mean USE per unit ligament area when using BS 131: Part 2: 1972 striker [14]

For relatively high absorbed energies (above 1 J/mm^2), thin specimens absorb less energy per unit fracture area than thick ones (Figures 2.32 and 2.33). At low absorbed energy levels, however, there is little evidence of an effect of specimen thickness. If anything, the evidence indicates that thinner specimens absorb more energy per unit ligament area.

Due to the fact that an increased fraction of the fracture area consisted of a shear lip, USE per unit ligament area decreased with decreasing thickness. This concept applied to laminated specimens of very thin sheets (each section of the laminate usually being less than 2.5 mm in thickness), for which the absorbed energy was mostly the energy absorbed in the shear lip(s) of each component section. When this occurred, the absorbed energy per unit ligament area was found to be linearly proportional to the thickness of the individual sections.

Nevertheless, as observed experimentally in this study, if the shear lips did not develop fully, the effect of specimen size on absorbed energy was less pronounced. If shear lips were non-existent, such as at very low USEs, the increased constraint presented in thicker specimens instead resulted in lower absorbed energies per unit ligament area. This can be an explanation for the apparent trend of lower energies

per unit area being obtained in full-size specimens compared to sub-size specimens for the two materials with low USE, CA 105 and X56, in Figure 2.33. This effect is also illustrated in Figure 2.34.

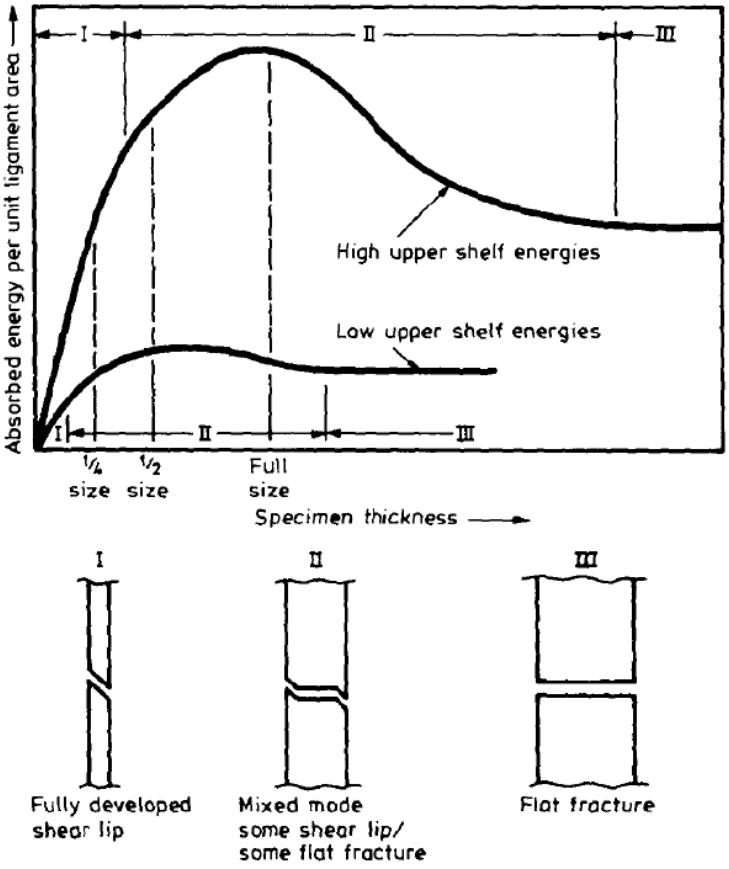

Figure 2.35 Effect of specimen thickness on USE per unit ligament [14]

The data considered in Towers's observation was extracted from Figure 2.33. The USE and specimen thickness data were fitted using power relationships. Results of the regression are provided in Table 2.1. For high-toughness materials, (USE >90 J), such as for 5.5% nickel steel, 316 S16 stainless steel, 310 S24 stainless steel, and CA106 Al–bronze, the power coefficients are close to 1.5 (between 1.4 and 1.45). For low-toughness materials such as the X56 line pipe used in these experiments and CA105 Al–bronze, the relationship is closer to linear or sub-linear behaviour.

Table 2.1 Collected data from Towers's work and regression results

Steel	Relationship	USE of the full-size specimen (J)
5.5% nickel steel	USE=8.375×$B^{1.402}$	210
316 S16 stainless steel	USE=6.412×$B^{1.438}$	177
310 S24 stainless steel	USE=6.093×$B^{1.414}$	155
CA106 aluminium bronze	USE=3.286×$B^{1.448}$	95
X56 line pipe	USE=4.726×$B^{0.862}$	34
CA105 aluminium bronze	USE=2.467×$B^{1.038}$	26

The well-known BTCM for fracture propagation and arrest, which was developed based on the results of experiments with traditional ("vintage") steels with low strength and low toughness (below 100 J), analyses the propagation or arrest by two curves: 1) crack velocity curve and 2) gas decompression curve. The crack velocity curve is a function of the Charpy absorbed energy normalized with respect to the surface area (CVN energy factor R=Cv/Ac). Here Cv is the Charpy V-notch absorbed energy and Ac is the fracture area. A linear Charpy energy/specimen thickness relationship is adopted in the BTCM. Modern low-carbon, low-sulphur steels have increased strength and toughness (> 100 J). It was suggested by Takahashi *et al* that the deviation from the predicted arrest energy in modern high strength steel was due to changes in steel properties such as separation and increased shelf energy [49].

It was also pointed out by Takahashi *et al* [49] that the effect of thickness on fracture toughness is one of the factors that cause the observed crack velocity to deviate from the predicted crack velocity in the BTCM. The dependence of the Charpy absorbed energy on specimen thickness is shown in Figure 2.35. Three types of line pipe steels, X80 TMCP, X70 conventional rolling (CR) and X70 QT, were compared. The Charpy absorbed energy was not seen to increase linearly with the specimen thickness *t*, but a non-linear relationship ($t^{1.5}$) was observed instead. It was concluded

that fracture toughness expressed as Charpy absorbed energy per unit area is not appropriate to estimate the toughness of heavy wall thickness pipe. A clear 1.5 power relationship between the CVN absorbed energy and specimen thickness have been found in Takahashi *et al'*s work.

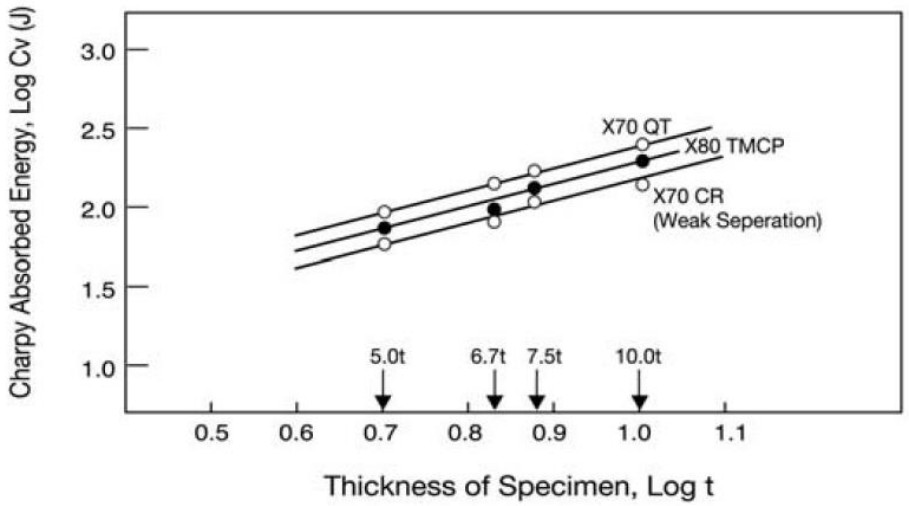

Figure 2.36 Effect of specimen thickness on upper shelf energy per unit ligament [49]

2.3.3.6. Summary

Ferguson [62] conducted a series of longitudinal Charpy tests on HSLA steel plates finish-rolled at 995°C, using full, one-half, one-third, and one-quarter specimen thicknesses. The absorbed energy of the full-size specimen was 183 J, and a no-linear power relationship of 1.36 was obtained between the varying specimen thicknesses. Towers [14] carried out experiments to assess the specimen thickness effect of various materials. A power relationship of 1.4 was observed for nickel, stainless steel, Al–bronze, and line pipe steel with full-size C*v* greater than 95 J. Studies by Corwin *et al* .[63], Abe *et al* .[55], and Louden *et al.* [64] also found an exponential relationship between C*v* and specimen thickness. Almost all the studies showed a non-linear relationship between specimen thicknesses and absorb energy for high toughness material

- Several normalisation methodologies have been developed to correlate the USE of full- and sub-size specimens, as summarized below:

Table 2.2 Summary of normalisation methodologies

Paper	USE- thickness(B) Model	Limitation & Observation
Corwin et al (1984)	Normalization by (Bb)1.5	Woks well for relatively high toughness materials (>~150J)
Louden et al (1988)	Normalization by Bb2/LK	Gives linear relationship between USE and B; applicable to relatively low toughness materials (<~150J claimed)
Kurishita et al (1994)	Normalization by (Bb)1.5	Normalized USE not constant for non-standard sub-size CVN
Kumar et al (1995 Schubert et al (1995)	$(\mathrm{N}) = \mathrm{Bb}^2/\mathrm{K}_t'\mathrm{L}$	Effect of pre-cracking considered
Manahan et al (1997)	$\frac{USE_{CVN}}{FPV_{CVN}} = (PZCF)\frac{USE_{MCVN}}{FPVLINE_{MCVN}}$	Required load-time curve obtained from miniature CVN specimens
Wallin et al (2001)	$\frac{KV_B \times 10}{KV_{10} \times B}$ $= 1 - \frac{0.5exp\left(\frac{2(KV_{10}/B - 44.7)}{17.3}\right)}{1 + exp\left(\frac{2(KV_{10}/B - 44.7)}{17.3}\right)}$	USE-B relationships for both low and high toughness plate steels. Not yet validated for high toughness line-

		pipe steels
Grubb et al (2007)	Normalization by B2b	Works well for Nickel alloy 22

- The area normalisation factor (Bb), namely the linear relationship between USE and B, works well for low toughness materials.

- (USE vs B) ~1.5 power relationships have been observed in many studies for high toughness materials. CVN tests on X70 and X80 line-pipe steels have confirmed the validity of 1.5 power relationship:

Table 2.3 Summary of power relationships between USE and B

Publication	**Material and USE- thickness(B) Relationship**		**USE of full-size specimen (J)**
Ferguson et al (1978)	HSL plate steel finish rolled at 995°C	$USE = 7.99B^{1.36}$	183
Towers (1986)	5.5% nickel steel	$USE=8.375\times B^{1.402}$	209.8
	316 S16 stainless steel	$USE=6.412\times B^{1.438}$	176.5
	310 S24 stainless steel	$USE=6.093\times B^{1.414}$	155.1
	CA106 aluminium bronze	$USE=3.286\times B^{1.448}$	94.5
	X56 line-pipe	$USE=4.726\times B^{0.862}$	33.6
	CA105 aluminium bronze	$USE=2.467\times B^{1.038}$	25.8
Takahashi et al (2009)	A clear 1.5 power relationship between the CVN absorbed energy and specimen thickness has been observed for high strength line-pipe steels (X70 and X80)		-

- Different USE vs B relationships have been developed to accommodate the change of the proportionality of shear lips.

- A new model is necessary to be developed to cover USE-B relationship for both low and high toughness line-pipe steels if the existing models cannot be applied.

2.4. Numerical fracture simulation

2.4.1. Fracture model

Two types of approaches have been widely used to describe fracture [65]. In the global approach, it is assumed that fracture resistance can be measured in terms of a single parameter, such as mode-I critical stress intensity factor (K_{IC}), *R* curve, *J*-integral (J_{IC}) and crack tip opening displacement. In the local approach, the modelling of fracture toughness is based on the local stress and/or strain fields at the front of the crack tip. The cohesive zone model is also used in some fracture simulations.

The global approach is useful, but it has a number of limitations, such as the absence of any prediction of size effects observed in brittle fracture and the lack of application in non-isothermal loading conditions. Its limitations were the driving force behind the development of the 'local approach to fracture' (LAF), which started in the 1980s. The LAF is based on local fracture criteria usually established from tests on volume elements, particularly notched specimens, to model fracture toughness. It requires that two conditions be fulfilled: (i) micro-mechanistically based models must be established and (ii) the crack tip stress/strain field must be modelled accurately [65].

The local fracture criterion is based on the elastic–plastic stress/strain history calculated at the point where fracture takes place in conjunction with the use of a micro-mechanistically based model for a given physical fracture process [66].

Information required for the application of local criteria is available through the development of finite element calculations.

It is well known that at moderately low temperatures, brittle fracture occurs when local critical fracture stress σ_f is exceeded by normal stress σ_{yy} ahead of the notch tip. The criterion for brittle fracture is simply that

$$\sigma_{yy} \geq \sigma_f \tag{2.22}$$

Engineering metals and alloys contain inclusions and second-phase particles at which, in the course of plastic deformation by either debonding or cracking, microvoids nucleate and grow until localised internal necking of the intervoid matrix occurs. The Gurson–Tvergaard–Needleman (GTN) model has recently become increasingly popular for simulating plastic flow localisation and ductile fracture problems.

2.4.2. Modelling of Charpy V-notch test

Eberle *et al.* [67] conducted both 2D and 3D explicit dynamic finite element analysis combined with the rate-dependent Gurson damage model to simulate Charpy tests. Not only did the calculated force vs. deflection curves represent good experimental curves, but the shape of the crack front calculated by a 3D FE analysis was also in close agreement with the measured crack front. The explicit dynamic simulations showed that it was possible to analyse the Charpy test to a high degree of confidence using damage parameters taken from quasi-static tests. Thus, the transfer of the parameters via numerical analysis to quasi-statically-loaded fracture mechanics specimens was possible.

Fumiyoshi *et al.* [68] studied the local approach to interpreting Charpy test results. The local approach used the Weibull stress, σ_w, as a driving force of fracture of ferritic materials. Instrumented Charpy tests and fracture toughness tests were performed in the lower-transition range for structural steels in the 490 and 780 MPa

strength classes. Stress fields were addressed by 3D-FEM, considering the strain rate effect and temperature increase during dynamic loading. It was shown that the critical Weibull stress at brittle fracture initiation was almost independent of the loading rate, which enabled the Charpy results to be transferred to the fracture toughness of the material.

Mudry and Sturel determined the micromechanical parameters of a cleavage model (Beremin model shown in Figure 2.36) from Charpy tests [69]. The properties of a simulated microstructure, representative of the most brittle area of the heat affected zone, were studied.

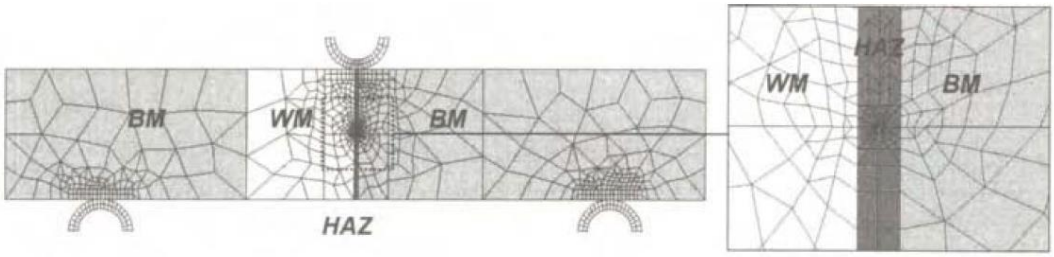

Figure 2.37 Mesh representative of a specimen sampled in the welded joint

The ductile–brittle transition of a weld was investigated with a full 3D transient analysis of Charpy impact specimens, as shown in Figure 2.37 [70]. The Gurson model was used to represent the ductile fracture. The material response was characterised by an elastic–viscoplastic constitutive relationship for a porous plastic solid, with adiabatic heating due to plastic dissipation and the resulting thermal softening accounted for. The onset of cleavage was taken to occur when a critical value of the maximum principal stress was attained. The mesh of accounting for the 3D Charpy geometry is illustrated in Figure 2.37.

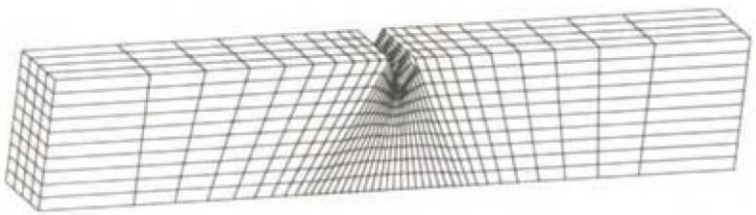

Figure 2.38 Charpy specimen and finite element half-thickness mesh [70]

Rossoll *et al.* [71] simulated a non-empirical relationship between CVN energy and fracture toughness K_{Ic} on the lower shelf of fracture toughness and on the onset of the ductile-to-brittle transition of a low-alloy structural steel. The methodology they used was based on the local approach. Brittle cleavage fracture was modelled in terms of the Beremin model, whereas the ductile crack advance preceding cleavage in the transition region was accounted for with the GTN model. Temperature and rate dependence of flow stress of the material were determined from tensile and compressive tests. Finite element analysis was used for modelling, and special consideration was taken into account to handle the dynamic effects in the Charpy impact test. On the lower shelf, fracture toughness could be predicted from the Charpy impact test results. In the transition region, the parameters of the Beremin model were found to deviate from those established on the lower shelf. Detailed fractographic investigations showed that the fractographic and microstructural features of regions of cleavage fracture initiation change with temperature.

Tanguy *et al*. [72] conducted a numerical simulation of the CVN test in the ductile–brittle transition regime. The material (A508 steel) was described using models to represent (i) tile viscoplastic temperature-dependent behaviour of the undamaged materials, (ii) crack initiation and growth caused by ductile damage, and (iii) brittle cleavage fracture. The ductile damage model was based on the Gurson-type model modified to account for viscoplasticity and temperature changes, and brittle fracture was described using the Beremin model. Finite element calculations were carried out to simulate ductile crack growth in the specimens. These calculations were post-processed to determine the probability of failure as a function of tile Charpy fracture energy for temperatures between -165°C and 0°C.

Poussard *et al.* [73] carried out numerical investigations to investigate the transferability of data obtained from un-irradiated, sub-size Charpy tests to full-size, conventional Charpy-V tests. Detailed finite element analysis was undertaken to investigate the influence of a number of factors that might govern the behaviour of the dynamic tests, both on the lower shelf for brittle failure and on the upper shelf for ductile tearing. It was concluded that only a full 3D finite element simulation allows

the retrieval of the experimentally observed global behaviour of the specimens. Quasi-static finite element simulations led to satisfactory results if the effect of strain rate on the true stress/strain curve was taken into account. The stress triaxiality ratio of the Charpy-V specimen (1.6) was found to be higher than that of the sub-size Charpy specimen (1.3). This finding partly explains the observed transition shift between the two geometries. The transferability of the Beremin cleavage criterion from sub-size Charpy to compact tension specimen was investigated at low temperatures. On the upper shelf, ductile tearing at 0°C was computed using the Gurson-type damage model. It has been demonstrated that this type of approach can successfully predict the behaviour of the dynamic tests provided that strain rate effects were accounted for. It has also been shown that adiabatic heating has little influence on the global mechanical behaviour or the crack propagation of the upper shelf. However, it might have to be considered at lower temperatures in the ductile–brittle transition region.

Oh *et al.* [74] developed a phenomenological model of ductile fracture for API X65 steel using the GTN model. Experimental tests and finite element (FE) damage simulations using the GTN model were performed on smooth and notched tensile bars, from which the parameters in the GTN model were calibrated. Comparisons of the experimental data of pre-strained, notched tensile, and fracture toughness tests with FE damage analysis showed good agreement, confirming the validity of the calibrated parameters. The developed GTN model was used to predict the pre-strain effect on deformation and fracture, and the results were compared with the experimental data.

Nonlinear dynamic finite element analysis (FEA) was conducted by Yu and Jeong [75] to simulate the fracture of un-notched Charpy steel specimens under pendulum impact loading by a dedicated oversized, non-standard bulk fracture Charpy machine (BFCM). To predict material failure, a phenomenological stress triaxiality-dependent fracture initiation criterion and a fracture evolution law in the form of strain softening were incorporated into the constitutive relationships. The results of the energy of the BFCM impact obtained from the FEA simulations compared favourably with the corresponding experimental data. In particular, the FEA

predicted accurately the correlations of the impact energy of the BFCM with such factors as specimen geometry, impactor tup width, and material type. The analysis showed that a specimen's progressive deterioration through the thickness dimension displays a range of shear to ductile fracture modes, demonstrating the necessity of applying a stress-state-dependent fracture initiation criterion. Modelling the strain-softening behaviour helped capture the residual load-carrying capability of the ductile metal or alloy beyond the onset of damage.

A coupled brittle/ductile fracture local approach model was developed in Ref. [76] to predict either Charpy energy or fracture toughness and to investigate conditions for correlations between them. A modification to the Beremin model was introduced to assess the failure of individual elements and to make the model compatible with the Gurson model for implementation as a user subroutine for the ABAQUS program. A probabilistic-based fracture criterion was introduced to monitor the damage within individual elements by either cleavage or ductile tearing. The fracture toughness and Charpy energy of a nuclear industry steel, BPL A508, were determined for the transition temperature range using finite element analysis with 3D solid elements for both the standard 25mm SE(B) three-point bend specimen and the CVN specimen. Critical fracture stress values in the modified Beremin model for brittle fracture and damage parameter values for ductile fracture were calibrated from experimental fracture toughness data. These same critical values were then used in the analysis of the Charpy specimens, including allowance for strain rate effects. Good agreement was observed between the predicted and experimental energy absorption values.

Koppenhoefer and Dodds [77] used plane strain, finite element analysis to model ductile crack extension in pre-cracked Charpy specimens subjected to static and impact loading. The GTN model for voided materials described the degradation of material stress capacity. Fixed-size, computational cell elements defined over a thin layer along the crack plane provided an explicit length scale for the damage process continuum. Outside of this layer, the material remained undamaged by void growth, which was consistent with metallurgical observations. The finite strain constitutive models included the effects of high strain rates on the flow properties of the material. Parametric studies focusing on numerically generated *R*-curves quantified the

relative influence of impact velocity, material strain rate sensitivity, and properties of the computational cells (thickness and initial cell porosity). In all of the cases, impact loading elevated the *R*-curve significantly by increasing the amount of background plasticity. The strong effects of impact loading on the driving force for cleavage fracture were illustrated through the evolution of the Weibull stress. The analysis suggested a negligible, additional effect of tearing on the Weibull stress under impact loading. Validation of the computational cell approach to predict loading rate effects on *R*-curves was accomplished by comparing the static and impact experimental sets of *R*-curves of three different steels.

Tanguy *et al.* [78] developed a FE simulation of the Charpy test to model the ductile-to-brittle transition curve of a pressure vessel steel, as shown in Figure 2.38. The simulation included a detailed description of the viscoplastic deformation of the material over a wide temperature range. Ductile behaviour was modelled using the Gurson-type model, and the Beremin model was used to describe brittle fracture. The Charpy test was simulated using full 3D mesh and accounting for adiabatic heating and contact between the specimen, the striker, and the anvil. The developed model was well suited to represent ductile tearing. Using brittle failure parameters identified below -150°C, it was possible to represent the transition curve up to -80°C, assuming that Beremin stress parameter σ_u was independent of temperature. Above this temperature, a temperature-dependent Beremin stress parameter, σ_u, must be used to simulate the transition curve correctly, after which quasi-static and dynamic tests can be modelled consistently.

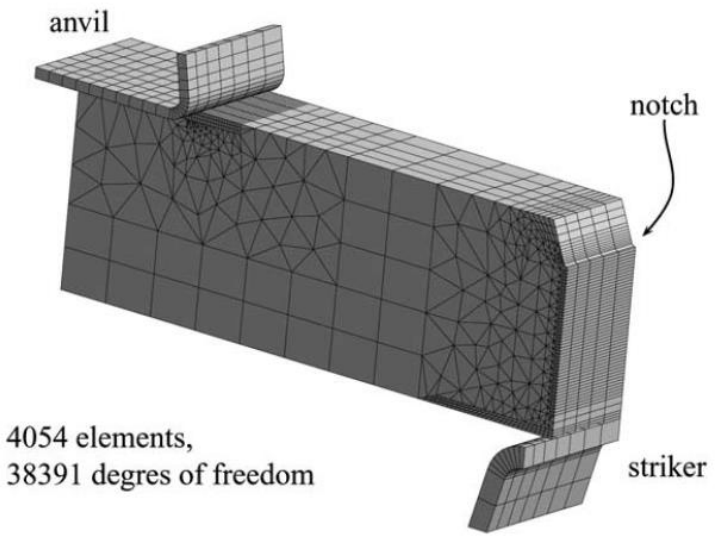

Figure 2.39 Charpy specimen and finite element mesh of half of the thickness [70]

Dynamic FEM of the fracture behaviour of fatigue pre-cracked Charpy specimens was performed in Ref. [79] to determine the effect of single variable changes in ligament size, width, span, and thickness on USE. A tensile fracture/strain-based method for modelling crack initiation and propagation was used. It was found that the USE of pre-cracked specimens is proportional to b^n, where b is the ligament size and n is a factor that varies from about 1.6 for sub-size specimens to 1.9 for full-size specimens. The USE was found to be proportional to $(\text{width})^{2.5}$. The dependence on span was found to be nonlinear, and the dependence on thickness was found to be linear for all cases studied. Some of the data from the FEM analysis were compared with experimental data and were found to be in reasonable agreement.

Thibaux *et al.* [80] performed instrumented Charpy tests and notched tensile tests on an X70 material. The same tests were also simulated using the finite element method and the GTN damage model. The combination of supplementary experimental information coming from the instrumentation of the Charpy test and finite element simulations delivered a different insight about the test. It was observed that the crack did not break the sample into two parts in the ductile mode. After 6–7 mm of propagation, the crack deviated and stopped. The propagation stopped when the crack met the part of the sample that became wider due to bending. FE simulations proved that it resulted in a quasi-constant force during a displacement of the hammer

of almost 10 mm. The consequence was that more than 25% of the energy was dissipated in a different fracture mode at the end of the test. FE simulations also proved that damage was already occurring at the maximum of the load, but the damage had almost no influence on the load for two-thirds of the displacement at the maximum. In the investigated steel, it meant that more than 27J, as often mentioned in standards for avoiding brittle failure, were dissipated by plastic bending before the initiation of the crack. From the findings of this study, one could conclude that the results of the Charpy test are very sensitive to crack initiation and that only a limited part of the test is meaningful for describing crack propagation. Therefore, it is questionable whether the Charpy test can be adapted to predict the crack arrest capacity of steels with high crack-initiation energy.

Koppenhoefer and Dodds [81] investigated the effects of specimen size and loading rate on brittle fracture of ferritic steels tested in the ductile-to-brittle transition region for the application of pre-cracked Charpy specimens. This investigation used 3D, nonlinear, FE analysis to assess crack-front stress triaxiality in quasi-static and impact-loaded pre-cracked CVN specimens, with and without side grooves. Crack front conditions were characterised in terms of Weibull stress, which reflects the statistical effects on brittle fracture. These 3D computations indicated that a less strict size/deformation limit, relative to the limits indicated by previous plane–strain analysis, was needed to maintain small-scale yielding conditions at fracture under quasi-static and impact-loading conditions. For impact toughness values that violated these size/deformation limits, a toughness scaling methodology was described to remove the effects of constraint loss. The new scaling model also enabled the prediction of the distribution of quasi-static fracture toughness values from a measured distribution of impact toughness values (and vice versa). This procedure was applied to experimental data obtained from a Cr-Ni-Mo-V pressure vessel steel, and it accurately predicted quasi-static fracture toughness values in specimens from impact-loaded, pre-cracked CVN specimens. These 3D analyses also yielded η-total values for use in impact testing to infer thickness average and mid-thickness J-values from measured work quantities.

Tanguy *et al.* [82] developed a constitutive model that integrated anisotropic behaviour and ductile damage for an X100 pipeline steel. The model was based on a set of experiments on various smooth, notched, and cracked specimens and on a careful fractographic examination of the damage mechanisms. The model was based on an extension of the GTN model, which included plastic anisotropy. Provided brittle delamination was not triggered, the developed model can accurately describe the plastic and damage behaviour of the material. The model was then used as a numerical tool to investigate the effect of plastic anisotropy and delamination on ductile crack extension. It was shown in particular that it is not possible to obtain a unified description of rupture properties for notched and cracked specimens tested along different directions without accounting for plastic anisotropy.

Hausild *et al.* [83] examined the relationship between fracture energy and the ductile area measured on the fracture surface. Instrumented Charpy tests and fracture toughness tests were performed in the transition temperature range, as well as at lower temperatures. Quantitative fractographic analysis of Charpy specimens revealed a certain proportion of ductile fracture even if the Charpy test was conducted at low temperatures, below the transition temperature. The ductile fracture area situated next to the notch was correlated with fracture energy at all temperatures. In the transition temperature range, fracture energy and the ductile area exhibited a large scatter. Since the limiting event in the development of the ductile area was the initiation of cleavage, the maximum principal stress was computed in different specimens using the FEM. It was shown that the propagating ductile crack did not increase the stress level, but it did increase the probability of brittle fracture through an expansion of the plastic volume where weak points could be found.

In Ref. [84] instrumented Charpy tests were performed on an X70 material. The tests were then simulated using the finite element method and the GTN constitutive model. The finite element simulations delivered a new insight in the Charpy test from the following of the crack propagation during the impact test. Furthermore, an analysis of each test using a single specimen method to identify the crack length during the test was performed. Such a method would allow a more accurate description of the crack propagation behaviour than the one provided by current impact energy approaches. The method was mainly based on the slope of the load

drop once the crack is initiated. The application of the Charpy test as a measure of the crack arrest capacity of a material was discussed. Finite element simulations showed that the energy absorbed during an impact test has a limited maximum value in the range 400-500J, which can be calculated as a case where no crack initiates. Increasing the impact energy of the material led mainly to an increase of the crack initiation resistance, but it did not guarantee an improved crack propagation resistance. In that sense the current requirements of crack propagation could be inadequate.

The numerical evaluations of Charpy V-notch tests have been carried out are summarized in table 2.4 below.

Table 2.4 Summary of Modelling of Charpy V-notch Test

Publication	**Model applied**	**Major findings**
Eberle *et al* (2002)	Rate-dependent Gurson	Enabling the possibility of transferring of the parameters via numerical analysis to quasi-statically-loaded fracture mechanics specimens.
Fumiyoshi *et al* (2002)	3D FE	Weibull stress at brittle fracture initiation was almost independent of the loading rate.
Mudry (2002)	Beremin Gurson	The model is able to determine the micromechanical parameters of a cleavage model.
Rossoll *et al* (2002)	Beremin & GTN	In the transition region, the parameters of the Beremin model were found to deviate from those established on the lower shelf.
Tanguy *et al* (2002)	Beremin & Gurson-type	The model account for viscoplasticity and temperature changes.
Poussard *et al* (2002)	Beremin & Gurson-type	The stress triaxiality ratio of the Charpy-V specimen was found to be higher than that of the sub-size Charpy specimen.
Oh *et al*	GTN	Comparisons of the experimental data of

(2007)		pre-strained, notched tensile, and fracture toughness tests with FE damage analysis showed good agreement.
Folch *et al* (1999)	Beremin & GTN	A coupled brittle/ductile fracture local approach model was developed to predict either Charpy energy or fracture toughness and to investigate conditions for correlations between them.
Koppenhoefer and Dodds (1998)	GTN	The analysis suggested a negligible, additional effect of tearing on the Weibull stress under impact loading.
Tanguy *et al* (2005)	Gurson type & Beremin	Incorporated temperature effect in FEM.
Sidener (1996)	Dynamic FEM	Reveal the relationship between the USE of pre-cracked specimens and ligament size.
Thibaux *et al* (2009)	GTN	It is questionable whether the Charpy test can be adapted to predict the crack arrest capacity of steels with high crack-initiation energy.
Koppenhoefer and Dodds (1997)	3D non-linear FE model	Investigated the effects of specimen size and loading rate on brittle fracture of ferritic steels tested in the ductile-to-brittle transition region for the application of pre-cracked Charpy specimens.
Tanguy *et al* (2008)	Extended GTN	It is not possible to obtain a unified description of rupture properties for notched and cracked specimens tested along different directions without accounting for plastic anisotropy.
Thibaux (2009)	GTN	Increasing the impact energy of the material led mainly to an increase of the crack initiation resistance, but it did not guarantee an improved crack propagation resistance.

		In that sense the current requirements of crack propagation could be inadequate.

2.4.3. Modelling of drop weight tear test

Marotta [85] discussed the influence of crack tunnelling in DWTT through experiments and simulations, and presented a method of obtaining an economical measurement of the crack tunnelling. The results, by FEM, agreed significantly with the experiments and suggested it could be considered an effective equivalent crack position in accordance with the numerical results. This equivalent position allowed for tuning of the classical kinematic methods in a more reliable way. The DWTT model from this study is presented in Figure 2.39 below.

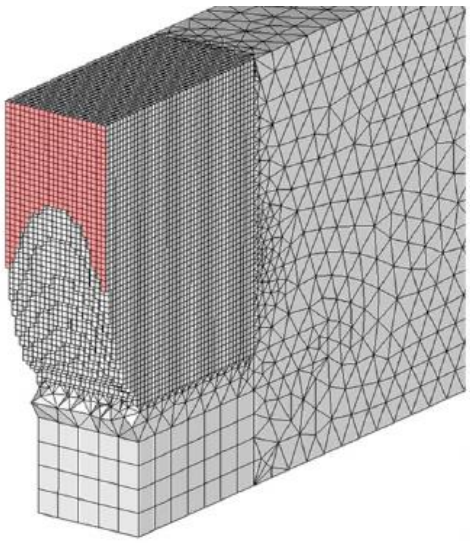

Figure 2.40 Finite element mesh for DWTT model [85]

Salvini *et al.* [86] presented a technique that was able to predict ductile fracture propagation occurrences in large metallic structures by means of an appropriate application of FEM. This technique took into account a cohesive zone in the vicinity of the crack tip, where a nodal release technique was implemented. Two parameters governing the process zone of the material under investigation have to be determined: the process zone dimension (‘D distance’) and the critical value of the

crack tip opening angle (CTOA). CTOA can be determined through experiments. D distance was determined by minimising the differences of the FE results towards the experimental data of an instrumented DWTT.

In Ref. [87] two aspects were considered for fracture control of pipelines: (1) the calculation of the maximum CTOA for a given geometry and loading and (2) the determination of the critical material property for fracture. The vehicle for CTOA calculations was a fluid/structure/fracture interaction inelastic dynamic computational model for fast, long-running fractures in pipelines. Validation of the approach used in this analysis was provided through quantitative comparisons with measured full-scale burst test data. A convenient two-specimen DWTT was used to determine the CTOA of line pipe steels. The linking of the latter with the quantification of a maximum CTOA for steady-state ductile fracture using the numerical model provided the basis for an approach that evaluates the conditions needed to ensure crack arrest.

2.4.4. Modelling of full-scale pipe fracture

Shim *et al.* [88] developed a dynamic ductile crack growth model to simulate an axially running crack in a pipe using FE analysis. The model was developed, using the FE program ABAQUS/Explicit, as presented in Figure 2.40. A cohesive zone model was used to simulate ductile crack propagation. The interaction between gas decompression and structural deformation was simulated with an approximate 3D pressure decay relationship from the experimental results. The dynamic ductile crack growth model was used to simulate 152.4mm (6”)-diameter pipe tests, where the measured fracture speed was used to calibrate the cohesive model parameters. In the simulation, the CTOA values were calculated during the dynamic ductile crack propagation. In order to validate the calculated CTOA value, DWTT experiments were conducted on the pipe material, where the CTOA was measured with high-speed video during the impact test. The calculated and measured CTOA values showed reasonable agreement. Finally, the developed model was used to investigate the effect of pipe diameter on fracture speed in small-diameter pipes.

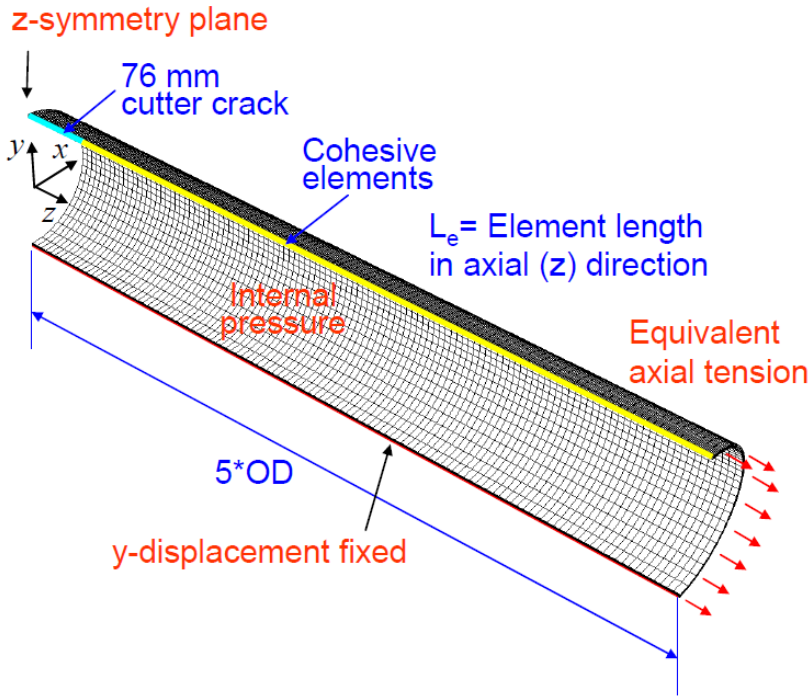

Figure 2.41 Finite element model for full-scale pipe [88]

Misawa *et al.* [89] presented a model of unstable ductile crack propagation and arrest of pressurised gas pipeline. The model coupled pipe deformation and fracture with gas decompression and took account of backfill effects. Pipe deformation and pressure changes were obtained by solving one-dimensional differential equations. The validity of the model was checked against published full-scale burst test data. The model was able to predict the history of crack velocity and arrest crack length with fairly good accuracy. Thus, this model can be applied to wide ranges of gases, pipe grades, and pipe sizes because it does not rely on parameter adjustments by experimental datasets.

2.5. Summary

Section 2.1 provides an overview of the fracture propagation control methodology for gas pipeline. Section 2.2 reviews the performance of the 85% DWTT shear area criterion and the lower diameter limit specified in pipeline standards. DWTT is not required below different lower diameter limits in the major pipeline standards, such

as API 5L. Work on CVN impact tests was carried out to estimate the FPTT, offering a substitute for DWTT. However, the literature indicated that the temperature shifts and sampling issues caused increasingly large uncertainties in predicting full-scale transition temperature using Charpy testing. Furthermore, there were cases of 355mm and 457mm welded pipes in which high CVN impact energy and SA% coexisted with a low DWTT SA% and where there was, therefore, a risk of brittle fracture, even though the Charpy results were good. Thus, to ensure the absence of brittle fracture in small-diameter pipes, it has become necessary to carry out related research and seek a resolution. This is particularly relevant for the Australian pipeline industry, as the pipeline network is dominated by relatively small-diameter, thin-walled pipe sections.

Section 2.3 discussed the importance of the relationship between Charpy absorbed energy and specimen thickness in ductile fracture control. The published research on the effect of specimen thickness on CVN absorbed energy was also reviewed. It should be noted that only a small number of studies on this topic have been conducted using line pipe steels. Most of the reviewed papers focused on pressure vessel steels for nuclear reactors, and it is unclear whether the findings can be applied to line pipe steels of different grades. Furthermore, there has not been an in-depth numerical evaluation of this trend until now. However, almost all studies demonstrated a power-law relationship with an exponent around 1.5 between specimen thicknesses and absorb energy for relatively high toughness materials. Chapter 6 investigates the power relationship in both low- and high-toughness line pipe steels, as well as the mechanisms of the power relationship between Charpy absorbed energy and specimen thickness.

Section 2.4 reviewed the numerical evaluations that have been carried out for steel fracture behaviour analysis. The GTN model is the damage model used most commonly in computational fracture mechanics to characterise the toughness of line pipe steels. While there have been a large number of numerical works on CVN tests, there has not been an in-depth numerical evaluation of the relationship between Charpy absorbed energy and specimen thickness until now. Numerical works carried

out to simulate the DWTT focused mainly on evaluation of the CTOA. None of the evaluations adopted the gull-wing DWTT specimen. Most of the numerical works on line pipe steel focused on relatively thick wall material; information on parameters and simulation results for thin-wall material are rather limited.

CHAPTER 3

EQUIPMENT AND SOFTWARE

This chapter will briefly describe the equipment and software packages used to carry out the research.

3.1. Tensile test

For all the line pipe materials acquired, tensile tests were carried out on specimens extracted from both longitudinal and circumferential directions, as demonstrated in Figure 3.1.

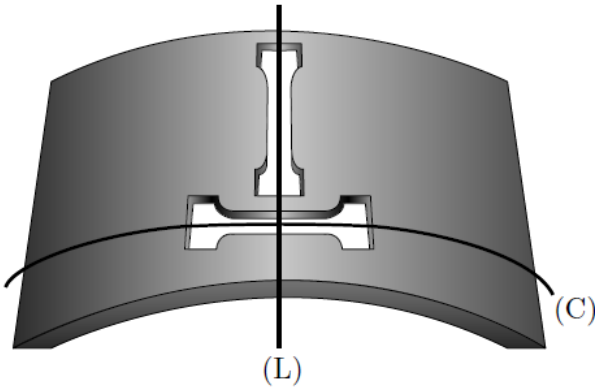

Figure 3.1 Depiction of the extraction of tensile extraction of tensile specimens in longitudinal (L) and circumferential (C) orientations

The tests were performed according to API 5L [31] with a strain rate predicted by ASTM A370 [90]. A stress rate of 52 MPa/s was applied to the upper yield point, and a maximum strain rate of 0.0008/s was applied through the yield point and up to 5%. Thereafter, a maximum strain rate of 0.008/s was applied.

All the tensile tests in this study were conducted on an Instron 1332 hydraulic tensile testing machine with a capacity of 500kN, shown in Figure 3.2.

Figure 3.2 Instron model 1332 hydraulic tensile testing machine

3.2. Drop weight tear test

DWTT is one of the major tests developed to evaluate the ductile-to-brittle transition temperature. Ductile-to-brittle transition curves obtained from full-scale burst tests nearly coincided with those obtained from DWTTs. In the current study, DWTT was used to determine the transition temperature. The specimen was a rectangular bar of full material thickness with a length of 305 mm and a width of 76 mm. All specimens in the current study were extracted from the circumferential direction of the pipe, as shown in Figure 3.3.

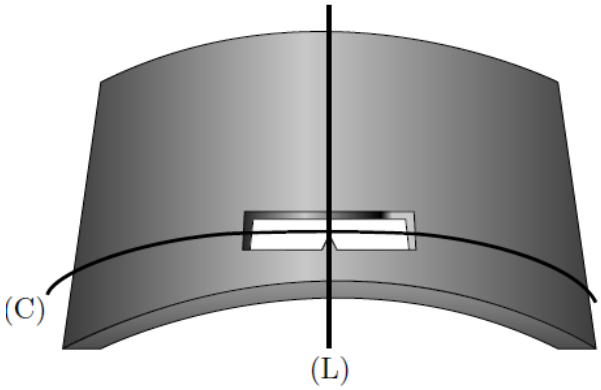

Figure 3.3 Depiction of the extraction of DWTT specimen in circumferential (C) orientation

In this study, DWTTs were performed at different temperatures using a DWTT tower with 15,000J impact energy. The drop weight applied was about 400 kg, and the impact hammer was released from a height of 3.8 m.

The specimens were conditioned in a cooling bath at the designated temperature for ten minutes before being loaded into the DWTT tower.

Figure 3.4 DWTT tower and cooling chamber

3.3. Charpy V-notch impact test

CVN impact testing is a pendulum-based, notched-bar impact test. It is a standardised high-strain-rate test that determines the amount of energy absorbed by materials during impact with a hammer, which typically causes complete or partial fracture of the specimen. The energy absorbed by the specimen is a measure of the material's toughness, and the percentage of shear area on the fracture faces is a measure of the fracture mode. CVN is used widely in industry because sample preparation and realisation of the test are relatively simple procedures that facilitate rapid and inexpensive data generation. The dimensions of standard CVN specimens are 10x10x55mm. Sub-sizes with reduced thickness can be used when a standard specimen is not available due to thin pipe wall thickness. All CVN specimens in the present study were extracted from the circumferential direction of the pipe, as shown in Figure 3.5.

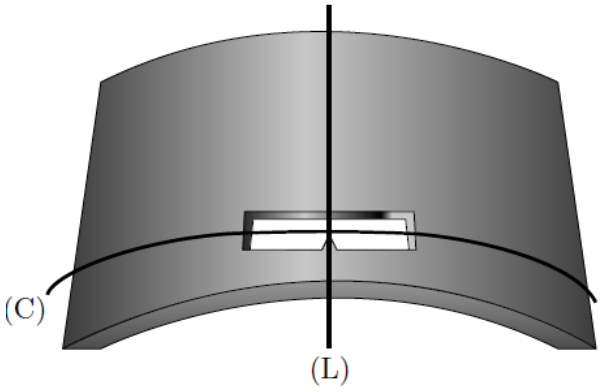

Figure 3.5 Depiction of the extraction of Charpy specimen in circumferential (C) orientation

ASTM A370 [90] allows the Charpy specimen to contain some outer diameter surface when the specimen is extracted from a tubular component, as depicted in Figure 3.6. All CVN specimens tested in this work were extracted from line pipes with relatively small diameters (OD <323.9 mm) and wall thicknesses (<11 mm). Some original OD surface was present in the sub-size specimens with thicknesses of 7.5 and 6.7 mm due to the large curvature. Therefore, there was minimal machining on the inner surface near the specimen centre, and thickness was reduced by machining from the outer surface.

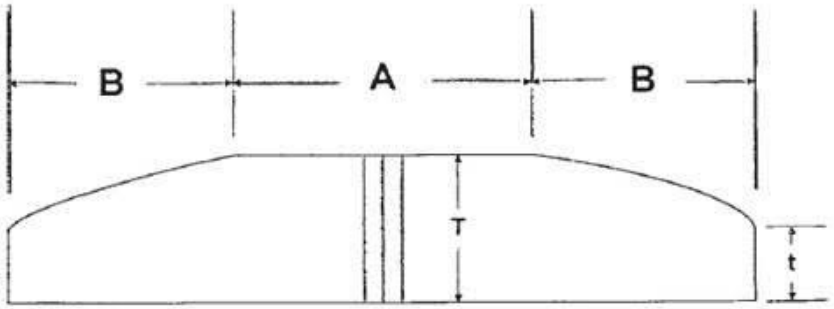

Dimension	Description	Requirement
A	Machined Surface	28 mm Minimum
B	Original OD Surface	13.5 mm Maximum
T	Specimen Thickness	Figure 11
t	End Thickness	½ T Minimum

Figure 3.6 Tubular impact specimen containing original outer diameter surface [90]

In this study, the CVN test was used to measure the toughness of sub-sized specimens extracted from small-diameter and thin-walled line pipes. The Instron MPX750 instrumented Charpy impact machine, with an impact energy of 750J, was used for all CVN tests.

Figure 3.7 Instron MPX7500 Charpy impact test machine and cooling chamber

3.4. Finite element method (FEM)

In addition to the experiments conducted in this study, a numerical method was engaged to analyse and explain the complex fracture behaviours of the line pipe steels.

3.5. FEM software

The numerical method used in this study was applied with the support of the following software products:

- ANSYS/LS-DYNA version 13.0-14.5

- LS-PREPOST version 3.2-4.0

ANSYS/LS-DYNA was introduced in 1996 as a collaborative effort between Livermore Software Technology Corporation (LSTC) and ANSYS, Inc. This commercial engineering simulation software is specially designed for structural analysis, including linear, nonlinear, and dynamic studies. A complete set that includes element behaviour, material models, and time-tested explicit solver is provided for a wide range of mechanical design problems. Since fractures in line pipe steel involve dynamic and nonlinear problems, ANSYS/LS-DYNA is an ideal tool for solving the equations stated in the literature review.

LS-PREPOST, also delivered by LSTC, is an advanced pre- and post-processing tool, with comprehensive LS-DYNA keyword support. The latest version of this software can be downloaded freely from the official LSTC website. In this research, most of the basic steps for building up the impact model were carried out in the ANSYS Mechanical environment, whereas some further implementations and post-processing were required to be completed in LS-PREPOST.

3.6. High performance computer (HPC) cluster

The superior technical devices available today have supported researchers extensively in overcoming the key barriers to gaining excellent results. Computers that are more powerful have been developed, with advanced performance, and their capabilities have been upgraded yearly.

In this study, the FEMs were constructed using a Dell computer with an Intel Core i7-2500 3.3GHz central processing unit with 8 Gb installed random access memory, running on Windows 7 (Professional). Very fine mesh was produced in the impact region of the model to achieve the best results.

A disadvantage of the FEM is that the finer the mesh that is generated, the longer is the calculation time required, due to the increasing numbers of nodes and elements.

Therefore, high-end computing resources are essential for carrying out the simulations. The University of Wollongong provides a number of high-performance computers to researchers from many disciplines, and parallel computing of the FEM model was carried out on a high-performance computer cluster (22 x 64 core Dell Power Edge C6145). It typically took five days for each DWTT simulation job and three days for each CVN job, running with four Cores at 2.3 GHz.

CHAPTER 4

INVESTIGATION OF BUCKLING IN DWTT OF SMALL DIAMETER PIPE

Most pipeline standards specify a minimum requirement of 85% shear area in a DWTT to ensure that the steel will not exhibit brittle fracture behaviour during operations. However, according to API and ISO specifications, the DWTT is only required for pipes with a diameter of 500 mm and above, despite instances of brittle fracture propagation being recorded in smaller-diameter pipelines.

Thus, to ensure the absence of brittle fracture in small-diameter pipes, it has become necessary to carry out related research and seek a resolution. This is particularly relevant for the Australian pipeline industry, as the pipeline network is dominated by relatively small-diameter, thin-walled pipe sections.

In this chapter, the difficulties associated with the manufacturing and testing of a DWTT specimen on small-diameter, seam-welded pipes were investigated. DWTTs were performed on both gull-winged and flattened DWTT specimens for API 5L X42 and X70 line pipe, and buckling was measured quantitatively. Additional information was collected by simulating the DWTT process using FEM with the GTN ductile fracture model. The simulated results were in good agreement with the experimental results. The applicability of DWTT on seam-welded line pipes with diameters as small as 168 mm and the effects of flattening are discussed.

4.1. Material properties and experimental procedures

DWTTs were performed on API 5L X42 and API 5L X70 HFERW seam-welded pipes. The diameters of the tested pipes ranged from OD 168 to OD 406 mm, and the thicknesses ranged from 4.8 to 12.7 mm. The tensile properties of each pipe, in both circumferential and longitudinal directions, are summarised in Table 4.1.

Table 4.1 Tensile properties of the X42 and X70 pipes

Sample Marking	Pipe Grade	Proof Stress Rt0.5% (MPa)	Tensile Strength (MPa)	Yield / Tensile Ratio	Uniform Elongation (%)	Total Elongation (%)
168 C	API 5L X42	389	497	0.78	18	29
168 L		425	491	0.86	18	28
219 C		380	475	0.80	20	31
219 L		448	508	0.88	14	32
323 C		431	506	0.85	14	42
323 L		442	510	0.87	8	39
406 C		420	496	0.85	11	42
406 L		417	510	0.82	12	45
323 C1	API 5L X70	606	662	0.92	11	27
323 C2		611	658	0.93	11	29
323 L1		585	645	0.91	12	32
323 L2		573	641	0.89	13	30

Note: C = circumference direction; samples were flattened for tensile test.
L = longitudinal direction

All DWTT specimens were extracted from the 3 o'clock position in a transverse direction and a pressed-notch was applied. A 15kJ drop weight tester with a

maximum drop height of 3.8m was used for all tests. Tests and evaluations were performed in accordance with AS1330:2004 [23].

For grade X42 pipes, DWTTs were performed on four pipe dimensions, as shown in Table 4.2. For the OD 168 pipe, both gull-winged and flattened specimens were used. The chemical composition of each line pipe material is presented in Table 4.3.

Table 4.2 Test summary of API 5L X42 pipes

Pipe OD (mm)	Wall Thickness (mm)	Pipe Grade	Notch Type	Type of Specimen
168	4.8	API 5L X42	Pressed notch	Gull-winged flattened
219	8.2			Gull-winged
323.9	9.5			Gull-winged
406.4	12.7			Gull-winged

Table 4.3 Chemical composition of API X42 line pipe Materials

168 x 4.8 mm API X42 line pipe								
C%	P%	Mn%	Si%	S%	Ni%	Cr%	Mo%	Cu%
0.135	0.017	0.7	0.12	0.005	0.013	0.016	<0.002	0.011
Ca%	AI%	Ti%	Nb%	Sn%	V%	N%	B%	
0.003	0.032	<0.002	<0.001	<0.002	<0.003	0.0046	<0.0003	
219 x 8.2 mm API X42 line pipe								
C%	P%	Mn%	Si%	S%	Ni%	Cr%	Mo%	Cu%
0.146	0.012	0.7	0.13	0.005	0.011	0.015	0.003	0.012
Ca%	AI%	Ti%	Nb%	Sn%	V%	N%	B%	
0.0039	0.037	<0.002	0.001	<0.002	<0.003	0.0052	<0.0003	
323.9 x 9.5 mm API X42 line pipe								
C%	P%	Mn%	Si%	S%	Ni%	Cr%	Mo%	Cu%

0.08	0.009	0.67	0.14	0.003	0.014	0.014	<0.002	0.02
Ca%	AI%	Ti%	Nb%	Sn%	V%	N%	B%	
0.0028	0.023	0.011	0.025	<0.002	<0.003	0.0063	<0.0003	
406.4 x 12.7 mm API X42 line pipe								
C%	P%	Mn%	Si%	S%	Ni%	Cr%	Mo%	Cu%
0.145	0.015	1.02	.013	0.004	0.017	0.02	0.003	0.021
Ca%	AI%	Ti%	Nb%	Sn%	V%	N%	B%	
0.0033	0.036	<0.002	0.001	<0.002	<0.003	0.0041	<0.0003	

Specimens extracted from OD219, 323, and 406mm pipes were gull-winged according to a two-step procedure: (1) flattening of both ends while keeping the curvature in the centre unchanged over a length of 50 mm and (2) gull-winging of both ends using formers or spacers. The procedure for OD168 was slightly more complex due to the extreme curvature. A zone of 50 mm on each side of the centre line was left unflattened for the first step. Then, both ends were gull-winged using two or more different-size spacers while keeping the curvature in the centre unchanged over a length of 50 mm. The alignment of each specimen was checked after the gull-wing process.

DWTs were conducted further on OD323.9mm API 5L X70 seam-welded line pipe as listed in Table 4.4. The chemical composition of the line pipe is shown in Table 4.5.

Table 4.4 Test summary for API 5L X70 pipe

Pipe OD (mm)	Wall Thickness (mm)	Pipe Grade	Notch Type	Type of Specimen
323.9	8.8	API 5L X70	Pressed notch	Gull-winged flattened

Table 4.5 Chemical composition of 323.9x8.8mm API X70 line pipe material

C%	P%	Mn%	Si%	S%	Ni%	Cr%	Mo%	Cu%
0.07	0.014	1.37	0.35	0.002	0.016	0.016	0.1	0.012
Ca%	AI%	Ti%	Nb%	Sn%	V%	N%	B%	
0.0012	0.038	0.018	0.06	<0.002	<0.003	0.0044	<0.0003	

4.2. Experimental results

4.2.1. Results for API 5L X42 seam welded line pipe

Excessive plastic deformations at the impact point were observed at the impact point (Figure 4.1, top) of all of the samples in the region of the upper shelf, and some in the region of the temperature transition. In the gull-winged specimens, the notch sides were mostly straightened (Figure 4.1, bottom) after the test. Nonetheless, the fracture surfaces were examined for SA%. Some of the specimens were not completely broken in the region of the upper shelf (Figure 4.2). Since these specimens exhibited fully ductile fracture, 100%SA was assigned. No case of inverse fracture was observed at any temperature.

Figure 4.8 Specimen with excessive deformation

Figure 4.9 Incompletely broken DWTT specimen

DWTTs were conducted over a range of temperatures from ambient to -60°C; the results are shown in Figure 4.3. Transition curve was obtained for each pipe. Scattering occurred at some temperatures. The OD168 flattened specimens tested at -45°C demonstrated both 100%SA with excessive plastic deformation and 5%SA without excessive plastic deformation. Most of the excessive plastic deformation occurred at the upper shelf. Exceptions were observed in the OD168 and OD323 gull-winged specimens.

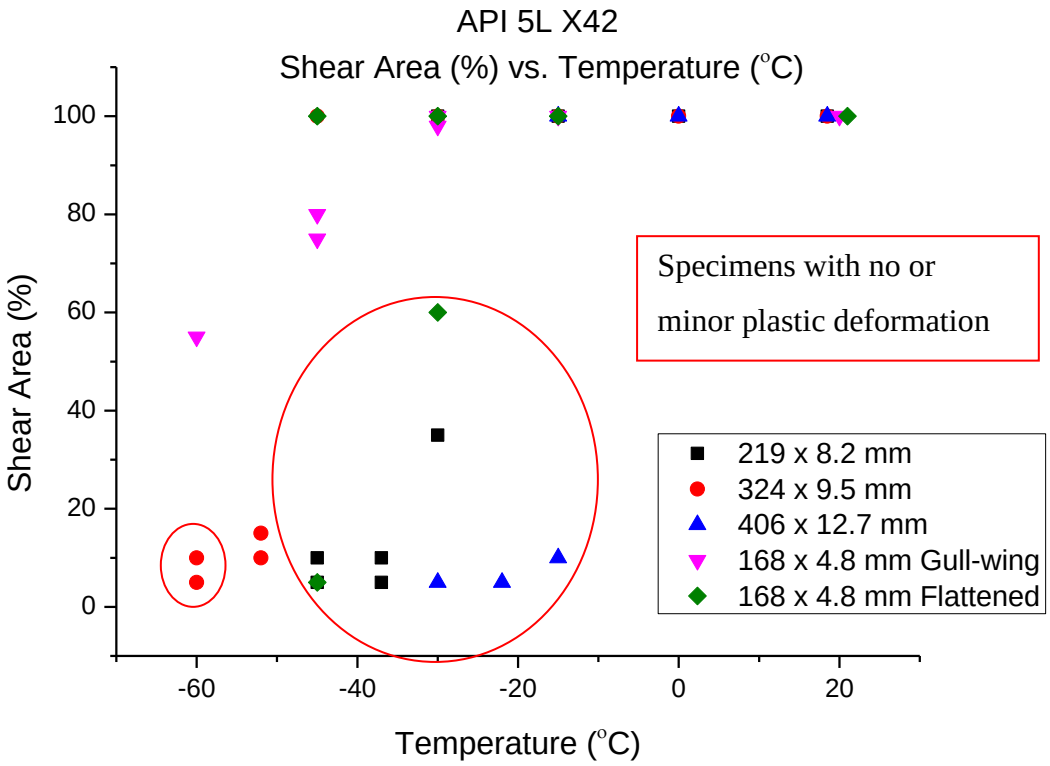

Figure 4.10 DWTT transition curves for pipe grade API 5L X42

4.2.2. Results for API 5L X70 seam weld line pipe

Similar to the previous tests on X42 pipes, incomplete breaks and excessive plastic deformation were observed for all specimens at the upper shelf. None of the specimens exhibited inverse fracture. The gull-wing curvature in the cross-section from the anvil to the notch zone has a tendency to flatten due to the important tensile loading induced at the bottom of the specimen by the impact process. Typical specimens, both gull-winged and flattened, with or without excessive plastic deformation, are shown in Figures 4.4 and 4.5, top and bottom, respectively.

Figure 4.11 API 5L X70 gull-winged specimens

Figure 4.12 API 5L X70 flattened specimens

The test results depicted in Figure 4.6 show the transition curves for both flattened and gull-winged specimens. A small difference was observed between the two types of specimens.

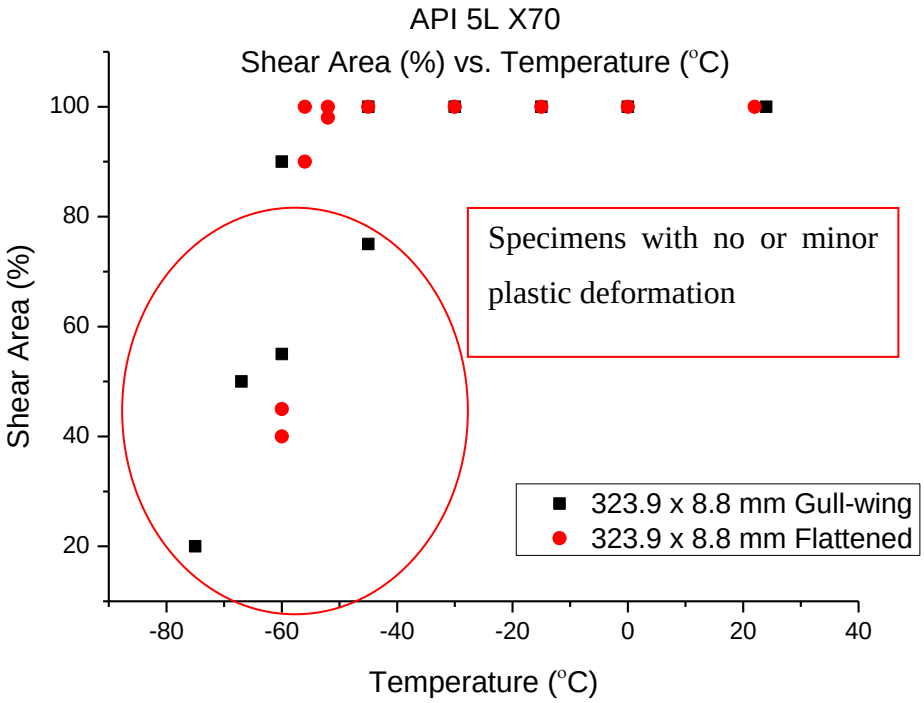

Figure 4.13 DWTT transition curves for pipe grade API 5L X70

Because all excessive plastic deformation occurred on or near the upper shelf, it is concluded that the deformations result from an increase in the ductility of the material. More than 70% of the presented tested specimens exhibited excessive plastic deformation. The SA% was calculated according to AS1330 [23]. If the assessment follows API 5L3, then a valid specimen need to be completely broken in one impact without the presence of buckling. The method of evaluation has a strong influence on what is perceived as valid.

4.2.3. Buckling

The maximum lateral displacement L_d, as shown in Figure 4.7, that occurred at the impact point was measured for both halves of the completely broken specimens. The average ratio of L_d to wall thickness T of each specimen was recorded, and SA%

against this ratio was plotted in Figures 4.8 to 4.11. L_d could only be obtained from four flattened OD168 specimens out of eight due to incompletely broken specimens.

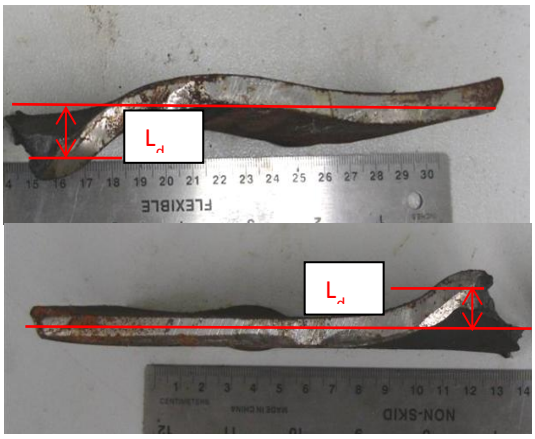

Figure 4.14 L_d measured in gull-wing and flattened specimens

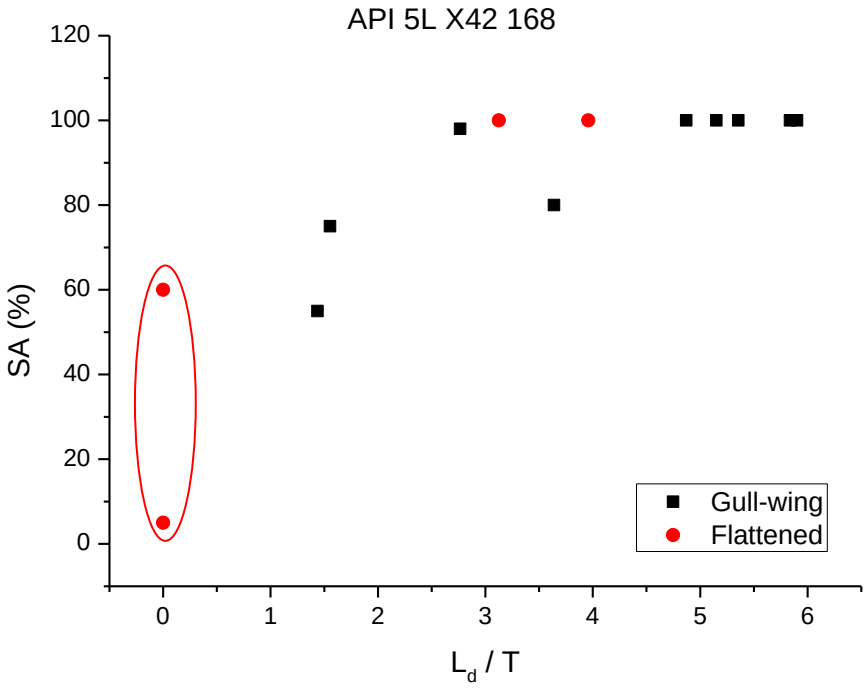

Figure 4.15 SA% vs. L_d / T for X42 168 gull-wing and flattened specimens

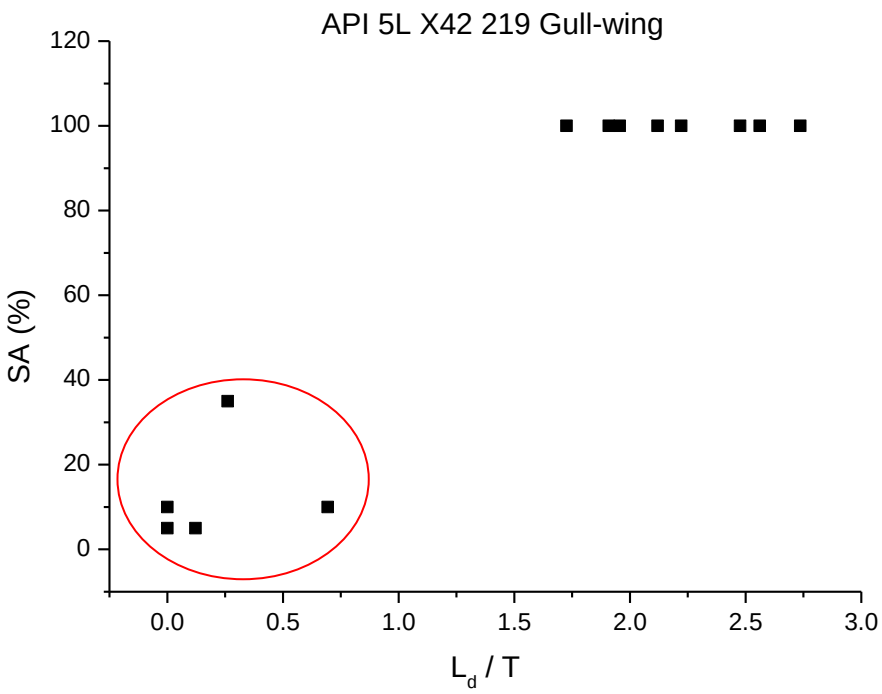

Figure 4.16 SA% vs. L_d / T for X42 219 gull-wing specimens

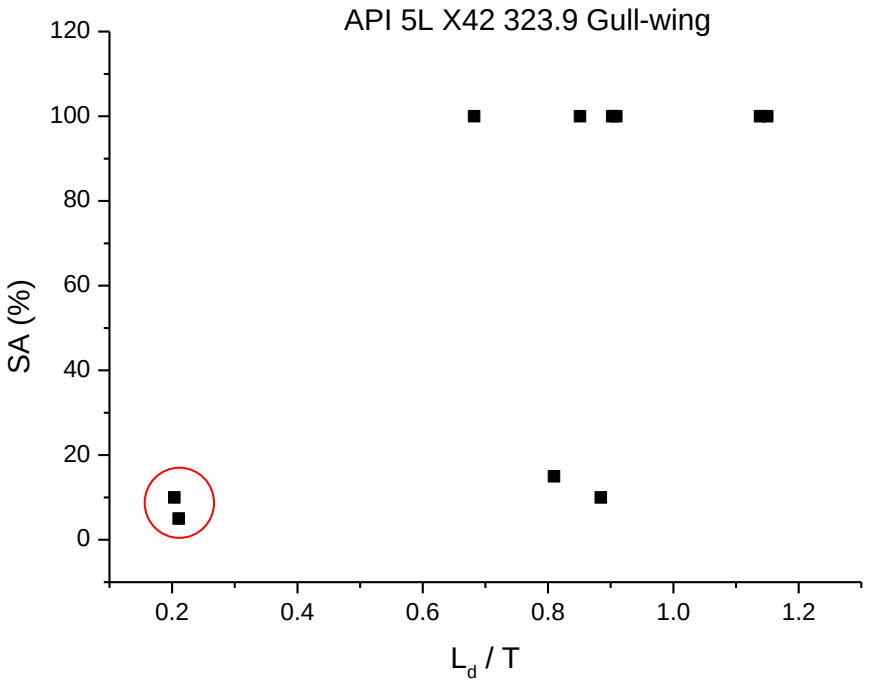

Figure 4.17 SA% vs. L_d / T for X42 323.9 specimens

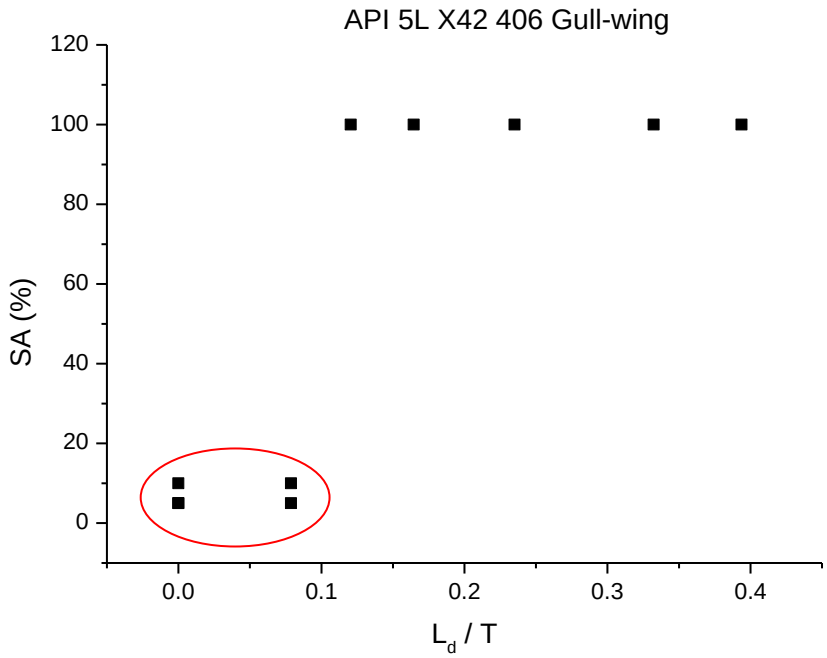

Figure 4.18 SA% vs. Ld / T for X42 406 specimens

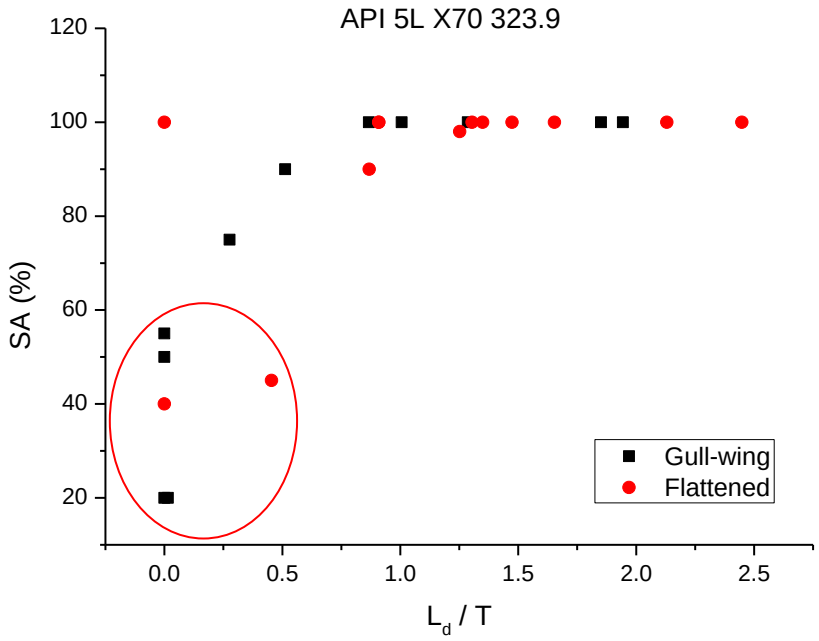

Figure 4.19 SA% vs. L_d / T for X70 323.9 gull-wing and flattened specimens

As shown in Figures 4-8 to 4-11, deformation on the X42 gull-winged specimens became less severe as the diameter and the wall thickness increased. The figures

show the same pattern of SA% vs. temperature. The gull-winged specimens of the OD168 pipe exhibited more severe deformation than the flattened ones. A lesser extent of deformation was observed in the gull-winged specimens of the X70 OD323.9 pipe; Figure 4.12 shows a clear increase in lateral displacement as the SA% increases in the gull-winged specimens. Almost all of the lower shelf specimens in the current study possessed an L_d-to-thickness ratio less than 0.5 (shown in Figure 4.6 and Figures 4.8 to 4.12). Since the extent of 'excessive' deformation is not indicated in any standard, a definition of 'minor lateral plastic deformation' is proposed. From our results, it is reasonable to consider lateral plastic deformation to be minor at an L_d/ T of 0.5 or below.

The effect of flattening was investigated. Average SA% and lateral displacement L_d were plotted against temperature for the gull-winged and flattened specimens. Figures 4.13 and 4.15 show that more conservative results were obtained with the flattened specimens of both grade X42 OD168 and X70 OD323.9 pipe.

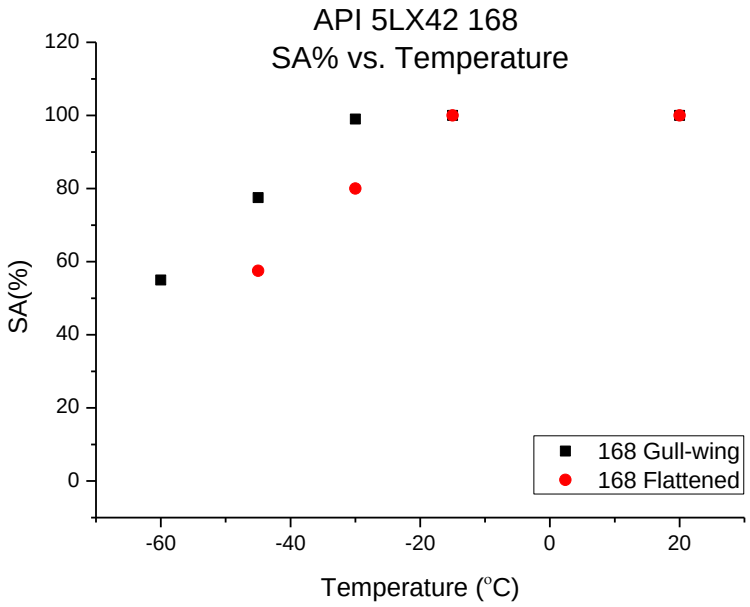

Figure 4. 20 Comparison of average SA% between X42 168 gull-wing and flattened specimens

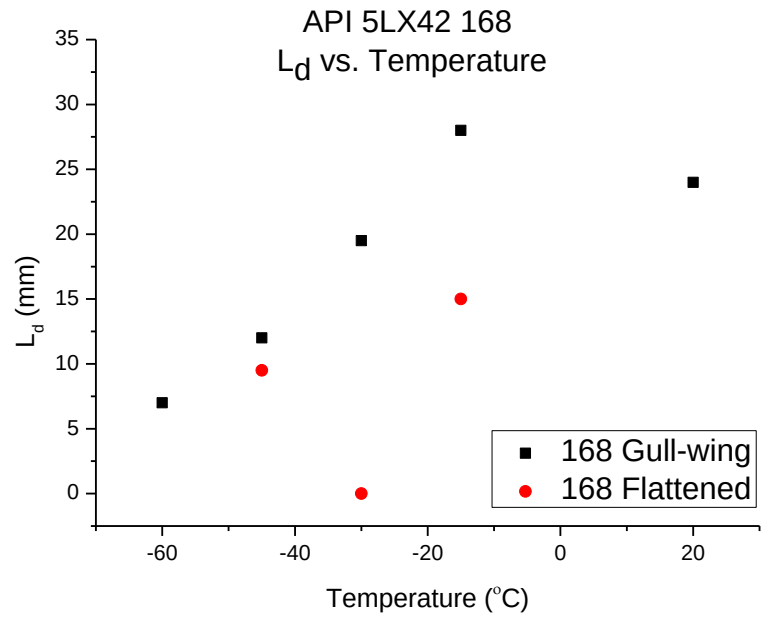

Figure 4.21 Comparison of averaged L_d between X42 168 gull-wing and flattened specimens

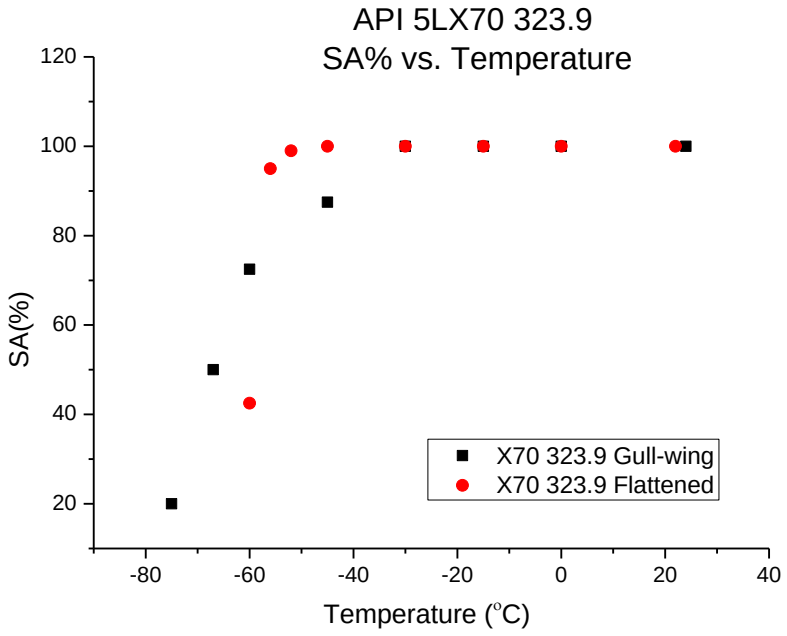

Figure 4.22 Comparison of averaged SA% between X70 323.9 gull-wing and flattened specimens

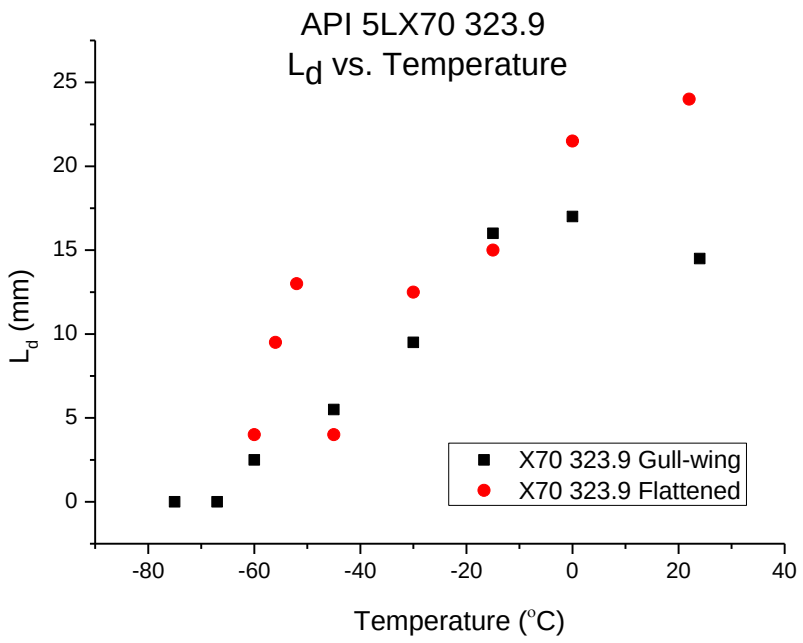

Figure 4.23 Comparison of averaged L_d between X70 323.9 gull-wing and flattened specimens

As mentioned previously, low grade OD168 gull-winged specimens were deformed to a higher extent than the flattened specimens (Figure 4.14). This trend is in opposition to the observation made in the high-grade OD323.9 case. Figure 4.16 shows that gull-winged specimens have a better resistance to lateral displacement compared to flattened specimens in grade X70 OD323.9 line pipes.

Average L_d values for all gull-winged specimens from each diameter are summarised in Figure 4.17. In the low grade pipes, the specimens were subjected to a higher extent of lateral displacement as the diameter decreased. At equal diameters, high-grade pipes exhibited a slightly higher extent of lateral displacement during DWTT.

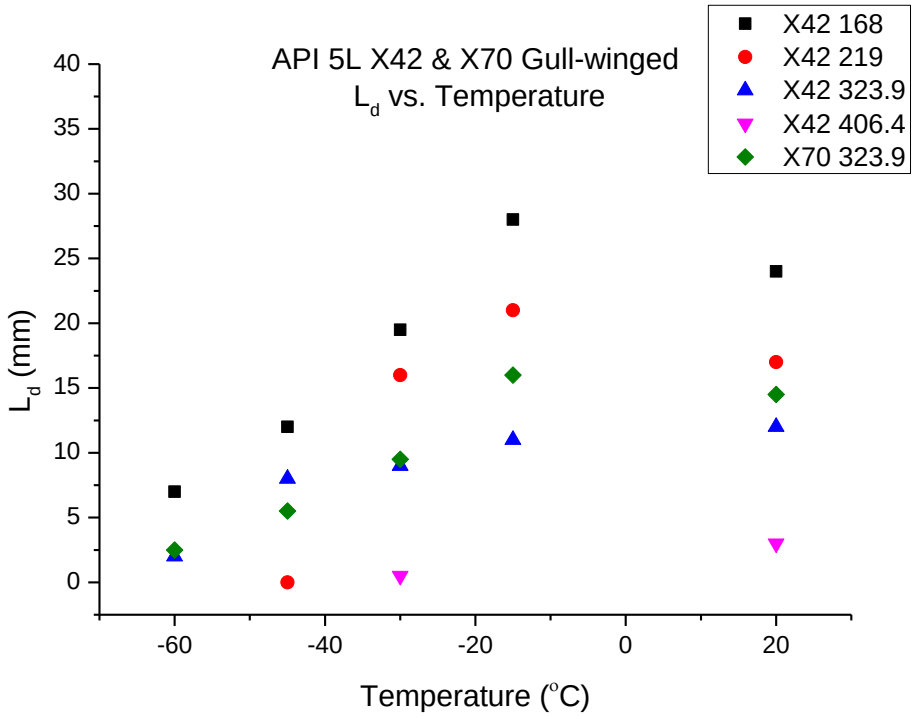

Figure 4.24 L_d vs. temperature in gull-winged specimens

4.3. Numerical work

4.3.1. FEM simulation model

The GTN model has become increasingly popular for simulating plastic flow localisation and ductile fracture problems. According to the GTN model, the yield function of a porous solid can be expressed with a randomly distributed volume fraction *f* of voids, as follow[91]:

$$\phi(\sigma, f, \bar{\sigma}) = \frac{\sigma_e^2}{\bar{\sigma}^2} + 2q_1 f cosh\left(\frac{3q_2\sigma_m}{2\bar{\sigma}}\right) - 1 - (q_1 f)^2 = 0 \qquad (4.1)$$

where the constants q_1 and q_2 are material parameters introduced by Tvergaard [92] to bring predictions of the model into closer agreement with full numerical analyses of a periodic array of voids. Here, σ_m and σ_e are the mean normal and effective part of the average macroscopic Cauchy stress σ_c, and $\bar{\sigma}$ is the yield stress of the matrix material.

Ductile fracture is correlated to the void volume fraction, *f*. The increase in *f* is controlled by local strains. In detail, the equation for the evolution of *f* consists of two terms- nucleation and growth:

$$\dot{f} = \dot{f}_{growth} + \dot{f}_{nucl} \tag{4.2}$$

As the matrix material around the voids is seen to be volume conservative, the void growth rate can be determined by the plastic volume dilatation rate,

$$\dot{f}_{growth} = (1 - f) \cdot \dot{e}^p_{kk} \tag{4.3}$$

with the components of the macroscopic plastic strain rate tensor, $\dot{e}^p_{kk}$.

The void nucleation rate can be determined by

$$\dot{f}_{nucl} = \dot{\varepsilon}^p \frac{f_n}{s_n\sqrt{2\pi}} exp\left(-\frac{1}{2}\left(\frac{\varepsilon^p - \varepsilon_n}{s_n}\right)^2\right) \tag{4.4}$$

where ε_n is the mean void nucleation strain and s_n is the corresponding standard deviation. f_n controls the amplitude of the nucleation rate.

Once the void volume fraction reaches critical void volume fraction f_c, the voids coalesce. Tvergaard and Needleman introduced Eqn. (4.5) to control gradual coalescence up to the ultimate void volume fraction f_u^*, the value at which the material is considered damaged [36].

$$f^* = \begin{cases} f & if\ f \le f_c \\ f_c + \dfrac{f_u^* - f_c}{f_f - f_c} \cdot (f - f_c) & if\ f > f_c \end{cases} \tag{4.5}$$

where f_c is the critical void volume fraction at which voids coalesce, f_f is the void volume fraction at final failure of the material $f_u^*$is the ultimate void volume fraction and $f_u^* = 1/q_1$.

In this study, explicit FEM code ANSYS/LS-DYNA with the built-in GTN model was used to simulate the DWTT process. The simulation parameters are shown in Table 4.6.

Table 4.6 Parameters used in simulations

Parameters	Value
Density, kg/m^3	7850
Young's Modulus, GPa	206
Yield stress, MPa	380 for 219 DWTT 600 for 323.9 DWTT
f^*	0.06
f_0	0.000125
f_c	0.03
f_n	0.0008
f_f	0.8
$\mathcal{E}_n$	0.3
S_n	0.1
q_1	1.5
q_2	1.0

A three-dimensional, gull-wing-shaped DWTT test was simulated. The pipe diameter and pipe wall thickness were 210 mm and 8.2 mm, respectively. The FE mesh used eight-node hexagonal elements. The elements around the expected fracture zone were much finer than elsewhere to improve the precision of this region. The model consisted of 124,864 elements and 127,002 nodes. As specified in the ASTM E436 [93], the DWTT specimen was loaded in three-point bending by a drop hammer with a weight of 400 kg and a loading span of 254 mm at an impact velocity of 7–10m/s. The simulated fracture test consisted of two steps, as shown in Figure

4.18: (1) pressing the notch and (2) fracturing the sample under the action of the hammer. During the DWTT process, the hammer descends with an initial impact speed of 7 m/s.

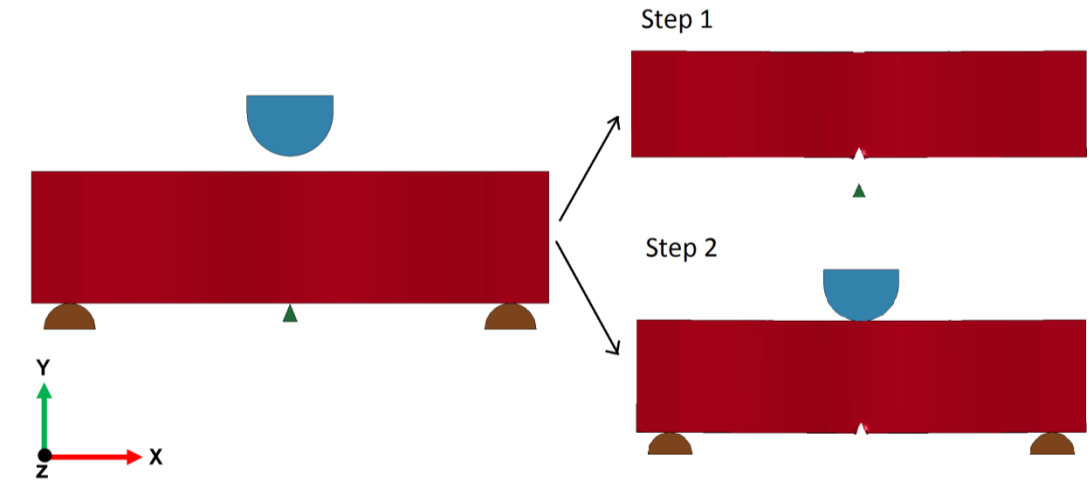

Figure 4.25 Geometry of the full simulation process

4.3.2. Simulation results

Figure 4.19 presents the DWTT simulation results at different simulation times t. Figure 4.19(a) shows the specimen shape before notching. In Figure 4.19(b), the hammer contacts the specimen at t=1.4ms. The fracture initiates at t = 2.2 ms (Figure 4.19(c)) and propagates through the specimen at t=6.4ms as shown in Figure 4.19(d). The specimen is separated at t = 9.6ms (Figure 4.19(e)).

Front View

Top view

(a) t = 0 s

(b) t = 1.4 ms

(c) t = 2.2 ms

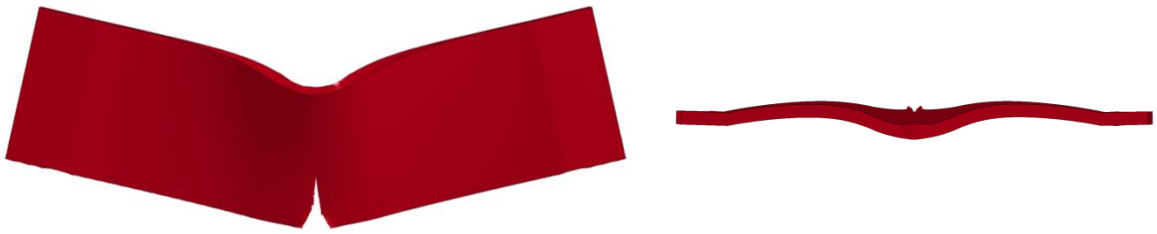

(d) t = 6.4 ms

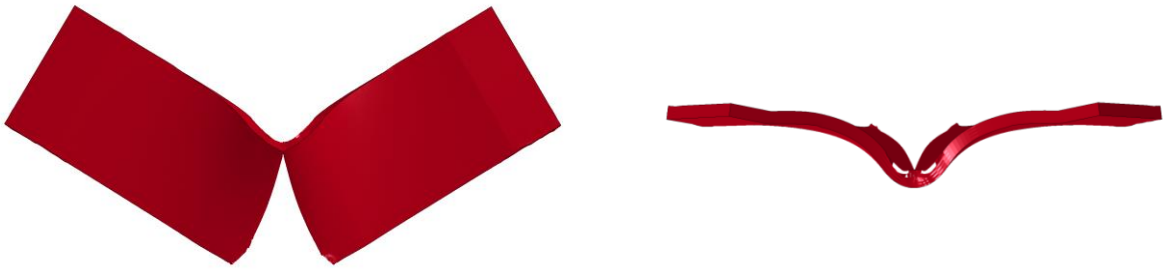

(e) t = 9.6 ms

Figure 4.26 DWTT simulation results at different simulation times

4.3.3. Comparison between experiment and simulation

Figure 4.20 compares the fracture morphology of the simulated gull-wing DWTT specimen and the experimentally tested specimen. A close agreement between them can be observed.

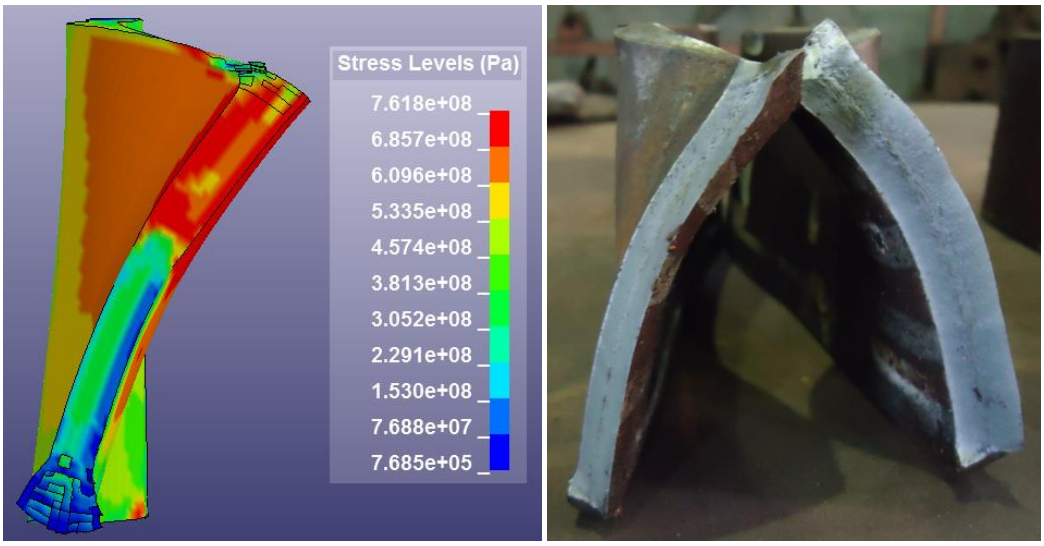

Figure 4.27 Fracture morphology of tested gull-wing DWTT specimen from simulation (left) and experiment (right)

Lateral deformation, L_d, from the model was measured and plotted as shown in Figure 4.21. The results show increased lateral deformation with the hammer displacement. The maximum lateral deformation was 24.52 mm. This result is quantitatively close to the average maximum deformation of 25 mm measured in the experimental DWTT specimen tested at ambient temperature.

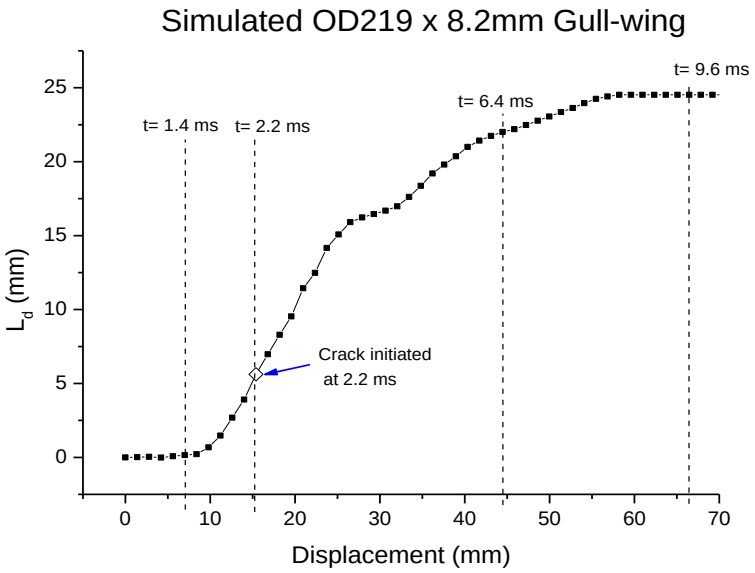

Figure 4.28 Force and lateral deformation vs. hammer displacement

The distributions of the stresses around the notch before initiation of the fracture are shown in Figure 4.22 (a) - (d). The stresses are no longer distributed symmetrically around the mid-plane due to the gull-wing geometry of the specimen and the development of buckling. However, the area near the notch tip is still subjected to tensile stress along three directions, similar to the DWTT flat specimens. The dominant tensile stress is in the x direction, suggesting that buckling does not affect stress state significantly near the notch until at least the initiation of the fracture.

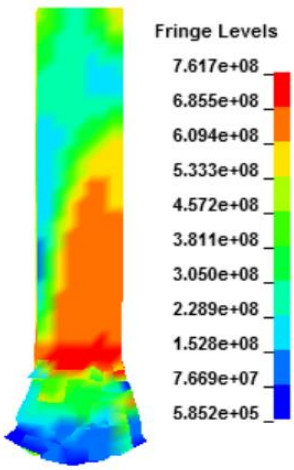

(a) Effective stress (Pa);

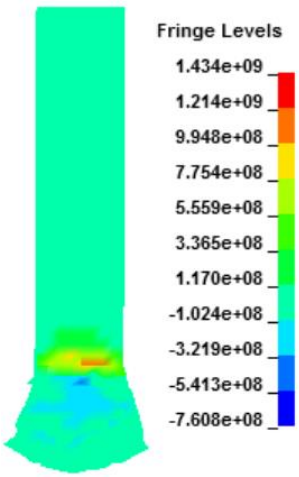

(b) Stress in the x direction (Pa)

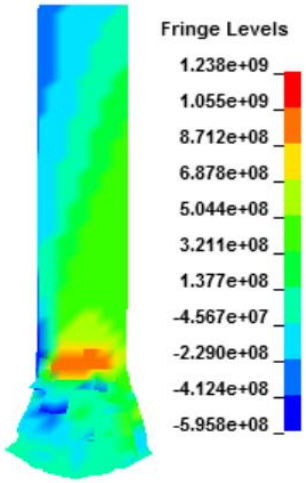

(c) Stress in the y direction (Pa);

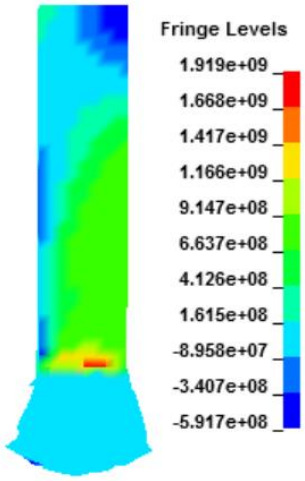

(d) Stress in the z direction (Pa)

Figure 4.29 Contour results of stresses near the notch before fracture initiation (t=2.2ms)

4.3.4. A new way to determine FPTT using conventional DWTT

Based on the fact that DWTT with buckling occurred mostly at the upper shelf and the transition zone, it is reasonable to assume that a non-buckled specimen in the lower shelf region is valid according to the API 5L3 acceptance criteria. It is suggested that DWTT start at low temperatures and proceed towards higher temperatures (as opposed to the conventional method of starting at high temperatures and proceeding towards lower temperatures). The maximum temperature, T_0, of the lower shelf region should correspond to the starting point of the transition from less buckling to more buckling. The temperature change over the narrow transition zone, ΔT, which is normally about 20°C, and the minimum temperature of the upper shelf region can be represented as $T_0+\Delta T$, as shown in Figure 4.23.

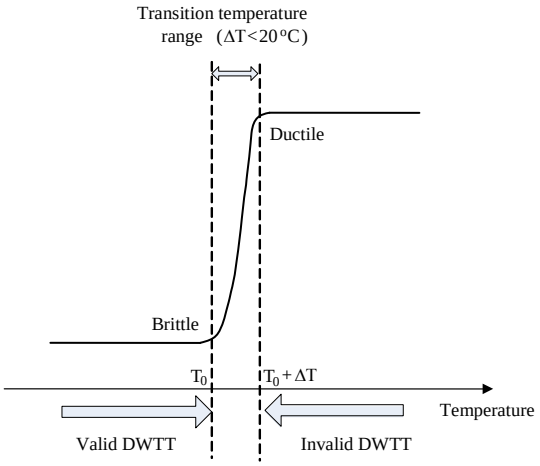

Figure 4.30 SA% vs. temperature transition curve

These observations lead to the following proposals:

- If the pipe operating temperature is less than T_0, the DWTT results are valid and the pipe is unsafe due to the possible occurrence of brittle fracture.
- If the pipe operating temperature is higher than T_0+ΔT+safety margin, the pipe is safe from brittle fracture.
- If the pipe operating temperature is higher than T_0 and less than T_0+ΔT, there is uncertainty. Further research and improved standards are needed to provide additional certainty.

4.4. Summary

The findings of the current chapter are summarised as follows:

(1) For 219mm diameter pipe and larger, the test specimens were conveniently gull-winged and tested, and transition curves obtained successfully, although buckling in the form of lateral deformations were observed in many specimens. However, it is not clear if any shift in the transition temperature was introduced by the lateral displacement.

(2) For OD168 pipe, the gull-wing process is slightly more complex but quite practical. Although some specimens are not perfectly symmetrical after gull-wing preparation, fracture surfaces were obtained successfully with a single impact.

(3) Evaluation method and acceptance criteria have a strong influence on the test results. More than 70% of the tested specimens exhibited large plastic deformation. The extent of allowable buckling or excessive plastic deformation categorised as invalid is not clearly defined in the standards.

(4) An L_d/T ratio less than 0.5 is proposed as a reasonable starting point to define a 'minor' level of lateral deformation.

(5) Flattened DWTT specimens generated more conservative results compared to gull-winged specimens in terms of transition temperature in low-grade line pipe steel. The opposite case was observed in high-grade line pipe steels in the current study.

(6) Grade API 5L X42 and X70 line pipe steels displayed relationships between shear area percentage and extent of lateral displacement. More tests are needed to investigate the effect of buckling on DWTT results, especially in high-grade line pipe steels.

(7) Flattened specimens exhibited higher extents of lateral displacement during DWTT compare to gull-winged specimens in high-grade line pipe steels. The opposite was true in low-grade line pipe steels, but many more incompletely broken specimens were generated by the flattened specimens compared to the gull-winged specimens.

(8) The specimens exhibited higher lateral displacement as the diameter decreased. No significant impact due to pipe grade was observed.

(9) A new evaluation method was proposed for future consideration.

(10) A FEM using the GTN damage model was applied to simulate the fracture process of pipeline steel during a DWTT. The simulated results are in close agreement with the experimental results in terms of stress distribution and fracture morphology. The simulated results suggested that buckling does not

have a significant effect on stress state near the notch until the instant of fracture initiation.

CHAPTER 5

IMPROVEMENT OF DWTT FOR SMALL DIAMETER PIPE

This chapter describes the design and use of a new DWTT specimen. Compared to the full-scale results, the new DWTT was able to predict a better transition temperature than the conventional DWTTs.

5.1. Full-scale pipe burst test

JFE Steel Corporation has performed full-scale burst tests in order to verify the applicability of the DWTT [94]. JFE collaborated with EPCRC by sharing the full-scale burst test data and donating a 1m-length pipe section that was cut off from the full-scale tested pipe for small-scale tests. The ductile–brittle transition curves were obtained from small-scale tests and compared with the full-scale burst test by the author.

The test pipes were the newly-developed HFW MightySeam line pipe by JFE Steel Corporation, which is an API X60M grade product with excellent low-temperature toughness. The outer diameter of the pipe is 323.9 mm and the wall thickness is 11.9 mm. Tensile properties of the base material in the longitudinal direction are presented in Table 5.1 for pipe longitudinal direction.

Table 5.1: Tensile properties of tested material in pipe longitudinal direction

X60M	YS* (MPa)	TS (MPa)	Y/T (%)	El (%)
Base Material	506	573	88.3	30.0

Nitrogen gas was used as the pressure medium in the full scale test, and the test pipe was cooled by using liquid nitrogen in the cooling baths. A girth welded pipe was used for the test. The test pipe was 6 m long, which is sufficient to observe the appearance of the fracture prior to the arrival of the reflected wave. Two cooling baths were set up separately at two sides of the pipe in order to obtain fracture behaviours at two test temperatures in one burst test.

The test was conducted at an initial pressure of 22.4 MPa, which is equivalent to 73% of SMYS. An initial longitudinally-oriented crack with a length of 600 mm was introduced by explosive charge. The initial notch was introduced into the pipe body 90° from the seam weld on one side of the girth weld and in the seam weld on the other side, as shown in Figure 5.1.

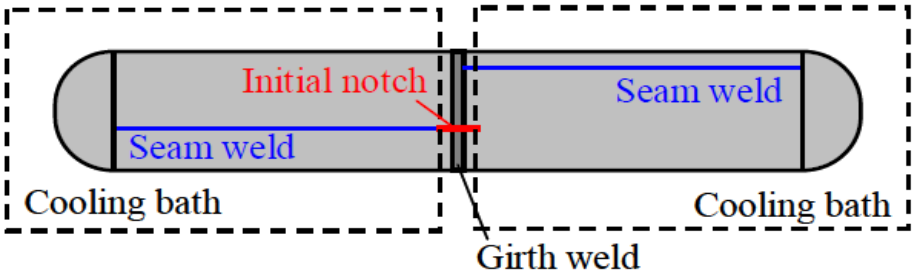

Figure 5.1 Initial notch location for the full-scale burst test

Thermocouples were mounted along the pipe to monitor temperature distribution. Figure 5.2 presents the temperatures measured by the thermocouples along the pipe just before the explosion. The average temperatures were -54°C at the seam weld side and -48°C at the pipe body side. There were some over-cooled locations that coincided with the locations directly under the liquid nitrogen cooling nozzles.

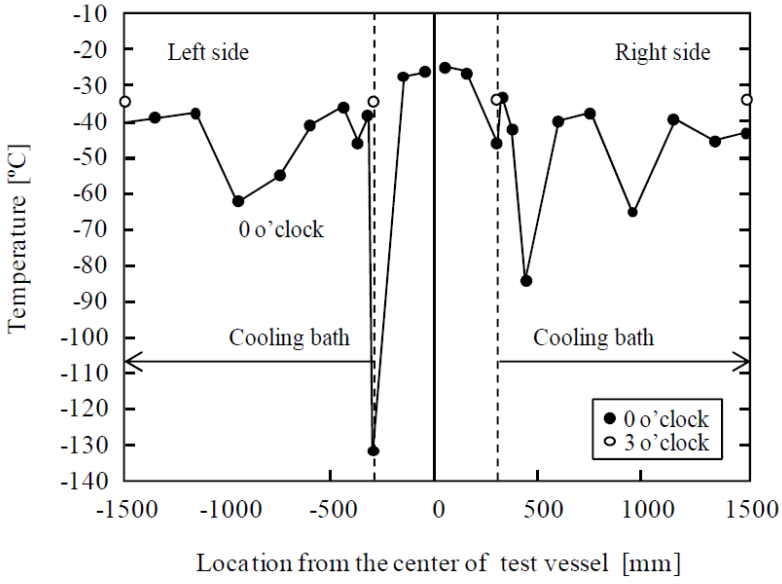

Figure 5.2 Temperature distributions of the full-scale pipe before the explosion

5.2. Improved DWTT and CVN test

After the full-scale pipe burst test, a non-deformed section was extracted from the pipe for further small-scale tests. JFE Steel Corporation developed a procedure for performing DWTT on thin-wall pipe [95], in which a flattened DWTT specimen with reinforcement plates is proposed to minimise the occurrence of buckling during impact. The specimens are flattened and two reinforcement plates are welded onto both ends of the specimen on the same side, as shown in Figure 5.3. The method is designed based on a pendulum-type machine.

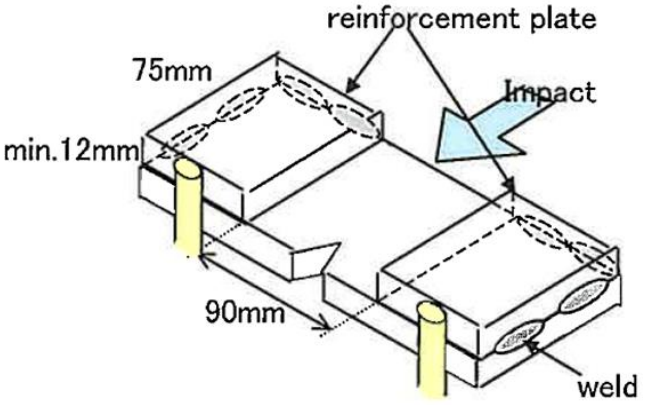

Figure 5.3 DWTT specimen with reinforcement plates [95]

The JFE specimen was modified in the present study. In order to increase stability, four reinforcement plates were welded onto the flattened specimens, at both ends and at both the front and back sides, as shown in Figure 5.4. The newly designed DWTT specimens were prepared from a 323.9x11.5mm Grade 60M pipe section. Gull-wing specimens were also tested to compare with the reinforced specimens and full-scale burst test results.

Six sets of both reinforced and gull-wing specimens were tested at the following temperatures: -20°C, -40°C, -45°C, -50°C, -60°C, and -70°C. The shear area percentage was measured immediately after the test according to API RP 5L3.

Figure 5.4 Reinforced and gull-wing DWTT specimens

Full-size 10x10x55mm Charpy specimens were used to obtain the ductile-brittle transition curve. The tests were conducted at 0°C, -20°C, -40°C, -60°C, -80°C, and -110°C, in accordance ISO 148-1 [96] (2mm striker). All specimens were conditioned at the designated temperature for ten minutes and struck within five seconds.

5.3. Experimental results

After the explosion in the full scale test, the length of the fracture propagation and the shape of the opening were measured on both the seam weld side and the pipe body side. The dimensions of the deformation of the tested pipe were measured and are presented in Figure 6.9 The initial notch propagated 1210 mm on the pipe body side and 1170 mm on the seam weld side, as shown in Figure 5.5.

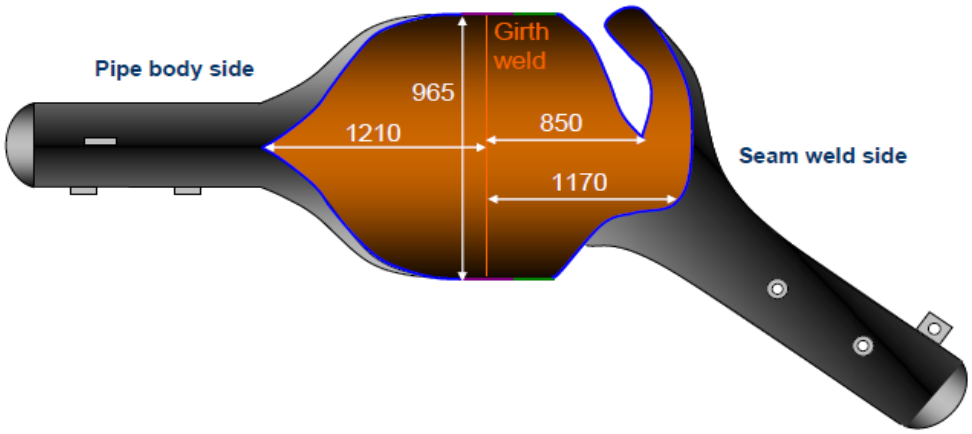

Figure 5.5 Illustration of appearance of the fracture in the tested pipe

Figure 5.6 Fracture propagation at the pipe body side (left) and seam weld side (right)

At the pipe body side, it was observed that a ductile crack initiated from the initial notch and propagated in a ductile manner for 1210 mm in a straight line along the pipe body, as illustrated in Figure 5.7 below:

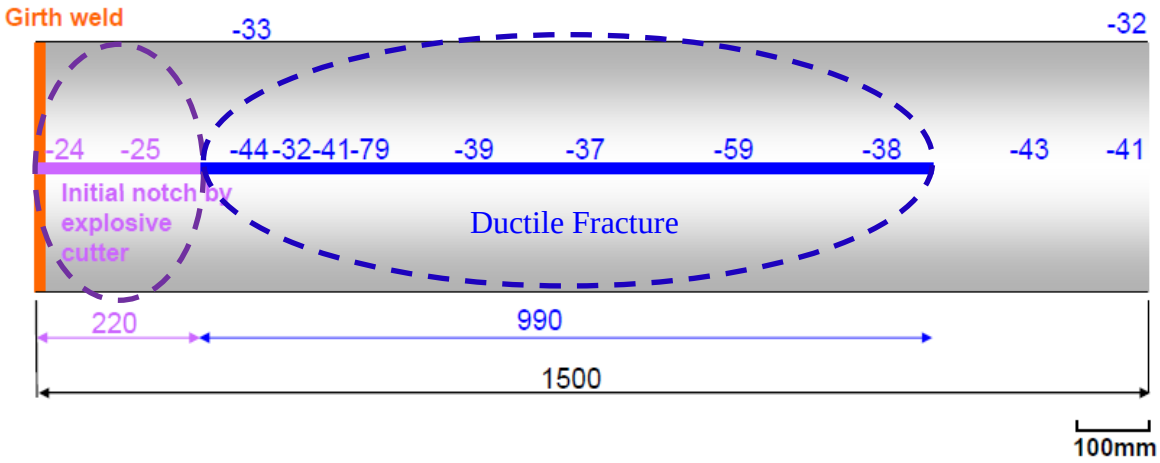

Figure 5.7 Illustration of fracture propagation on the pipe body side

On the seam weld side, a brittle crack began at the initial notch due to local over-cooling. The brittle crack propagated along the seam weld for 197 mm, then branched into the pipe body. These cracks propagated approximately 50 mm in the pipe body and then transitioned to a ductile manner. The transition from brittle fracture to ductile took place in the region where the temperature was between -35°C

and -43°C. The appearances of the fracture at the transition region and the ductile fracture region are presented in Figure 5.8.

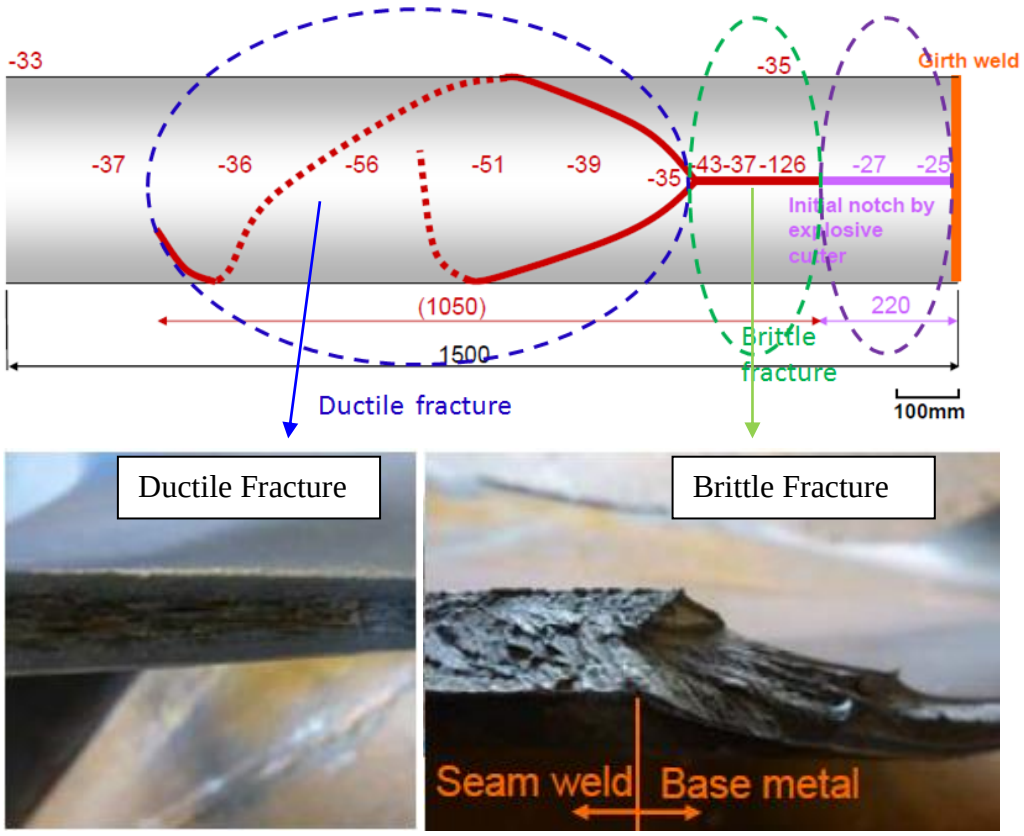

Figure 5.8 Illustration of the fracture propagation at seam weld side

The measured shear area percentages of the newly-designed, reinforced DWTT specimens and gull-wing specimens are plotted against test temperatures in Figure 5.9.

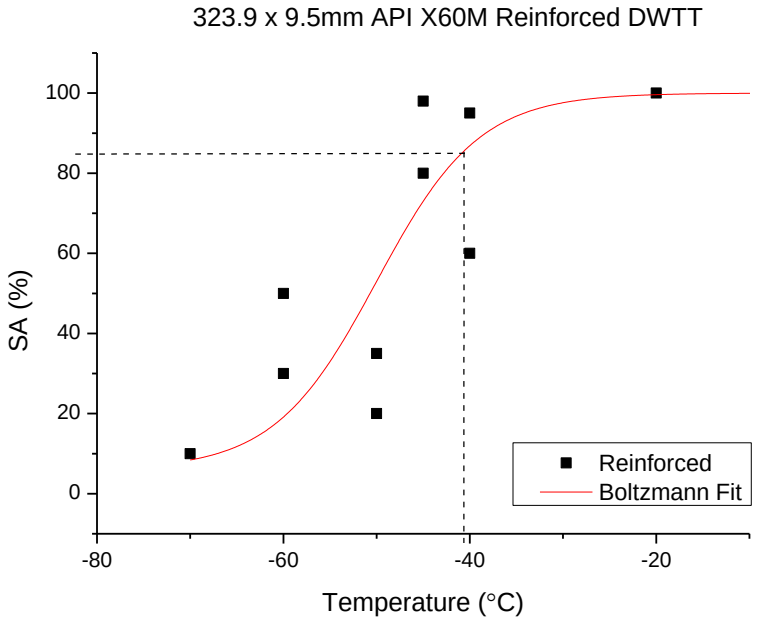

(a) Shear area percentage of reinforced specimens

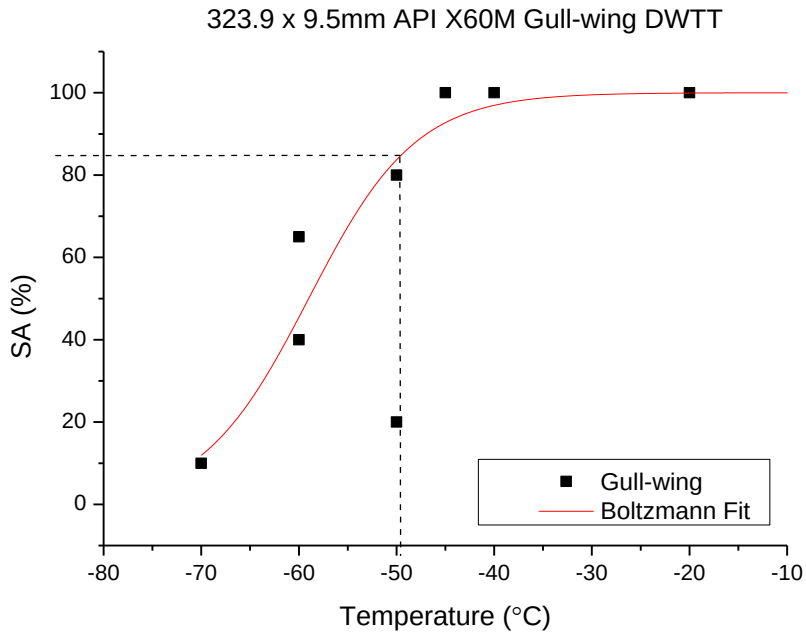

(b) Shear area percentage of gull-wing specimens

Figure 5.9 DWTT results

Wang *et. al* [97] suggested that the mathematic model of Boltzmann function is reliable for Charpy ductile-to-brittle transition curve fitting. This curve-fitting approach enforces a discipline in the interpretation of the test data, and the coefficients of the equation generating the fitted curve have a readily grasped physical meaning. Oldfield [98] also proposed a hyperbolic tangent function to generate the fitting curve for Charpy impact data, which is the same function as Boltzmann but in a different expression. The expression of the Boltzmann function is

$$A_{kv} = \frac{A_1 + A_2}{2} + \frac{A_1 - A_2}{2} \tanh\left(\frac{t - t_0}{\Delta t}\right) \tag{5.1}$$

where A_{kv} is the test response, A_1 is the upper shelf response, and A_2 is the lower shelf response. t is the test response corresponding temperature, t_0 is the transition temperature, and Δt is the transition range in which the response moves from one shelf to another.

The application of the Boltzmann curve fit was extended to generate a fitting curve for DWTT data.

The DBTTs obtained from Figure 5.9 were -41°C from the reinforced specimens and -49°C from the gull-wing specimens, which means that reinforced specimens provide a more conservative transition temperature than gull-wing specimens. It was observed that the tested gull-wing specimens at the upper shelf and some at the transition range exhibited buckling, while the reinforced specimens exhibited minimal buckling, as shown in Figure 5.10. Reinforced DWTT specimens generated a conservative transition temperature and successfully minimised occurrences of buckling. The better performance of the reinforced DWTT specimens could be attributed to the minimisation of buckling.

(a) Gull-wing DWTT specimens

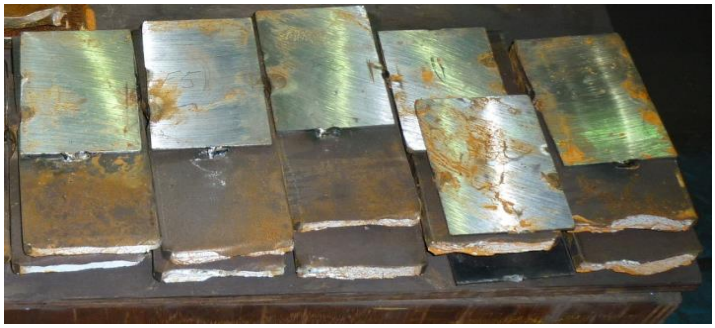

(b) Specimens with reinforced ends

Figure 5.10 DWTT specimens

Figure 5.11 shows the results of the CVN test. The transition temperature at 85% SA was observed to be -60°C, and the FPTT at 50% SA is -78°C which is much lower than those of the DWTT results. Relatively large scatterings were observed for the Charpy absorbed energy at some test temperatures.

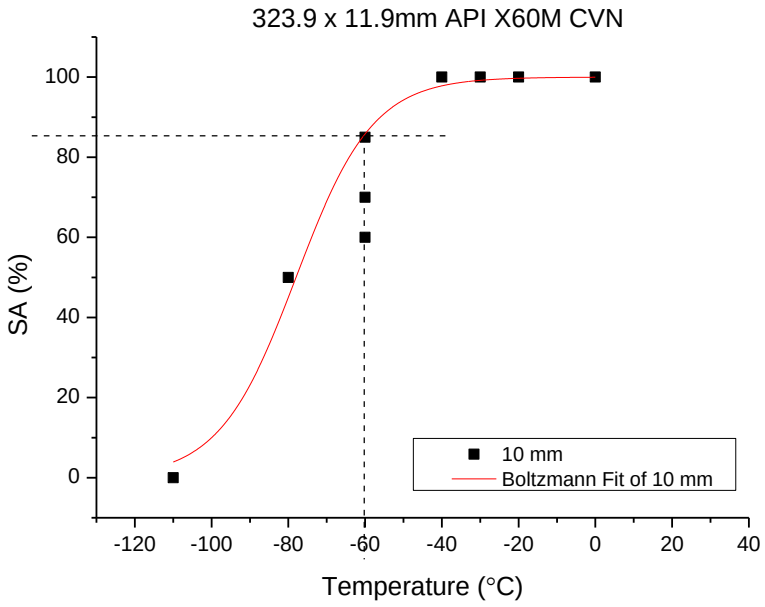

(a) Shear area percentage

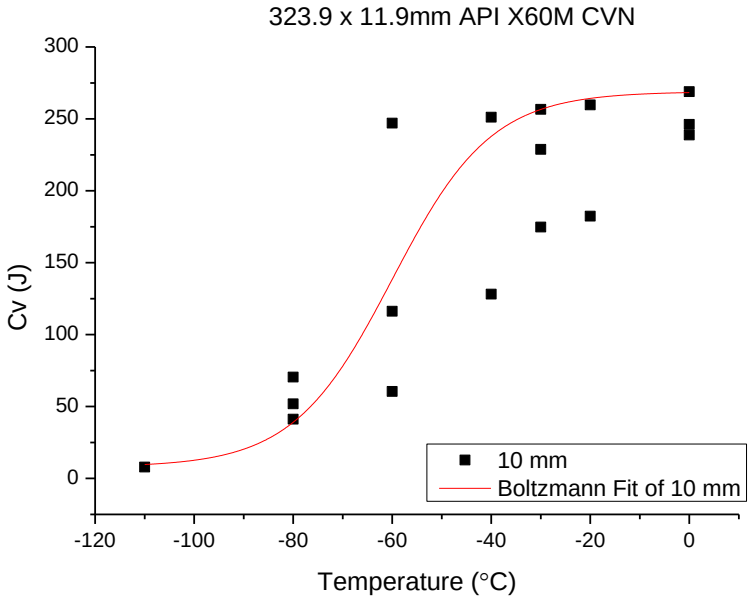

(b) Absorbed energy

Figure 5.11 CVN test results

The results of the CVNs and DWTTs are summarised and compared with full-scale test results in Figure 5.12. The transition temperature range of -35°C to -43°C

obtained from the full-scale test coincided with the -41°C from the reinforced DWTT specimens. The gull-wing DWTT result was slightly non-conservative, and the CVN result was far below that of the DWTTs and the full-scale test. The comparison confirms the validity of the Battelle DWTT 85% shear area criterion for small-diameter pipes and the capability of reinforced specimens to predict the transition temperatures of line pipe materials correctly.

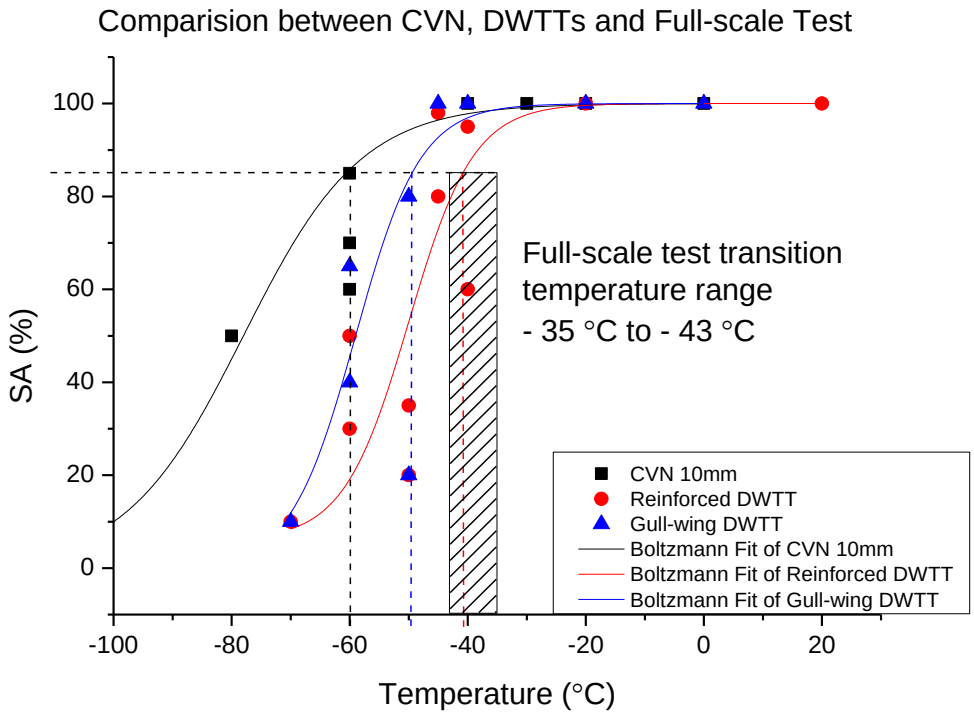

Figure 5.12 Comparisons of transition temperatures between CVN and DWTT small-scale and full-scale tests

5.4. Summary

The results and findings in this chapter show that Charpy transition curves are not conservative compare to DWTTs for both low- and high-grade, small-diameter line

pipes. DWTT is essential for predicting the DBTTs of small-diameter line pipes. Buckling was observed in the gull-wing DWTT specimens from the upper shelf and transition range, while newly designed reinforced specimens minimised buckling successfully and delivered a more accurate transition temperature prediction for full-scale line pipes. Therefore, it is recommended that the flattened DWTT specimen with reinforcement plates at the support points be used as alternative, especially for small-diameter thin-wall pipelines. However, this method will increase the practical difficulties encountered during DWTT and lead to extra works and costs. An easier and reliable alternative to the production test needs to be developed and validated.

CHAPTER 6

SPECIMEN THICKNESS EFFECT ON CHARPY ABSORBED ENERGY

Since its inception in the 1970s, the BTCM has been pivotal in determining the required material toughness to arrest running ductile fractures in line pipe steels. The BTCM provides a minimum required value of the Charpy absorbed energy as a function of pipe geometry, pipe grade, hoop stress, gas composition, and temperature [11].

Measuring the Charpy absorbed energy value (C*v*) starts with extracting a pipe specimen. For small-diameter and thin-walled pipes, this process encounters many difficulties. The standard CVN specimen has dimensions of 10x10x55 mm, which removes the possibility of specimen extraction from thin-walled pipe [12]. In such cases, specimens have a reduced thickness of 7.5, 6.7, 5.0, 3.3, or 2.5 mm [96].

The Battelle fracture model was developed using the absorbed Charpy energy when fracturing a two-thirds-thick specimen from low-toughness line pipe steels. When converting the absorbed energy of the sub-size specimen to a full-thickness specimen, a linear relationship is assumed. For example, a sub-size specimen with a thickness of 5.0 mm and C*v* of 50 J will assume a C*v* of 100 J for a full-thickness specimen. However, a large number of experiments have shown that a linear relationship only exists for low-toughness steel and the thickness correction varies

non-linearly for high toughness steel. It has been well known that when toughness values exceed 95 J, the BTCM produces non-conservative results[99]. The nonlinear thickness effect on absorbed energy has been identified as a factor leading to the deviation of the velocity of the observed fracture from the velocity predicted by the BTCM [49]. The implementation of the nonlinear thickness effect in the BTCM could provide a better prediction of the arrest toughness.

The published studies discussed in Chapter 2 indicated a power relationship of approximately 1.5 between Charpy absorbed energy and specimen thickness. However, a numerical investigation of the thickness effect has yet to be performed.

This chapter analyses the specimen thickness effect by comparing experimental data to numerical modelling. Charpy impact tests of three different thicknesses were carried out on X70 line pipe steel. A FEM was implemented to simulate Charpy tests with varying specimen thicknesses. The model looked at two cases of line pipe steels: clean and dirty. Clean steels have a smaller number of inclusions compared to dirty steels, giving clean steels a higher toughness value. More specifically, clean steels contain fewer impurity elements such as phosphorus, sulphur, oxygen, nitrogen, hydrogen, and inclusions [100]. For the remainder of this chapter, references to clean steels will conform to this definition, which will also be used to refer to modern steels. Dirty steels will refer to vintage line pipe steels that contain a higher impurity content when compared to clean, modern steels. A model was created based on experimental data gathered from a high-toughness, clean, line pipe steel mentioned above. The GTN model was implemented to characterise fracture behaviour. Studies have revealed that the initial void volume fraction of the material plays a key role in the observed power relationship.

6.1. Material properties and experimental procedure

All tensile and Charpy specimens were extracted from a grade API X70 line pipe with an outer diameter of 323.9 mm and wall thickness of 8.8 mm. The chemical composition is presented in Table 6.1. Tensile specimens were extracted from both

the circumferential (C) and longitudinal directions (L), while the Charpy specimens were only extracted from the circumferential direction (shown in Figure 6.1).

Table 6.1 Chemical composition of API X70 line pipe material

C%	P%	Mn%	Si%	S%	Ni%	Cr%	Mo%	Cu%
0.07	0.014	1.37	0.35	0.002	0.016	0.016	0.1	0.012
Ca%	AI%	Ti%	Nb%	Sn%	V%	N%	B%	
0.0012	0.038	0.018	0.06	<0.002	<0.003	0.0044	<0.0003	

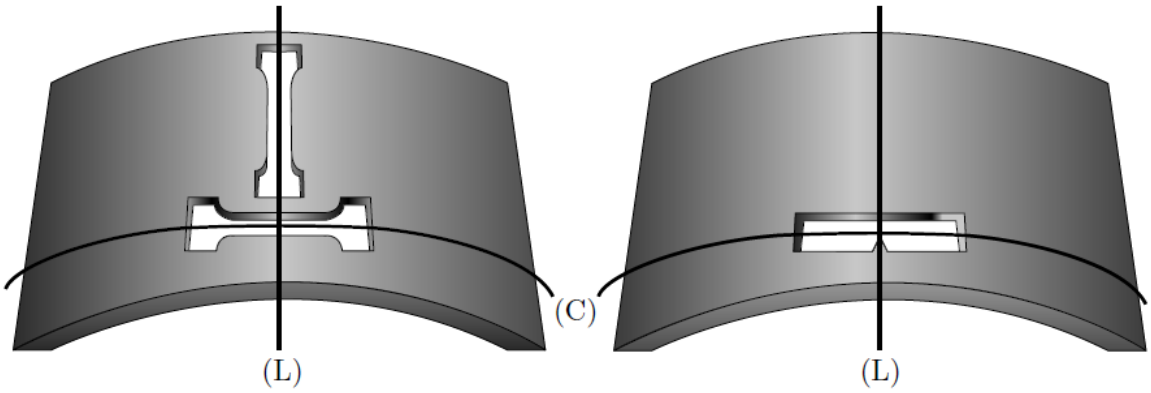

Figure 6.1 Depiction of the extraction of tensile and Charpy specimens in the longitudinal (L) and circumferential (C) orientations

Tensile tests were performed according to API 5L [101] with a strain rate predicated by ASTM A370 [90]. A stress rate of 52 MPa/s was applied to the upper yield point, and a maximum strain rate of 0.0008 /s was applied through the yield point and up to 5%. Thereafter, a maximum strain rate of 0.008 /s was applied. Sub-size Charpy specimens with thicknesses of 5.0, 6.7, and 7.5 mm were prepared according to ASTM A370 [90] and ISO 148-1 standard [96]. Charpy impact tests were carried out at ambient temperature, using an instrumented Charpy impact machine with a capacity of 600 J. The load was measured by a load cell installed on the striker and the displacement at the load point was measured by a transducer. The Charpy absorbed energy was then calculated from the determined load-displacement curve.

A 2mm-radius ISO striker was used for all tests. Load-deflection curves were collected for all specimens and are presented in this chapter.

6.2. Experimental results

The experimental results for the tensile and Charpy specimens are shown in Tables 6.2 and 6.3. Load-deflection curves were obtained for Charpy impact tests and are shown in Figure 6.2(a). Figure 6.2(b) shows the resulting absorbed energy values for the various specimen thicknesses. The relationship between absorbed energy (C*v*) and specimen thickness (B) is generally expressed as

$$Cv = k\mathrm{B}^{\mathrm{n}} \tag{6.1}$$

where *k* and *n* are material-dependent constants. From experimental evaluations an *n* value of 1.43 was observed, which coincides with previous evaluations described in Chapter 2.

Figure 6.2a shows that as specimen thickness increases, the peak load increases and the specimen deflects more before the maximum load is reached. Each specimen has approximately the same rate of loading and unloading; however, 6.7 and 7.5mm specimens display a plateauing effect before the load drops to zero.

Table 6.2 Tensile properties of X70 line pipe

Specimen Orientation/Number	**Yield Stress Rt0.5% (MPa)**	**Tensile Strength (MPa)**	**Uniform Elongation (%)**	**Total Elongation (%)**
C1	606	662	11	27
C2	611	658	11	29
L1	585	645	12	32

L2	573	641	13	30

Note: C = Circumference direction, samples were flattened for tensile test.
L = Longitudinal direction

Table 6.3 Absorbed energies of Charpy impact tests

Specimen number	**CVN thickness B (mm)**	**CVN energy (J)**	**Average CVN energy C*v* (J)**
1	7.5	164	165.4
2		168	
3		164	
4	6.7	124	128
5		128	
6		132	
7	5	84	91
8		96	
9		92	

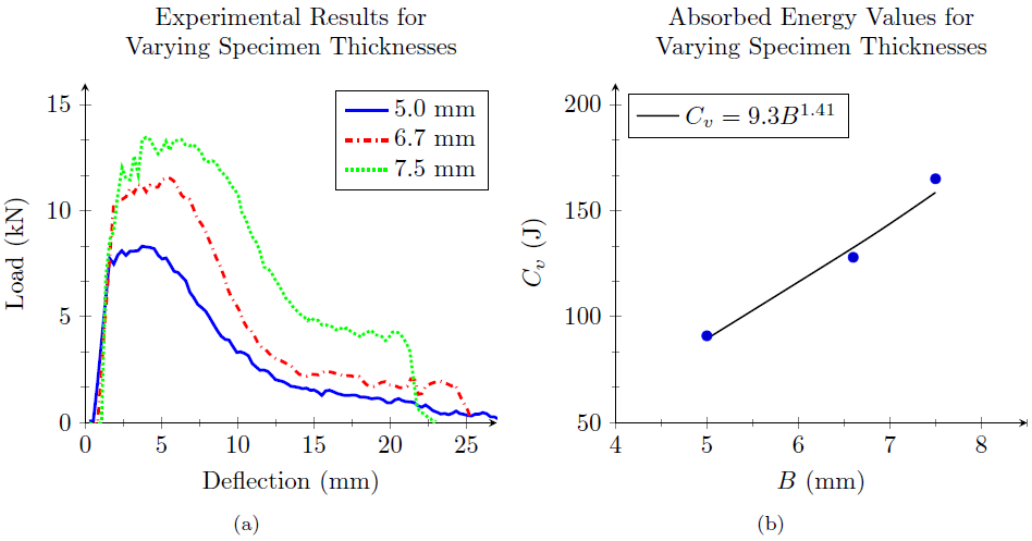

Figure 6.2 (a) Charpy impact test results. (b) Average absorbed energies for Charpy

impact tests with trend-line showing the power relationship

6.3. FEM model

The CVN tests with different specimen thicknesses were simulated using the commercial FEM software LS-DYNA with the built-in GTN model. The FE mesh made use of eight-node hexagonal elements, with the elements around the expected fracture zone being much finer than elsewhere to improve precision in this region. The model consisted of 302,700 elements and 322,462 nodes, as presented in Figure 5-3. Like all metals and alloys, line pipe steels contain inclusions and/or second-phase particles. During the course of plastic deformation, microvoids nucleate from these inclusions and second-phase particles. As the material continues to deform, microvoids coalesce and expand, creating the conditions for fracture. The GTN model applies the microscale behaviour of evolving voids to a macroscale model. The model does not explicitly account for individual void evolution but instead considers the voids to exist as a continuum in the material, causing the voids to behave like a material parameter.

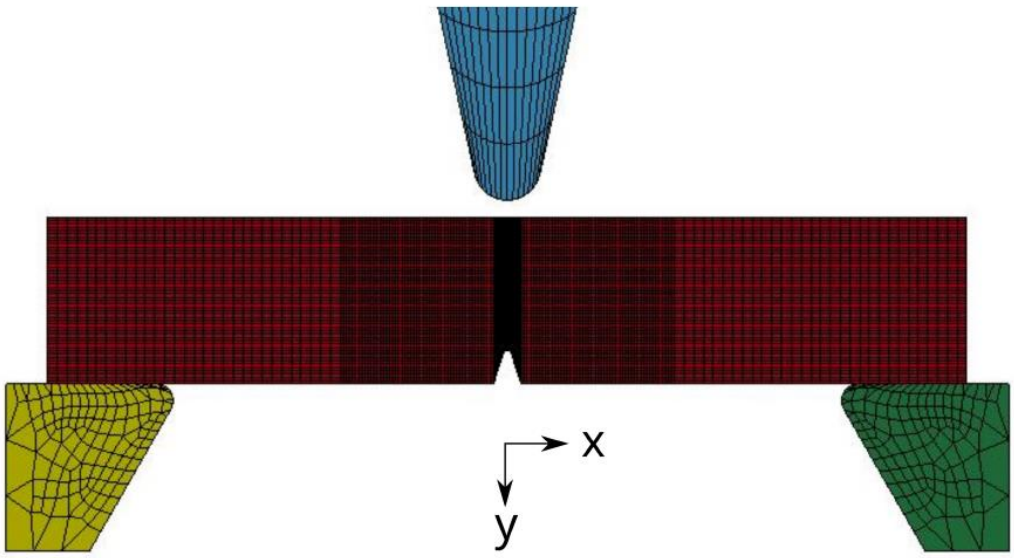

Figure 6.3 Depiction of the mesh of CVN specimen

In order to understand the effect of the specimen thickness on the absorbed energy, FE simulations were carried out to compare the behaviour of dirty line pipe steels to that of clean line pipe steels. This was done for Charpy specimen thicknesses of 5.0, 6.7, 7.5, and 10.0 mm. Generally, dirty steels are steels that have a large volume of inclusions and/or second-phase particles, with clean steels being the opposite. More specifically, dirty steels contain a larger volume percentage of sulphides (>0.007%) compared to clean steels (<0.005%) [102, 103]. To distinguish between dirty and clean steels in the simulations, two different initial void volume fraction (f_0) values were used. Numerical studies conducted by Yu *et al.* [104, 105] showed that a high volume of inclusions promotes the formation of voids.

The GTN model requires eight parameters—f_0, f_c, f_n, f_f, f_n, S_n, q_1, and q_2—which are described in Section 4.3.1. f_0 is the initial void volume fraction of the material. The implemented values, shown in Table 6.4, were used in the present simulations [106]. The parameters of the numerical model were determined by matching the load-deflection curve for the 7.5mm specimen. To match the numerical results with the experiment, initial void volume fraction and final void volume applied in the models were adjusted within the commonly applied range. These determined parameter values were then applied to models with specimen thicknesses of 6.7 and 5.0 mm.

Table 6.4 GTN parameter values used for dirty and clean line pipe steels

Parameters	Values
f_0 (Clean steel)	0.00015
f_0 (Dirty steel)	0.0015
f_c	0.013
f_n	0.0008
f_f	0.15
$\mathcal{E}_n$	0.3
S_n	0.10008
q_1	1.5

q_2	1.0

In order to account for strain rate effects, the GTN model provided in LS-DYNA allows for the stress-strain curves to be strain rate dependent. Because impact tests experience high strain rates, the model accounted for strain rate sensitivity by using the relationship

$$\sigma' = \sigma\left(1 + C\ ln\frac{\dot{\varepsilon}}{\dot{\varepsilon}_o}\right) \tag{6.2}$$

where σ' is the stress after applying the strain rate effect, σ is the true stress value provided by tensile results, $\dot{\varepsilon}$ is the strain rate, $\dot{\varepsilon}_o$ is the strain rate of the tensile test, and C is a constant determined empirically. The value of C was 0.0032. The phenomenological model was based on macroscopic parameters of typical conditions during high strain rate loading [107]. The stress-strain curves were generated at different strain rates by Eqn. (6.2) and implemented in the GTN model. The corresponding effective stress values were used for the numerical calculations. The strain rate range considered in the current study is 10^{-4} to 10^{4}/s.

6.4. Simulation results and discussion

Figure 6.4 shows the comparison of experimental results to numerical results for clean steels. It can be seen that simulation results are in good agreement with the experimental results for most parts of the curves except for the last stages of the tests (plateau regions). The numerical model does not provide the plateauing effect seen in the experimental results, which could be due to the limitations of the GTN model in describing the compressive stresses at the point of impact.

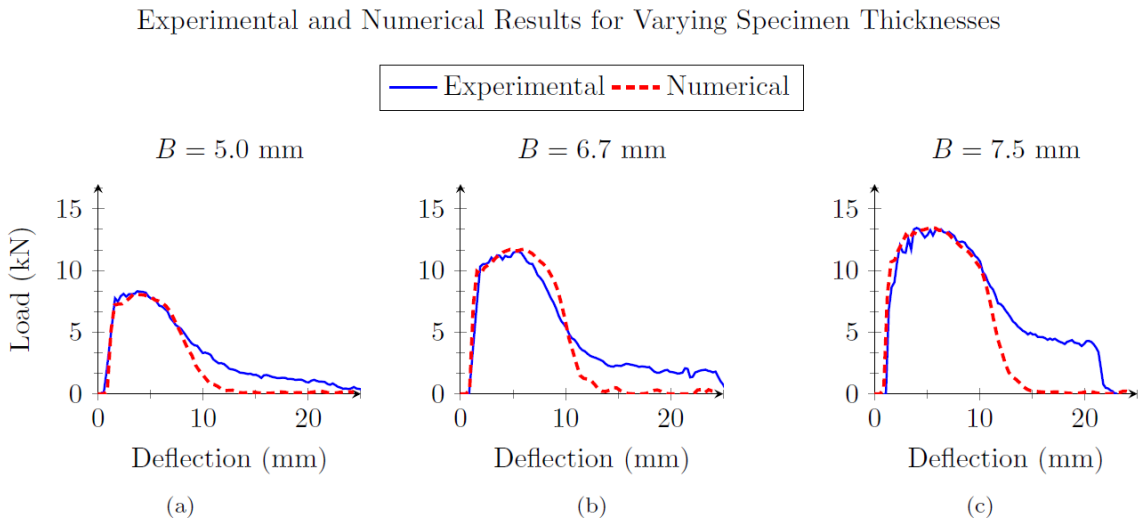

Figure 6.4 Comparison of experimental and numerical load-displacement curves

The load-deflection for dirty steel is presented in Figure 6.5(a). Fracture initiation for the dirty steel cases occurs at approximately the same amount of deflection, and the maximum load increases as the specimen thickness increases. The peak load for each thickness coincides with the point of fracture initiation. The area under each curve corresponds to the total Charpy absorbed energy for each specimen thickness. The determined energy values are 24, 32, 41, and 50 J for thicknesses 5.0, 6.7, 7.5, and 10.0 mm specimens, respectively. The absorbed energy/specimen thickness relationship is shown in Figure 6.5(b). The relationship of C*v* and B for dirty steels exhibits a near-linear *n* value of 1.06. This finding is consistent with the experimental observations regarding low-toughness steels discussed in Section 6.2.

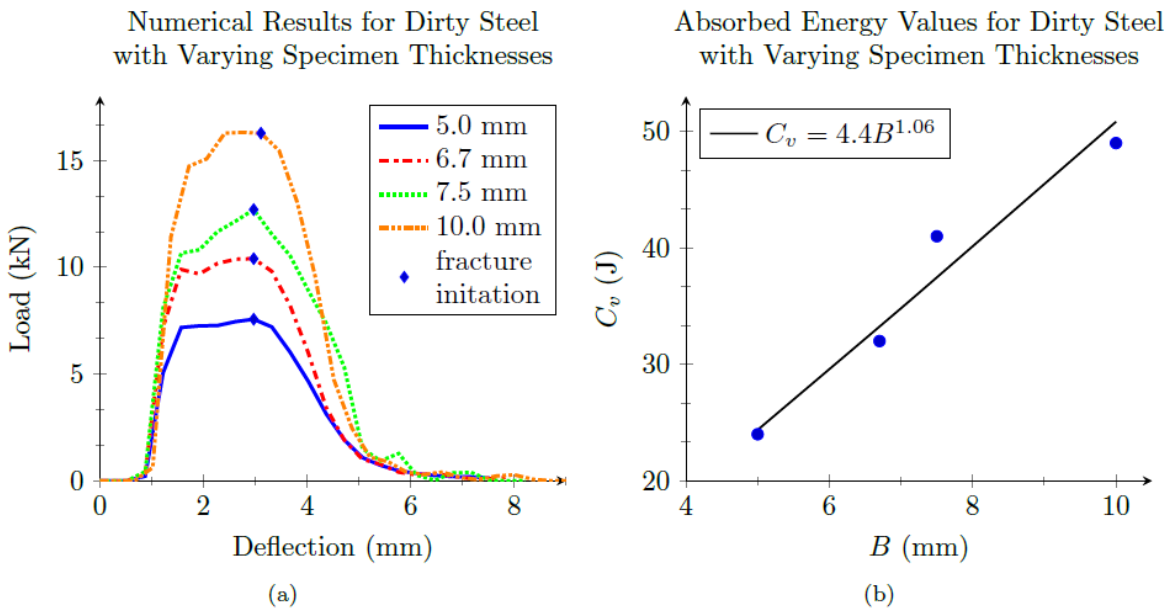

Figure 6.5 (a) Load-deflection curves for dirty steel (b) Absorbed energy /specimen thickness relationship for dirty steel

Figure 6.7(a) shows the fracture initiation position relative to the initial/undeformed fracture plane, A-A (Figure 6.6), of a 5.0mm dirty steel specimen. Fracture initiation occurs at a deflection of 2.87 mm and is represented by a blank region. The fracture initiates at a point approximately 0.16 mm above the notch tip. The von Mises stress is shown in Figure 6.7(b) in the deformed state. Two deformation zones are present along the fracture plane: one in the striker impact region and the other around the notch tip. Lateral contraction is observed along the specimen thickness, and it increases slightly as the fracture propagates further.

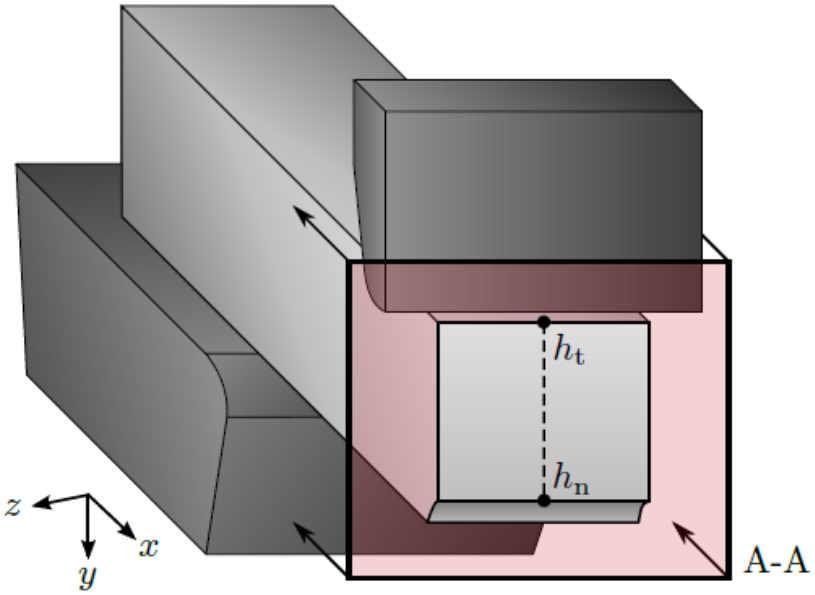

Figure 6.6 Geometry of the CVN impact test showing the cross-sectional area of fracture plane A-A and path *h*. h_n represent *h* at the notch tip and h_t represents *h* at the top or striker impact point of the specimen.

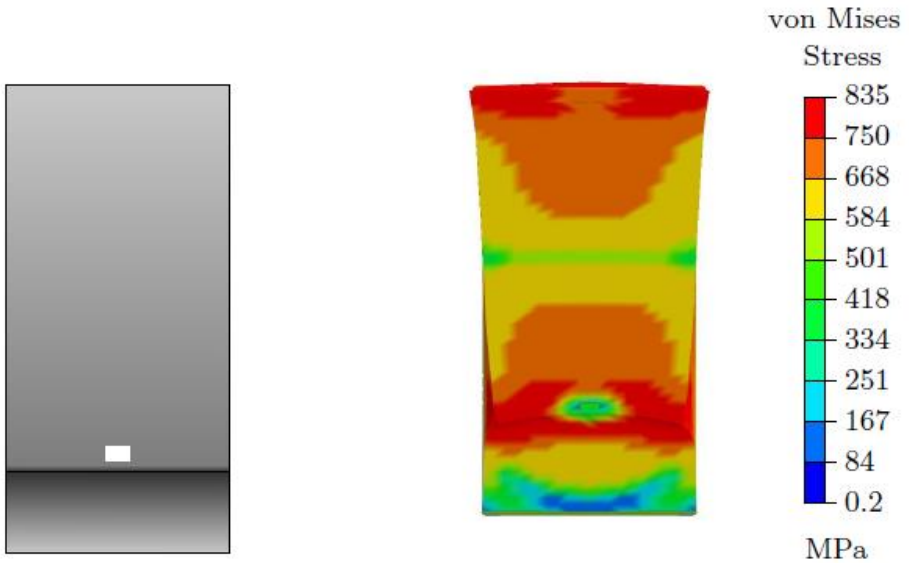

Figure 6.7 Fracture surface of dirty steel with a thickness of 5.0 mm: (a) starting fracture point with respect to un-deformed plane A-A; (b) deformed state

Similar to the 5.0mm specimen, the fracture in a 7.5mm dirty steel specimen initiates above the notch tip around 0.16 mm at a deflection length of 3.0 mm. A similar deformation state is also observed, as well as a similar amount of lateral contraction.

The load-deflection curves of clean steel specimens of four different thicknesses are shown in Figure 6.8(a).The obtained values of absorbed energy are 56, 97, 126, and 175 J for 5.0, 6.7, 7.5, and 10.0 mm, respectively. The relationship of C*v* to B gave a non-linear *n* value of 1.63.

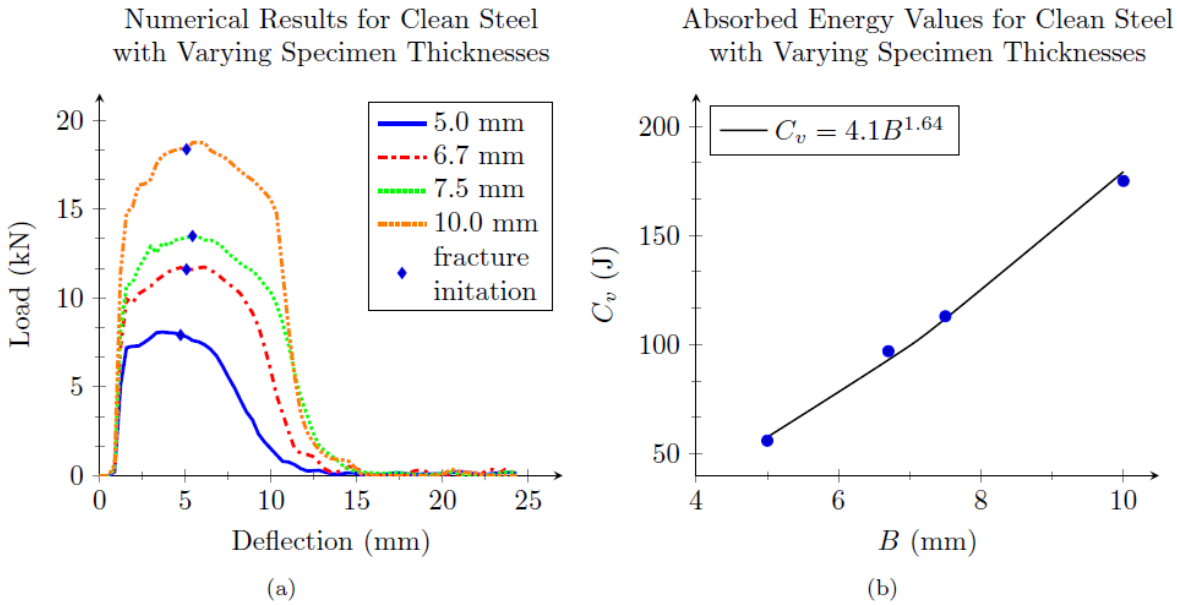

Figure 6.8 (a) Load-deflection curves for clean steel (b) Absorbed energy /specimen thickness relationship for clean steel

In the 5.0mm specimen, as illustrated in Figure 6.9(a), fracture initiates at a deflection of 4.7 mm, which is almost double the deflection of the dirty steel specimen. Because the initial void volume fraction of clean steel is much less than that of dirty steel, a larger amount of plastic deformation is required for voids to grow and coalesce. Unlike dirty steel, fracture initiates at the notch tip and not a distance from it.

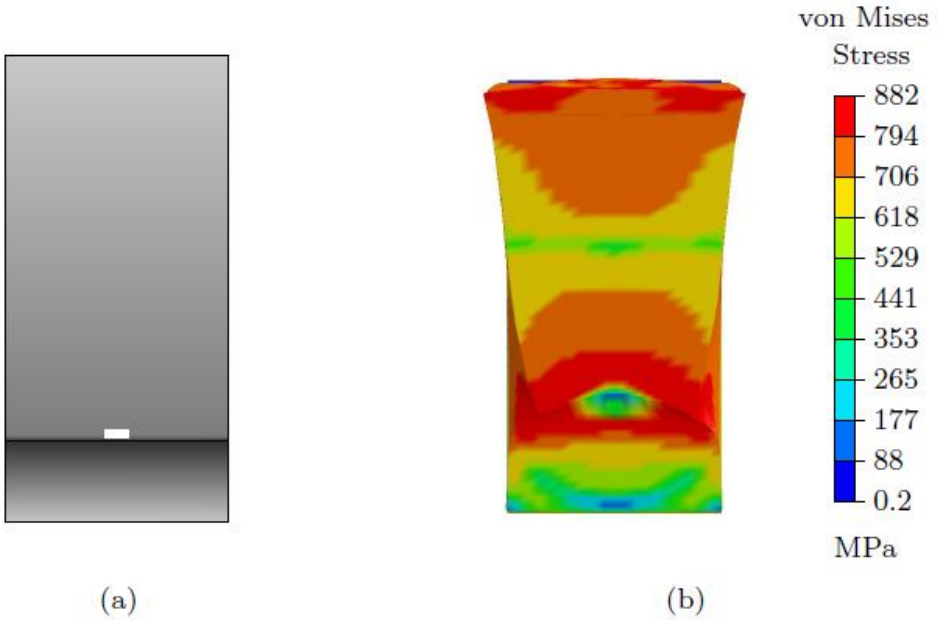

Figure 6.9 Fracture surface of clean steel with a thickness of 5.0 mm thickness: (a) starting fracture point with respect to un-deformed plane A-A; (b) deformed state

In the 7.5mm clean steel specimen, fracture initiates at a deflection of 5.33 mm, which is higher compared to 7.5mm dirty steel. Furthermore, the difference in the amount of deflection for fracture initiation in clean steel is higher than the difference for fracture initiation in dirty steel. A much more severe lateral contraction is observed in the clean steels compared with the dirty steels.

The distribution of void volume fraction and effective strain rate along path *h* immediately before fracture initiation in each dirty steel specimen is shown in Figure 6.10 for dirty steel. The deflection length of the 5.0mm specimen is 2.86 mm, and that of the 7.5mm specimen is 3.0 mm. For both specimens, the maximum void volume fraction occurs at a distance approximately 0.1 mm from the notch tip. The maximum effective strain rate occurs at around 0.33 mm and 0.20 mm from the notch tip in the 5.0mm and 7.5mm specimens, respectively. This causes the fracture initiation to occur away from the notch tip and promotes earlier fracture initiation in the 5.0mm specimen. Away from the fracture initiation region, the effective strain rate is far below the maximum strain rate. The peak values for void volume fraction and effective strain rate are similar in both dirty steel specimens prior to fracture initiation.

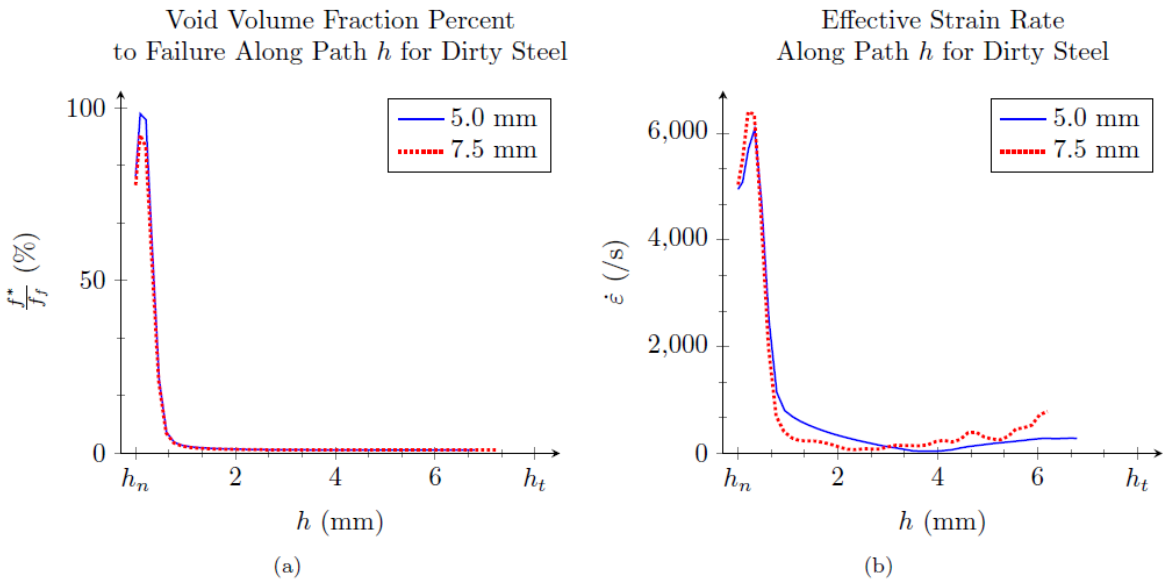

Figure 6.10 (a) Void volume fraction percent to failure along path *h* in dirty steel (b) effective strain rate along path *h* in dirty steel

Figure 6.11 shows the distribution of the void volume fraction and effective strain rate along path *h* immediately before fracture initiation in clean steel. The same time-step is observed to show the variation between void volume fraction and effective strain rate at different thicknesses. The deflection shown for both cases is 4.73 mm, which is immediately before fracture initiation in the 5.0mm specimen. The void volume fraction is at maximum at the notch tip, corresponding to the fact that fracture initiated at this point. The void volume fraction of the 7.5mm specimen is a quarter of the void volume fraction of the 5.0mm specimen at the notch tip, and the maximum effective strain rate of the 7.5mm specimen is approximately two-thirds that of the 5.0mm specimen. This results in earlier fracture initiation in the 5.0mm specimen compared to the 7.5mm specimen.

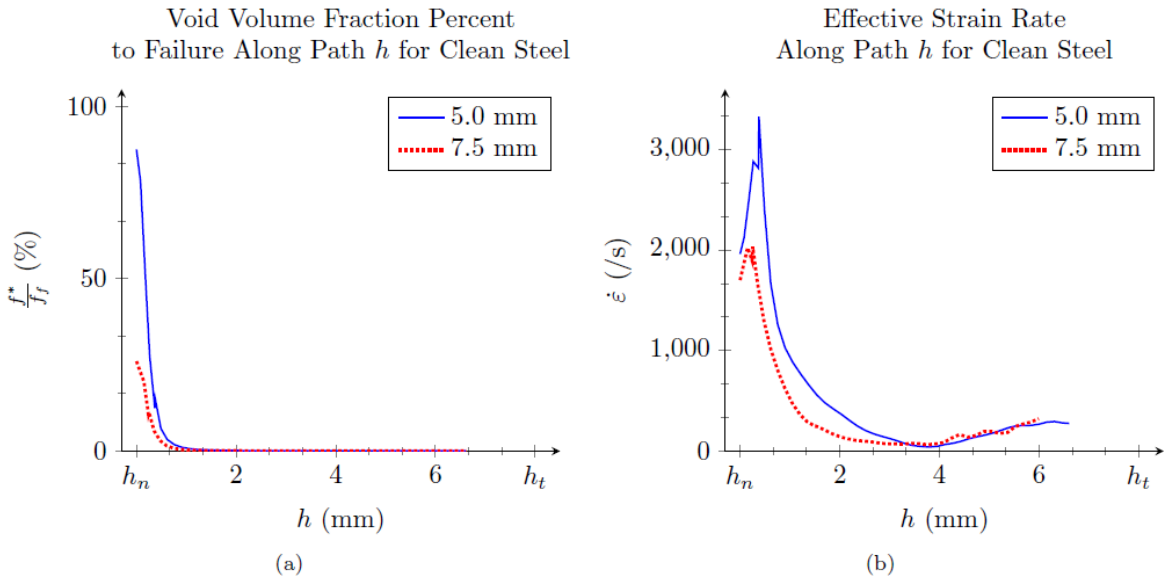

Figure 6.11 (a) Void volume fraction percent to failure along path *h* in clean steel (b) effective strain rate along path *h* in clean steel

Given that the initial void volume fraction in the 7.5mm clean specimen is well below that of the dirty steel specimen, clean steel requires much more deformation to reach a critical value of void volume fraction. In other words, the 7.5mm clean specimen requires a longer time to reach fracture initiation. The delay in fracture initiation between specimen thicknesses of clean steel is significantly longer than with dirty steel.

Fracture initiation depends on the initial void volume fraction (f_0), and the void growth rate is controlled by the strain rate in the GTN damage model. The dirty steel specimens have a larger initial void volume fraction, and only a small void growth rate is required to reach the critical void volume fraction for fracture initiation. As fracture initiates at the early stage of CVN deflection in dirty steel, the effect of specimen thickness on strain rate and then on void growth is insignificant. Therefore, fracture initiates at nearly the same deflection in dirty steel specimens of different thicknesses. As a result, the energy consumed prior to fracture initiation is linearly related to specimen thickness. After fracture initiation, the fracture propagates through the specimen. Fracture propagation energy depends on the area of the fracture surface or thickness, resulting in a relationship between linear absorbed energy and specimen thickness in dirty steel specimens.

The initial void volume fraction of clean steels is smaller than that of dirty steels. Thus, greater amounts of void growth and plastic deformation are required to reach a critical void fraction and initiate fracture. Specimen thickness affects the strain rate for large deformations significantly; thinner specimens have a larger effective strain rate. Because void growth is influenced by strain rate, thinner specimens initiate fracture at an earlier stage of deformation compared with thicker specimens. The delayed fracture initiation in thicker specimens significantly increases fracture initiation energy, and therefore, total energy. This creates the power relationship between Charpy absorbed energy and specimen thickness in high-toughness steels.

6.5. Implementation of exponential CVN energy /thickness relationship in BTCM

In the BTCM the fracture propagation velocity is usually expressed in analytical form as discussed in Section 2.3. The Battelle fracture velocity model was historically developed using the CVN absorbed energy obtained by breaking two-thirds-thickness CVN specimens. The two-thirds-thickness CVN energy was converted to full thickness CVN energy by assuming that the specific energy of fracture (R) was a constant of the material and independent of the scale.

Chapters 2 and 5 have shown that CVN energy does not increase proportionally to the specimen thickness, but follows a power law relationship in modern clean steels. This indicates that the specific energy is not a constant independent of specimen thickness. By considering that the Battelle fracture model was calibrated based on two-thirds CVN tests, Eqns. (2.1) and (2.2) in the form should be presented in Eqns. (6.3) and (6.4) respectively:

$$V = C\frac{\sigma_f}{\sqrt{R_{2/3}}}\left(\frac{P_d}{P_a} - 1\right)^m \tag{6.3}$$

$$P_a = \frac{2\sigma_f t}{3.33\pi r} arccos\left(e^{-\left(\frac{\pi R_{2/3} E}{24\sqrt{rt}{\sigma_f}^2}\right)}\right) \tag{6.4}$$

$$R_{2/3} = \frac{C_{v2/3}}{A_{2/3}} \tag{6.5}$$

where $R_{2/3}$, $C_{v2/3}$ and $A_{2/3}$ are the specific energy, CVN absorbed energy and the cross sectional area of a two-thirds CVN specimen, respectively.

The published works and experimental and simulation works presented in Chapter 5 showed that a power relationship of approximately 1.5 can be representative of modern clean steels. The following equations provide the relationship between the specific energy of a two-thirds-size CVN specimen and a full-size CVN specimen.

$$C_{v1/1} = k\, B_{1/1}^{1.5} \rightarrow R_{1/1} = \frac{k}{l}\sqrt{B_{1/1}} \tag{6.6}$$

$$C_{v2/3} = k\, B_{2/3}^{1.5} \rightarrow R_{2/3} = \frac{k}{l}\sqrt{B_{2/3}} \tag{6.7}$$

where the subscripts *1/1* and *2/3* refer to full-size and 2/3 size CVN specimens respectively, *k* is a constant and *l* is the length of the unbroken ligament of the CVN specimen (i.e. 8mm).

Substituting *k/l* from Eqn. (6.6) into Eqn (6.7) gives the relationship between the specific energy of a two-thirds CVN specimen and the energy of the full size specimen:

$$R_{2/3} = \sqrt{\frac{t_{2/3}}{t_{1/1}}}\, R_{1/1} = \sqrt{\frac{2}{3}}\, R_{1/1} \tag{6.8}$$

Substituting Eqn. (6.8) in Eqns. (6.3) and (6.4) provides the modified Battelle fracture velocity model based on the specific energy of the full-size CVN, using a 1.5-power law relationship on the thickness, namely

$$V = C\frac{\sigma_f}{(2/3)^{1/4}\sqrt{R_{1/1}}}\left(\frac{P_d}{P_a} - 1\right)^m \tag{6.9}$$

$$P_a = \frac{2\sigma_f t}{3.33\pi r} arccos\left(e^{-\left(\frac{\pi\sqrt{2/3}R_{1/1}E}{24\sqrt{rt}\sigma_f{}^2}\right)}\right) \tag{6.10}$$

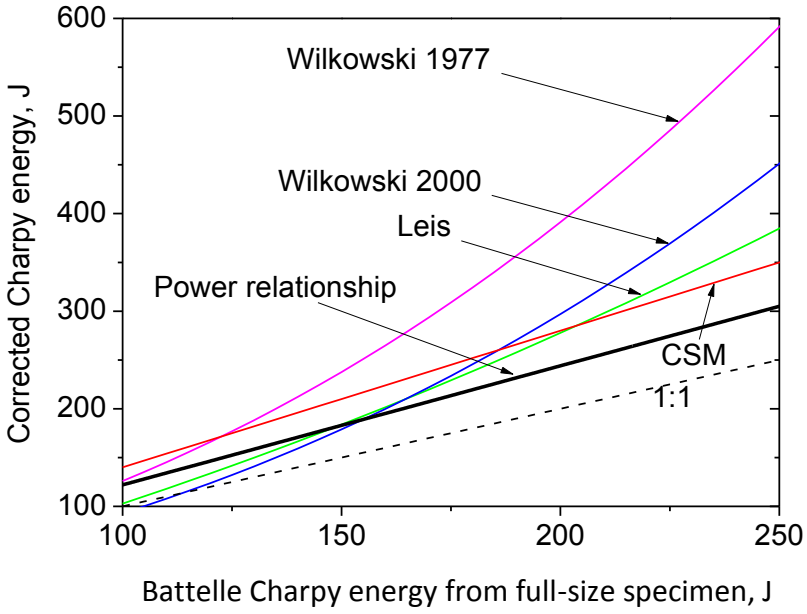

Figure 6.12 Comparison of different correction approaches

Eqns. (6.9) and (6.10) are used to calculate the arrest toughness. The results are called the corrected CVN energy using the power relationship. Figure 6.12 plots the corrected CVN energy as a function of the Battelle CVN energy for different correction approaches.

In the Battelle CVN energy range of 100 ~ 150 J, the corrected CVN energy by the power law relationship is located between the CSM prediction and predictions of the Leis model and the Wilkowski 2000 model. Note that the Battelle CVN energies for most of the full-scale fracture propagation tests of high toughness steels are within the range of 100 ~ 150 J.

The above finding indicates that the correction model developed in the current work

is comparable to the major popular correction approaches. It should be noted that other correction approaches were developed based on the curve fitting of full-scale fracture propagation test data.

6.6. Summary

The findings from the experimental and numerical studies in this chapter are summarised as follows:

- Both experimental results and numerical results show that in dirty steel, there is a near-linear relationship between CVN absorbed energy and specimen thickness, while a power relationship is observed in clean steel.

- In dirty steel specimens, a small amount of void growth is needed to reach a critical void volume fraction. The fracture in dirty steel specimens is initiated at an earlier stage of deflection, where the strain rate does not have a significant effect on void growth. This results in fracture initiating at nearly the same deflection in specimens of different thicknesses. The energy consumed prior to fracture initiation is linearly related to specimen thickness.

- Because clean steel has a smaller void volume fraction, more void growth is required to reach the critical value for fracture initiation. Fracture is initiated at a stage with larger deformation, where the strain rate has a significant effect on void growth. Thinner specimens exhibit larger strain rates, which initiate fracture at an earlier stage of deformation than thicker specimens. Therefore, fracture initiates at different deflection lengths in specimens of different thickness.

- The delayed fracture initiation in the thicker specimens increases fracture initiation energy significantly, and thus, the total energy. This leads to the

power relationship between energy and specimen thickness in high-toughness steels.

- The 1.5 power relationship between Cv and B is implemented in the BTCM. This correction approach stems from a new understanding of the specimen thickness effect on CVN energy in modern clean line pipe steels. Furthermore, the prediction from the BTCM with the exponential Cv–B relationship is comparable to other major correction approaches, but without resorting to the use of a correction factor or the term ‘fudge factor’ that is used in Australian standards.

CHAPTER 7

CORRELATION OF TRANSITION TEMPERATURES BETWEEN DWTT AND CVN TEST

The DWTT 85% shear area criterion is the approach to pipeline brittle fracture control recommended by current pipeline standards. As stated in Chapter 2, the major current pipeline specifications, introduced for practical reasons in 1969, require DWTT on pipes with a diameter of DN500 or higher. In the absence of DWTT requirements for smaller-diameter line pipe, pipe manufacturers often refuse to provide DWTT testing when filling small orders of smaller-diameter pipes. However, practical experiences have proved that small-diameter pipes are not immune to propagating brittle fracture. The CVN transition curve is offered as an alternative for small-diameter pipes in many standards. Different from the DWTT 85% SA transition temperature criterion, CVN transition temperature at 50% SA is widely served as a measure of the fracture propagation resistance (or FPTT) [108]. The other approach is to correct the CVN transition curves for differences in specimen-to-pipe wall thickness to obtain the 85% SA transition temperature. The thickness correction was developed in the X52 and X60 line pipe in 1980s [16]. In this chapter, transition curves from Charpy with various thicknesses and DWTTs with different specimen configurations were obtained and compared.

7.1. Material properties and experimental procedures

Chapter 4 described DWTT tests that were carried out on API 5L X42 and API 5L X70 HFERW seam welded pipes, while Chapter 5 described DWTT tests that were conducted on API 5L X60M HFW line pipes. In the current chapter, these pipe materials were used to determine the DBTTs using sub-size CVN specimens. The DBTTs from the Charpy specimens were compared with the results from previous DWTT tests. Table 7.1 summarises the specimen types from which the transition temperatures were obtained and compared in this chapter.

All Charpy specimens were extracted from the pipe circumferential direction. Charpy specimens of various thicknesses were prepared according to the ASTM A370 [90] and ISO 148-1 standards [96]. Charpy impact tests were carried out at ambient temperature, using an instrumented Charpy impact machine with a capacity of 600 J. The load was measured by a load cell installed on the striker and the displacement at the load point was measured by a transducer. The Charpy absorbed energy was then calculated from the determined load-displacement curve. A 2 mm radius ISO striker was used in all tests.

Table 7.1 Summary of specimen types used for DBTT comparisons

<table>
<tr><th>Pipe OD
(mm)</th><th>Wall Thickness
(mm)</th><th>Pipe
Grade</th><th>Charpy Specimens (Current Chapter)</th><th>DWTT Specimens (Previous Chapters)</th></tr>
<tr><td>219</td><td>8.2</td><td rowspan="5">API 5L X42</td><td>6.7mm (2/3)</td><td rowspan="8">Gull-wing DWTT Chapter 4</td></tr>
<tr><td rowspan="3">323.9</td><td rowspan="3">9.5</td><td>7.5mm (3/4)</td></tr>
<tr><td>6.7mm (2/3)</td></tr>
<tr><td>5.0mm (1/2)</td></tr>
<tr><td>406.4</td><td>12.7</td><td>7.5mm (3/4)</td></tr>
<tr><td rowspan="2">323.9</td><td rowspan="2">8.8</td><td rowspan="2">API 5L X70</td><td>7.5mm (3/4)</td></tr>
<tr><td>6.7mm (2/3)</td></tr>
</table>

			5.0mm (1/2)	
323.9	11.5	API 5L X60M	10.0mm (Full)	Gull-wing DWTT Chapter 5

Sub-size Charpy specimens (7.5, 6.7, and 5.0 mm) of 323.9 x 9.5mm X42 and 323.9 x 8.8mm X70 line pipes were tested. For 219 x 8.2mm X42 and 406.4 x 12.7mm X42 line pipes, only 6.7mm and 7.5mm specimens were tested, respectively. A full-thickness Charpy specimen was tested for 323.9 x 11.5 X60M line pipe, which was provided by JFE. The specimens were tested over a temperature range of -194 to 23°C to obtain the Charpy ductile–brittle transition curves.

7.2. Experimental results

The CVN tests were conducted using various specimen sizes of API X70 line pipes with a diameter of 323.9 mm and a thickness of 8.8 mm. The absorbed energy for specimen thicknesses 7.5 mm, 6.7 mm, and 5.0 mm were plotted as a function of test temperature as shown in Figure 7.1. Specimen size exhibits a significant influence on absorbed energy. As the thickness decreases, the transition temperature from the upper shelf to the lower shelf decreases as well. However, the difference is not significant.

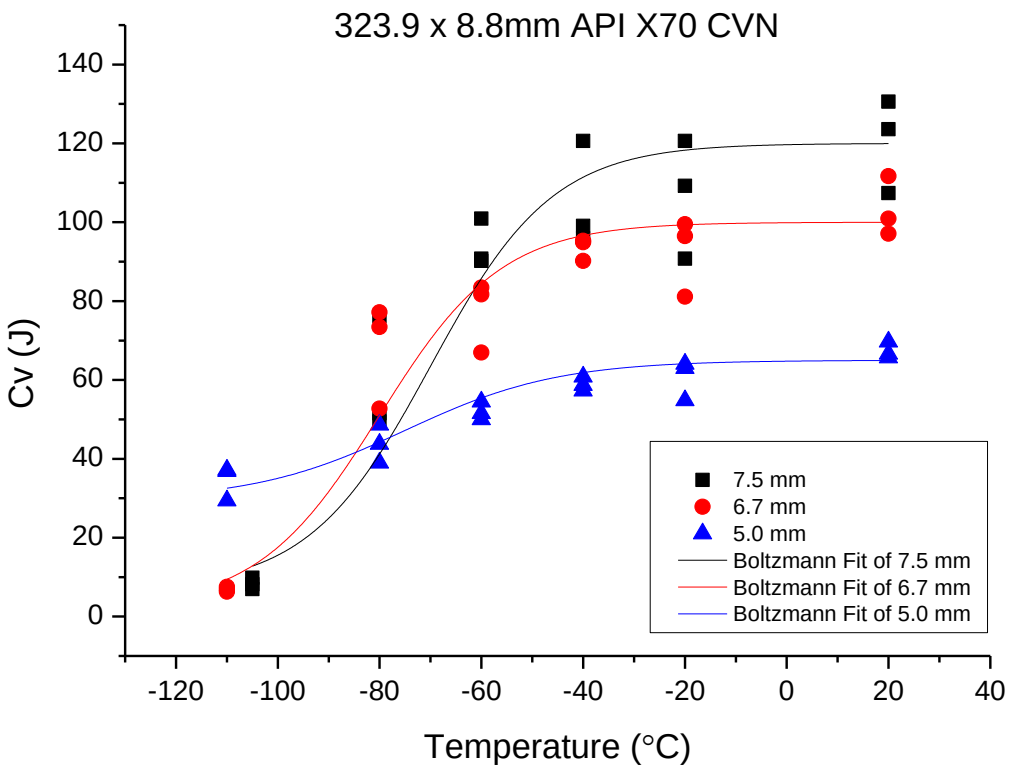

Figure 7.1 Charpy energy vs. temperature, 323.9 x 8.8mm X70 line pipe

The Charpy shear area percentage values were measured and are presented in Figure 7.2. Although the data points showed some scattering, a clear trend of shear to cleavage transition is observed. It can be seen that as specimen thickness decreases, transition temperature increases; this trend is consistent with the energy transition curves. The 85% transition temperatures are observed to be -78°C, -75°C, and -71°C for specimen thicknesses 7.5, 6.7, and 5.0 mm at 85% SA, respectively. The FPTT are observed to be -88°C, -84°C, and -86°C for specimen thicknesses 7.5, 6.7, and 5.0 mm at 50% SA, respectively. According to the results presented in Chapter 4, the 85% transition temperatures obtained from DWTTs were -51°C and -55°C for gull-wing and flattened specimens, as shown in Figure 7.3.

All of the Charpy transition temperatures are lower than the DWTT temperatures; in other words, the 50% Charpy shear area criterion is much less conservative compared to DWTT, using either gull-wing or flattened specimens.

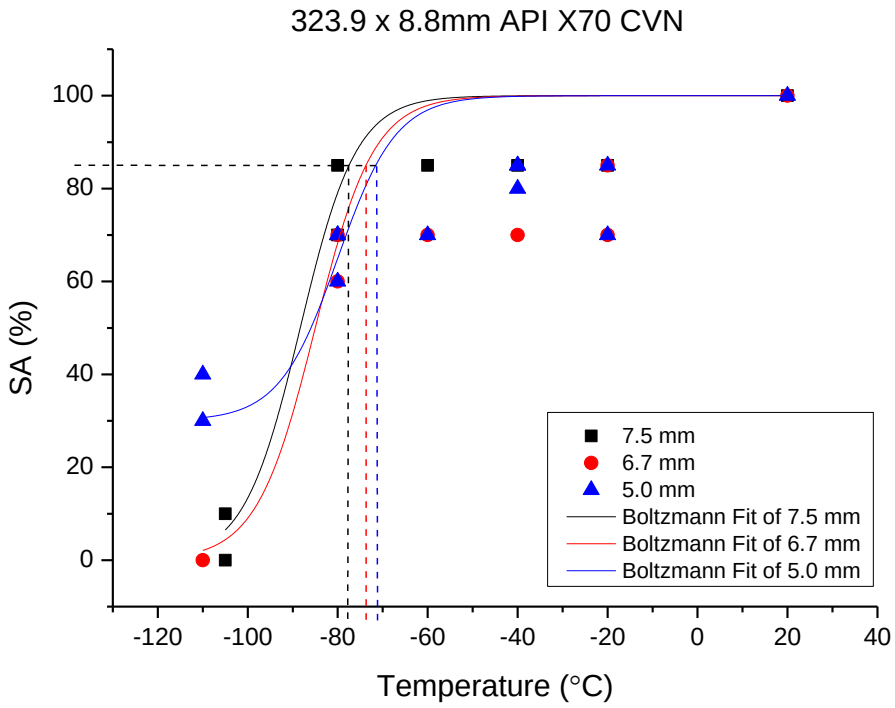

Figure 7.2 Charpy SA% vs. temperature, 323.9 x 8.8mm X70 line pipe

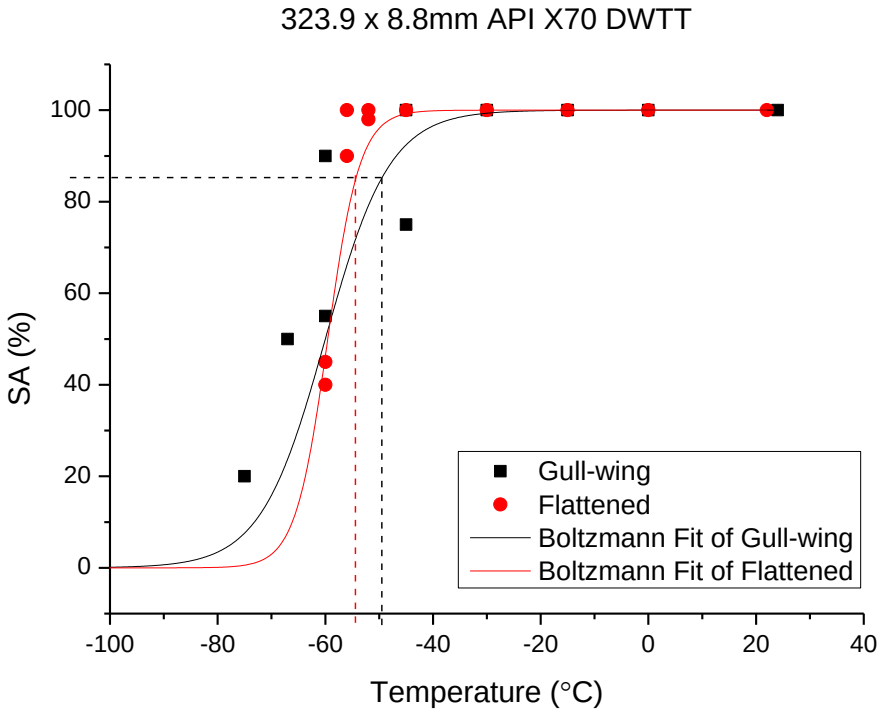

Figure 7.3 DWTT SA% vs. temperature, 323.9 x 8.8mm X70 line pipe

CVN tests and DWTTs using gull-wing specimens were also conducted on API X42 line pipe material with a diameter of 323.9 mm and a thickness of 9.5 mm. The Charpy energies obtained from specimens with thicknesses of 7.5, 6.7, and 5.0 mm are plotted against test temperatures in Figure 7.4. The energy transition curve findings for the X42 line pipe are similar to the findings obtained for X70 line pipe. As the specimen thickness decreases, transition temperature decreases as well.

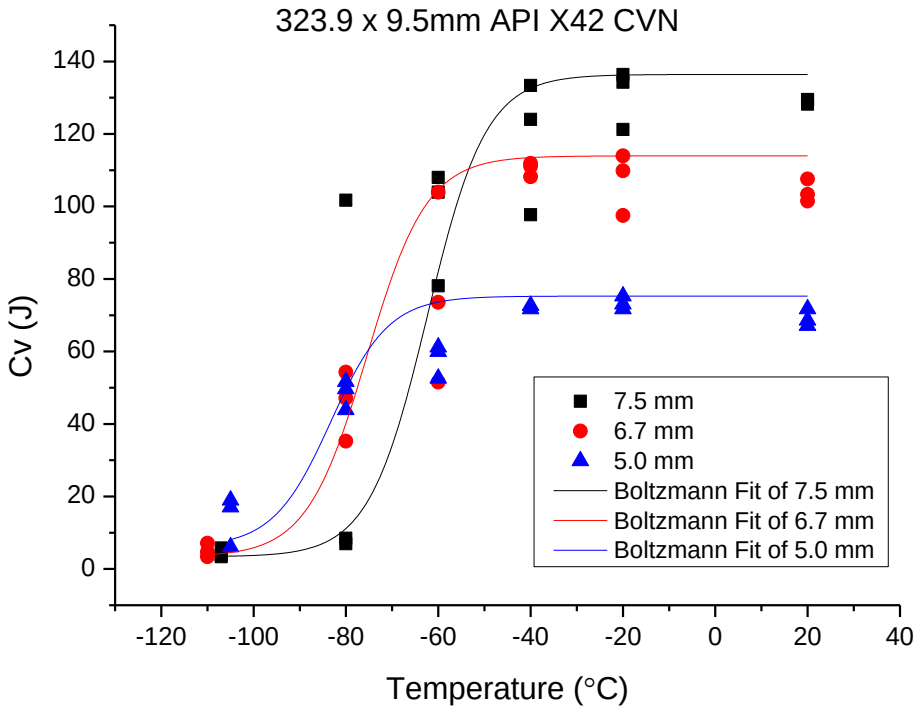

Figure 7.4 Charpy energy vs. temperature, 323.9 x 9.5mm X42 line pipe

However, the shear area transition curves show a different trend. As the specimen thickness decreases from 7.5 to 6.7 mm, the transition temperature at 85%SA decreases slightly, from -64°C to -65°C. When the specimen thickness decreases further, to 5.0 mm, the transition temperature also decreases further, to -68°C, as demonstrated in Figure 7.5. The trend is opposite to the X42 energy transition curves and all transition curves for the X70 line pipe material. The FPTT are observed to be -75°C, -77°C, and -80°C specimen thicknesses 7.5, 6.7, and 5.0 m at 50% SA, respectively. Again, all the Charpy FPTTs are much lower than that of the gull-wing DWTT specimens, which is -44°C, as shown in Figure 7.6.

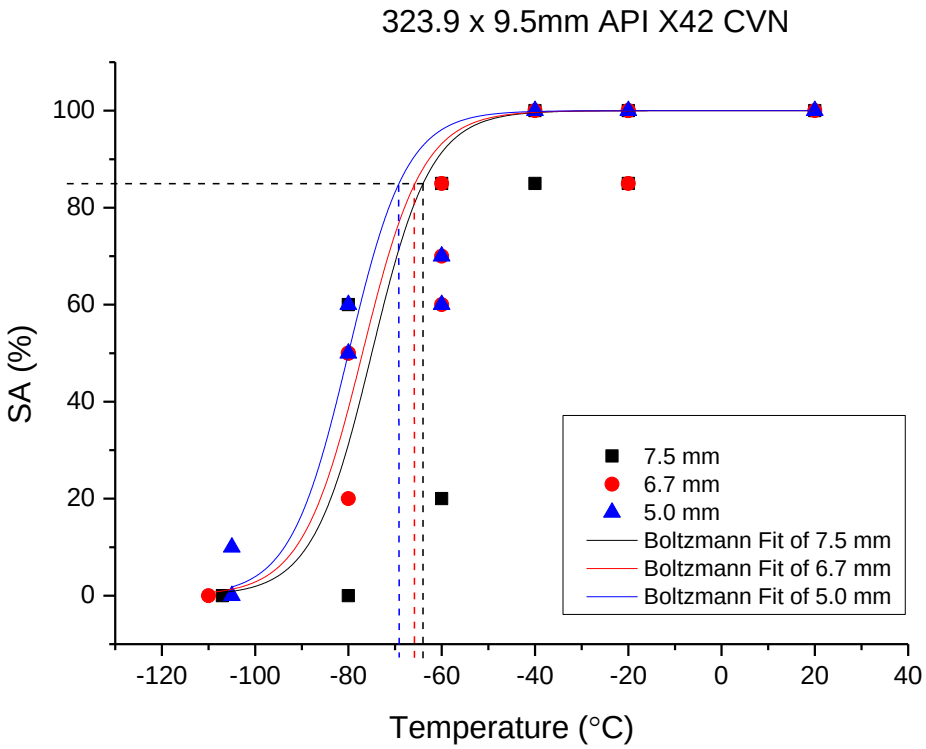

Figure 7.5 Charpy SA% vs. temperature, 323.9 x 9.5mm X42 line pipe

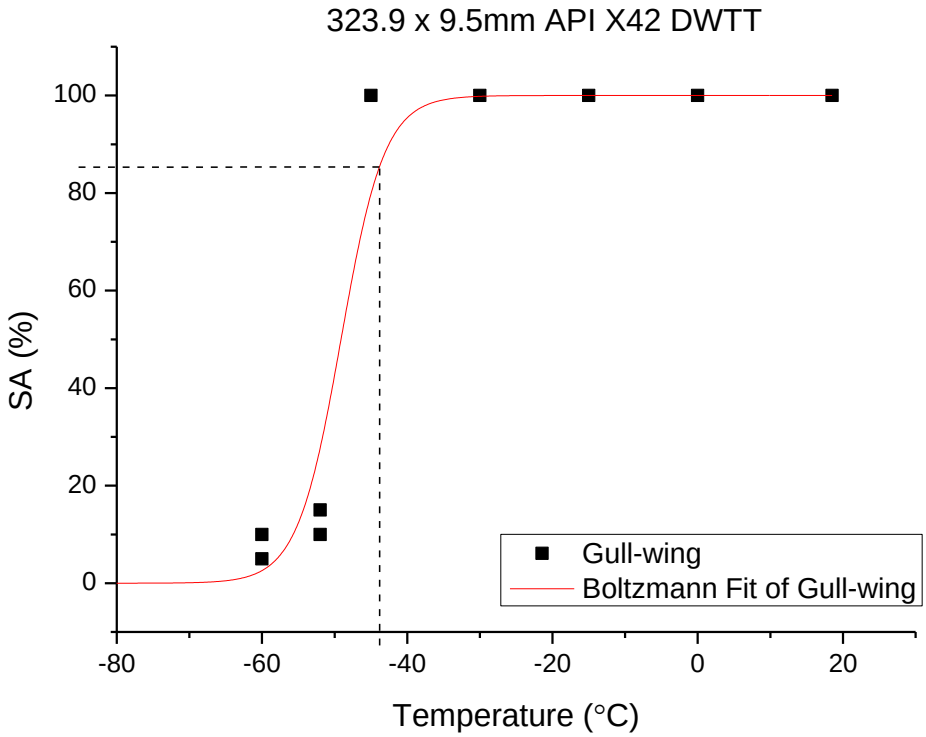

Figure 7.6 DWTT SA% vs. temperature, 323.9 x 9.5mm X42 line pipe

Only one Charpy specimen thickness is tested in 406 x 12.7mm X42, 219 x 8.2mm X42, and 323.9 x 11.5mm X60M line pipes. The DWTT and Charpy shear area transition temperatures are plotted in Figures 7.7, 7.8 and 7.9 respectively.

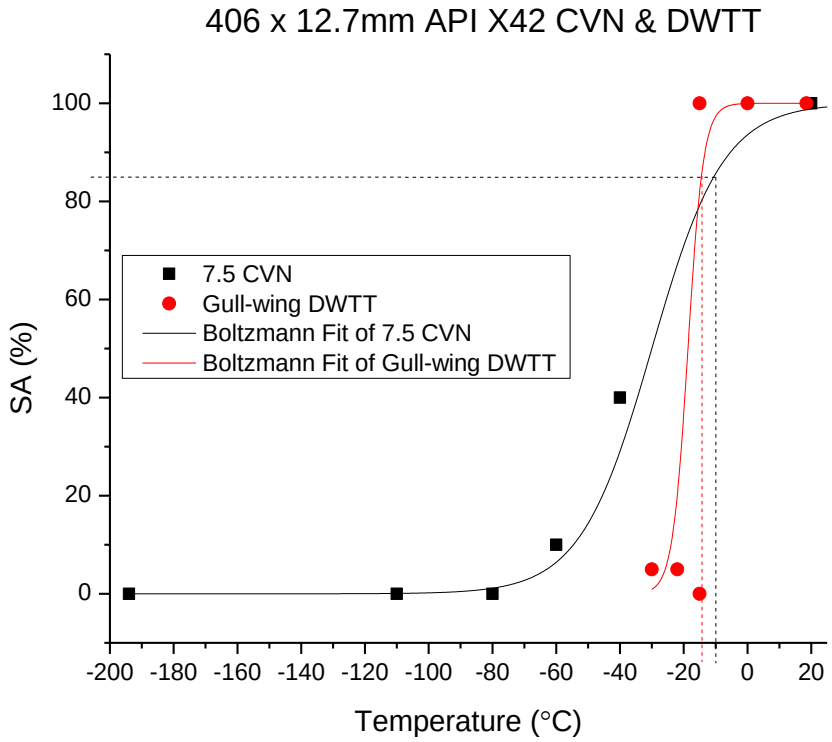

Figure 7.7 DWTT and CVN SA% vs. temperature, 406 x 12.7mm X42 line pipe

As shown in Figure 7.7, the transition temperature at 85% SA is -10°C for 7.5mm Charpy tests and -14°C for gull-wing DWTT tests. The difference between the two transition temperatures is small. However, 85%SA FPTT of -30°C is obtained from Charpy tests which is much lower than that from DWTT. The same phenomenon is observed in 219 x 8.2mm X42 line pipe, shown in Figure 7.8. The transition temperature at 85% SA is found to be -25°C for 6.7mm Charpy tests and -28°C for gull-wing DWTT tests, but the FPTT from Charpy test reduced further to -45°C at 50% SA.

In 323.9 x 11.5mm X60M line pipe, a transition temperature of -60°C at 85% SA is obtained for full-thickness Charpy tests and -46°C is obtained for gull-wing DWTT tests as showed in Figure 7.9. The 50%SA FPTT from Charpy specimens is further reduced to -78°C.The DWTT FPTTs are more conservative than the full-thickness Charpy results for this thicker wall case.

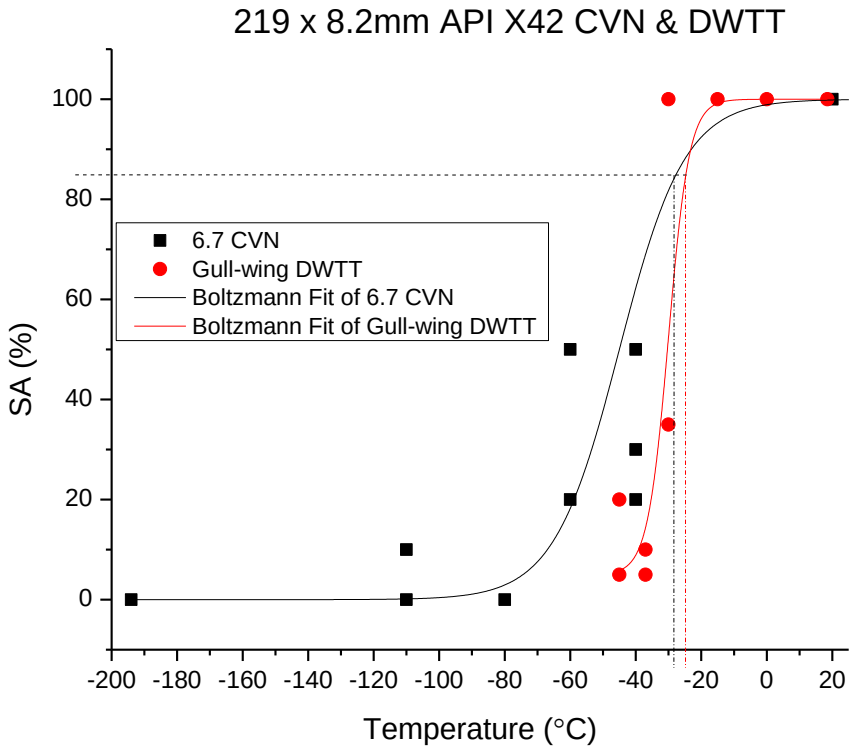

Figure 7.8 DWTT and CVN SA% vs. temperature, 406 x 12.7mm X42 line pipe

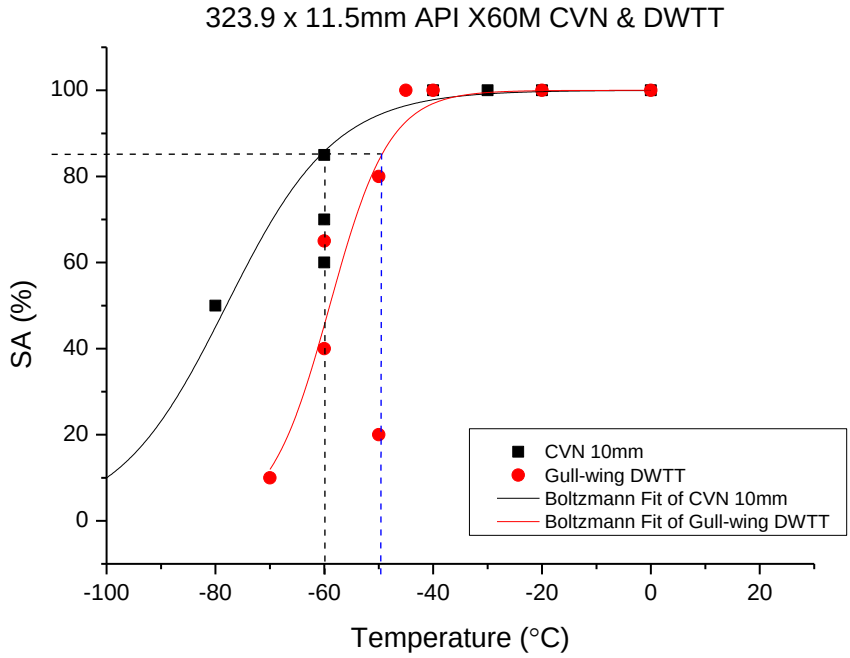

Figure 7.9 DWTT and CVN SA% vs. temperature, 323.9 x 11.5mm X60M line pipe

7.3. Comparison of transition temperatures

Figure 10 demonstrates correlations between the Charpy 85% SA transition temperature (T_c) and the DWTT 85% SA transition temperature (T_D) as a function of pipe wall thickness [16], which has been widely used in the pipeline industry. These correlations were developed using X52 and X60 data in 1980s [109].

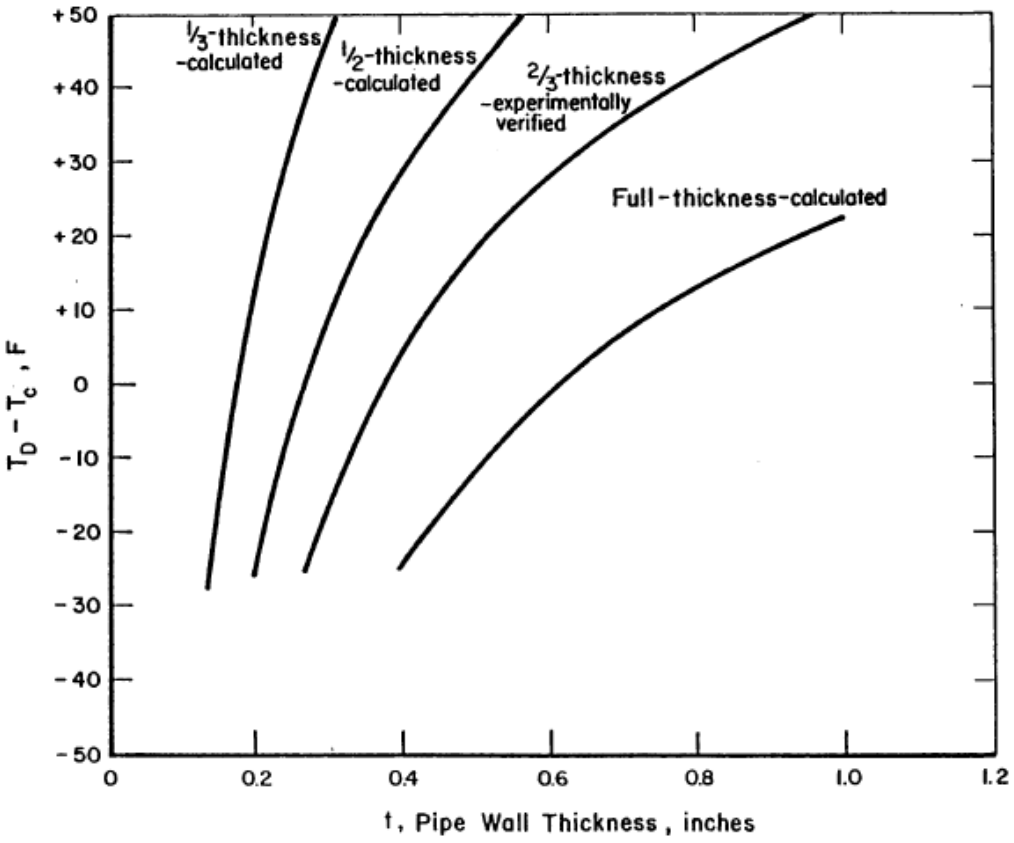

Figure 7.10 Thickness correction for 85% SA transition temperature shift as a function of pipe wall thickness [16]

All of the transition temperatures at 85% SA from the DWTT (T_d) and CVN tests (T_c) with various specimen thicknesses in this work are summarised in Table 7.2 and plotted in Figure 7.11 to compare with the 85% SA transition temperature shift presented in Figure 7.10.

Table 7.2 Summary of T_d and T_c from DWTT and CVN

Grade	Diameter	Thickness	Thickness	Td*	Td*	CVN Specimen	Tc	Tc	Td-Tc
	mm	mm	inch	°C	°F		°C	°F	°F
X42	323.9	9.5	0.374	-44	-47.2	3/4	-64	-83.2	36.0
X42	323.9	9.5	0.374			2/3	-65	-85.0	37.8
X42	323.9	9.5	0.374			1/2	-68	-90.4	43.2
X42	406	12.7	0.500	-14	6.8	3/4	-10	14.0	-7.2
X42	219	8.2	0.323	-25	-13.0	2/3	-28	-18.4	5.4
X65M	323.9	11.5	0.453	-49	-56.2	Full	-60	-76.0	19.8
X70	323.9	8.8	0.346	-51	-59.8	3/4	-78	-108.4	48.6
X70	323.9	8.8	0.346			2/3	-75	-103.0	43.2
X70	323.9	8.8	0.346			1/2	-71	-95.8	36.0

Note*DWTT transition temperatures were obtained from gull-wing specimens.

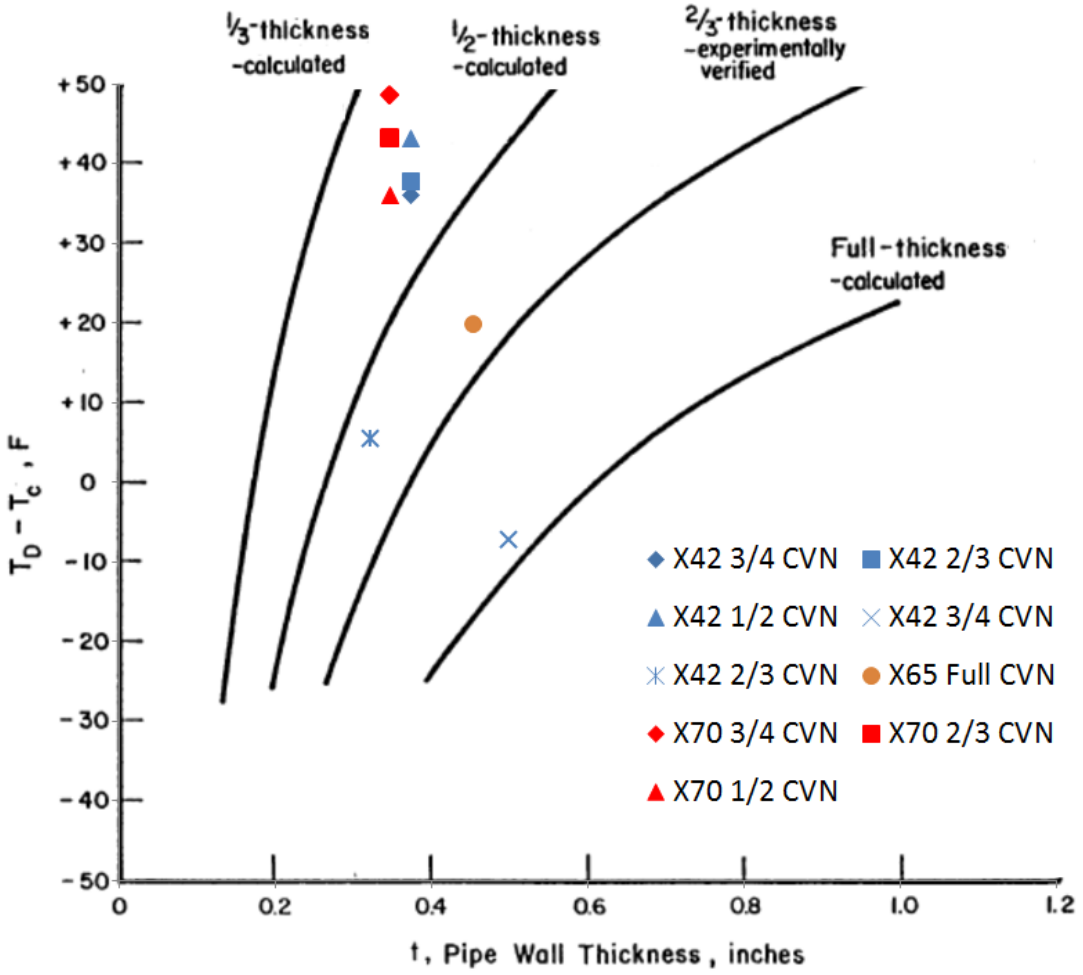

Figure 7.11 Thickness correction for 85% SA transition temperature shift as a function of pipe wall thickness for sub-size CVNs

As can be seen in Figure 7.11, the results obtained in the current work no longer follow the correlations between DWTT and Charpy given in Figure 7.10. The shift in the transition temperature at 85% SA between DWTT and Charpy observed in this study is significantly larger than the prediction given in Figure 7.10. For X42 line pipe materials, sub-size specimen results show that the transition temperature shift becomes larger as the specimen thickness becomes smaller, which agrees with the trend of the correlation given in Figure 7.10. However, large scatters in the transition temperature shift are observed in some sub-size specimens from pipes with different wall thicknesses. As for the X70, it is observed that the shift becomes greater as the specimen thickness increases, which is the opposite trend of the correlation given in Figure 7.10. The comparisons indicate that the correlation of the transition temperatures developed decades ago is no longer accurate and it significantly underestimates the transition temperature shift between the DWTT and Charpy test with sub-size specimens for both X70 and X42 small-diameter line pipes.

7.4. Summary

For small-diameter, thin-walled line pipes, full-size Charpy might not be able to extract specimens for testing. Various sub-size specimens of reduced thicknesses need to be used if the Charpy test is applied instead of full-thickness DWTT to obtain the transition curves. However, the findings in this section show that Charpy FPTTs at various thicknesses are much lower than the DWTT results, whether gull-wing or flattened specimens. Furthermore, the trend of transition curves shifting due to the reduction in specimen thickness is different for low-grade and high-grade line pipe materials. The Charpy test may no longer be adequate for transition temperature prediction by using the 50% SA transition temperature criterion, especially in small-diameter, thin-walled pipes where various sub-size Charpy specimens are needed. The performance of full-thickness DWTT is more reliable and it eliminates the uncertainties. Furthermore, the existing correlation of the transition temperatures between DWTT and Charpy as a function of pipe wall thickness, which was

developed based on X52 and X60 line pipes, is no longer able to predict the shift and correct the Charpy transition curves accurately in either low-grade (X42) or high-grade (X70) line pipe materials. However, a very large scatter was observed in the relationship presented in the reference[16] for existing correlation of transition temperatures. The correlations significantly underestimate the 85% SA transition temperature shift between DWTT and Charpy.

CHAPTER 8

CONCLUSIONS AND RECOMMENDATIONS

The findings are distributed in four key chapters:

- ***Chapter 4*** investigates the buckling phenomenon in drop weight tear test of small-diameter, thin-walled line pipes;
- ***Chapter 5*** proposes a new DWTT approach and compares the transition temperatures determined from full-scale tests, CVN, DWTT gull-wing specimens and reinforced specimens;
- ***Chapter 6*** investigates the Charpy energy/specimen thickness relationships experimentally and numerically for line pipe steels and implements the exponential relationship in the BTCM to improve the prediction of arrest toughness for ductile fracture;
- ***Chapter 7*** compares the shear area transition curves from DWTT and CVN with specimens of various thicknesses for different pipe dimensions and grades.

In this chapter, the findings are synthesized and the improvements for fracture propagation control methods are recommended.

8.1. Conclusions

The ‘no buckling’ acceptance criterion in API RP5L is no longer adequate for the DWTT in modern, high-toughness line pipes. There has been no reliable alternative when invalid tests have occurred due to specimen ‘buckling’. Furthermore, the absence of the DWTT requirement for small-diameter pipe (<OD508 mm) may lead to brittle fracture, as it has been proven that small-diameter pipelines are not immune to brittle fracture, and the alternative CVN transition temperature has been shown to be insufficient for brittle fracture control.

Small-diameter, thin-walled line pipes may not be able to be extracted for full-size Charpy testing. Various sub-size specimens of reduced thicknesses need to be used if the Charpy test is applied instead of full-thickness DWTT to obtain the transition curves. However, in both high-grade and low-grade line pipe materials, Charpy FPTTs from various thicknesses are much less conservative than DWTT results, whether gull-wing or flattened specimens. The Charpy test is no longer suitable to predict the FPTT by using either the 50% SA transition temperature criterion or the 85% SA transition temperature with a thickness-correction applied, especially in small-diameter, thin-walled pipes, where various sub-size Charpy specimens could create more uncertainties. The performance of full-thickness DWTT is more reliable, and it eliminates the uncertainties.

Therefore, it is no longer adequate for the standards to allow Charpy transition curves as the alternative to DWTT for small-diameter pipes. DWTT is essential for predicting the DBTTs of small-diameter line pipes. Flattened DWTT specimens with reinforcement plates successfully minimised buckling and delivered more accurate transition temperature predictions in full-scale line pipes. Therefore, to use reinforced DWTT specimens to obtain accurate ductile-brittle transition temperatures is recommended for thin-walled line pipe material to ensure the pipeline is immune to brittle fracture propagation. However, the additional practical difficulties introduced by this method made it a less efficient production test.

Both the experimental and numerical investigations show an exponential relationship between CVN absorbed energy and specimen thickness in modern, high-toughness line pipe materials. Under current standards, the linear Charpy energy/specimen thickness relationship is widely used in the BTCM to predict fracture arrest toughness. In the current study, the exponential relationship has been found to be applicable for high toughness steels and the exponential relationship has been implemented in the BTCM to improve the BTCM predictions for high-toughness line pipe steels. The prediction result is comparable to the major popular correction approaches that were developed based on the curve fitting of full-scale fracture propagation test data for moderate Charpy values (up to ~160 J from full size specimen).

8.2. Recommendations to the standard

The brittle and ductile fracture control methodologies used in current standards were mostly developed in the 1960s and 1970s. However, the toughness of line pipe steel manufactured today has improved significantly, and the approaches recommended in the standard for pipeline fracture control are no longer adequate. The following recommendations are made based on the outcomes of the current study:

- Lower the diameter requirement in API RP5L from 508 mm to 300 mm above which DWTT is required to be carried out to demonstrate that no brittle fracture propagation will occur in the pipeline above the minimum operating temperature.

- It is strongly recommended that the ‘no buckling’ acceptance criterion for DWTT be reviewed and revised. It is also recommended that the alternative approach of using CVN to predict pipeline FPTT be removed and replaced with another approach.

- It is recommended that flattened DWTT specimens with reinforcement plates at the supports be used to reduce the effect of buckling, especially in thin-walled line pipe material, to ensure the pipeline is immune to brittle fracture propagation.

- In order to improve the prediction of ductile fracture arrest toughness for higher-toughness, clean steels, it is recommended that the linear relationship between Charpy absorbed energy applied in the BTCM to be replaced with the exponential relationship.

8.3. Recommendations for future work

- Reliability study of the proposed new method in Chapter 4 for determining the FPTT is recommend to be performed. The method suggested that to start DWTT at low temperatures and proceed towards higher temperatures based on the fact that buckling often occurred at upper shelf and transition region. This method is potentially an easier and efficient alternative than DWTT with reinforcement to determine the FPTT accurately.

- Studies on thickness correction for 85% SA transition temperature shift as a function of pipe wall thickness for modern line pipe are recommended if DWTT and CVN are continued to be used as experimental approaches for obtaining FPTT.

- As shown in current study, the ‘no buckling’ requirement for DWTT is no longer adequate for modern line pipe. In order to provide foundations for proposing new acceptance criteria in API standard, investigation on the effect of buckling on the shifting of DWTT SA transition temperature is recommended to be continued.

- Development of an alternative production test to CVN is highly recommended to be carried out to achieve brittle fracture propagation control in modern, high-toughness pipelines.

- Full-scale burst tests are recommended to be carried out for line pipe with higher-toughness (above 150J) to validate the arrest toughness predicted by BTCM after the 1.5 power relationship being implemented.

REFERENCES

[1] H. O. Nordhagena, S. Kragsetb, T. Berstada, A. Morinc, C. Døruma, and S. T. Munkejordb, "A new coupled fluid–structure modeling methodology for running ductile fracture," *Computers & Structures*, vol. 94-95, pp. 13-21, 2012.

[2] D. L. Rudland, G. M. Wilkowski, Z. Feng, Y.-Y. Wang, D. Horsley, and A. Glover, "Experimental investigation of CTOA in linepipe steels," *Engineering Fracture Mechanics*, vol. 70, pp. 567-577, 2003.

[3] T. Berstad, C. Dørum, J. P. Jakobsen, S. Kragset, H. Li, H. Lund, *et al.*, "CO2 pipeline integrity: A new evaluation methodology," *Energy Procedia*, vol. 4, pp. 3000-3007.

[4] "Oil and gas pipelines network of Australia, http://www.mapsofworld.com/australia/thematic-maps/oil-and-gas-network.html," 2009.

[5] J. Jorissen. *Gas Pipeline Explosion at Ghislenghien*. Available: http://www.afac.com.au/docs

[6] P. Tuft and S. Cunha, "Comparing international pipeline incident rates," presented at the 19th Biennial Joint Technical Meeting, APIA, EPRG and PRCI, Sydney, Australia, May 1-3, 2013.

[7] M. Kanninen and P. E. O'Donoghue, "Research challenges arising from current and potential applications of dynamic fracture mechanics to the integrity of engineering structures " *International Journal of Solids and Structures*, vol. 32, pp. 2423-2445, 1995.

[8] P. Hopkins, *Comprehensive Structural Integrity Volume 1: The Structural Integrity Of Oil And Gas Transmission Pipelines*: Elsevier, May 2002.

[9] G. M. McClure, R. J. Eiber, G. T. Hahn, F. W. Boulger, and K. Masubuchi, "Research on the Properties of Line Pipe," in *Battelle Columbus Division's report to the American Gas Association, AGA Catalogue No.L00290*, ed, 1962.

[10] "API RP 5L 3: Recommended Practice for Conducting Drop-Weight Tear Test on Line Pipe," 3 ed: American Petroleum Institute, 1996.

[11] G. Mannucci and G. Demofonti, "Control of ductile fracture propagation in X80 gas linepipe," *Journal of Pipeline Engineering*, vol. 10, 2011.

[12] O. L. Towers, "Testing sub-size Charpy specimens Part 1 -The influence of thickness on the ductile-brittle transition," *Metal construction*, vol. 18, pp. 171-176, 1986.

[13] C. R. Killmore, F. J. Barbaro, J. G. Williams, and A. B. Rothwell, "Limitations of the Charpy test for specifying fracture propagation resistance," in *Seminar on Fracture Control in Gas Pipelines, Welding Technology Institute of Australia*, Sydney, Australia, 1997, pp. 4-1 - 4-19.

[14] O. Towers, "Testing sub-size Charpy specimens. Pt. 2: the influence of specimen thickness on upper shelf behaviour," *Metal Construction*, vol. 18, p. 254, 1986.

[15] G. Vogt, "Full-scale fracture behavior of pipelines (EPRG)," in *6th AGA Symposium of Line Pipe Research, American Gas Association*, Houston, Texas, 1979, pp. M1-M15, Paper M.

[16] R. J. Eiber and B. N. Leis, *Fracture control technology for natural gas pipelines circa 2001, Report No. PR-003-00108 to PRCI*, 2001.

[17] W. A. Maxey, "Fracture propagation studies," in *6th AGA Symposium of Line Pipe Research, American Gas Association*, Houston, Texas, 1979, pp. J1-19, Paper J.

[18] R. W. E. Shannon and A. A. Wells, "Brittle crack propagation in gas filled pipelines—A model study using thin walled unplasticised PVC pipe," *International Journal of Fracture*, vol. 10, pp. 471-486, December 1, 1974.

[19] W. D. Biggs, *The brittle fracture of steel*: Macdonald and Evans Ltd, 1960.

[20] A. Cosham, D. G. Jones, K. Armstrong, D. Allason, and J. Barnett, "Ruptures in Gas Pipelines, Liquid Pipelines and Dense Phase Carbon Dioxide Pipelines," in *9th International Pipeline Conference*, Calgary, AB; Canada, 2012, pp. 465-482, IPC2012-90463.

[21] B. N. Leis and R. J. Eiber, "Fracture propagation control in onshore transmission pipelines," in *2nd Onshore Pipeline Technology Conference* Istanbul November 1998, pp. 2.1 - 2.35.

[22] A. Cosham, D. G. Jones, R. Eiber, and P. Hopkins, "Don't drop the drop weight tear test," *The Journal of Pipeline Engineering*, vol. 9, pp. 69-84, 2010.

[23] "AS 1330: Metallic materials - Drop weight tear test for ferritic steels," 2004 ed: Standards Australia.

[24] R. J. Eiber, "Correlation of Full Scale Tests With Laboratory Tests," in *3rd Symposium on Line Pipe Research, American Gas Association* 1965, pp. 83-118.

[25] R. M. Andrews and V. Pistone, "European pipeline research group studies on ductile crack propagation in gas transmission pipelines," in *From Charpy to Present Impact Testing* vol. 30, ed: Elsevier Science Ltd, 2002, pp. 377-384.

[26] G. Demofonti, G. Mannucci, D. Harris, L. Barsanti, and H.-G. Hillenbrand, "Fracture behaviour of X100 gas pipelines by full-scale tests," presented at the International Conference on Application and Evaluation of High Grade Linepipe in Hostile Environments, Yokohama, Japan, November 7-8, 2002.

[27] L. Fletcher, "Unpublished work presented in discussion session on DWTT, 18th Biennia Joint Technical Meeting, APIA, EPRG and PRCI," ed. San Francisco 2011.

[28] G. D. Fearnehough, "Fracture Propagation Control in Gas Pipelines: A Survey of Relevant Studies, International Journal of Pressure Vessels and Piping," vol. 2, pp. 257-282, October 1974.

[29] H. Makino, I. Takeuchi, and R. Higuchi, "Fracture Propagation and Arrest in High-Pressure Gas Transmission Pipeline by Ultra High Strength Line Pipes," *ASME Conference Proceedings*, vol. 2008, pp. 39-48, 2008.

[30] G. Demofonti, G. Mannucci, and P. Roovers, "Existing methods for the evaluation of material fracture resistance for high grade steel pipelines," presented at the 6th Biennial Joint Technical Meeting, APIA, EPRG and PRCI, Canberra, Australia, 2007.

[31] "ANSI/API 5L: Specification for Line Pipe," 44 ed: American Petroleum Institute, 2007.

[32] "ISO 3183: Petroleum and natural gas industries — Steel pipe for pipeline transportation systems," 2012 ed: International Organization for Standardization, 2012.

[33] "AS 2885.1—Gas and liquid petroleum Part 1: Design and construction," ed: Standards Australia, 2012.
[34] "ASME B31.8 : Gas Transmission and Distribution Piping Systems, ASME Code for Pressure Piping," ed: The American Society of Mechanical Engineers 2014.
[35] "CSA Z245.1: Steel Pipe," 2014 ed: Canadian Standard, 2014.
[36] "BS EN 10208: Steel pipes for pipelines for combustible fluids - Technical delivery conditions, Part 2: Pipes of requrement class B," ed: British Standard, 2009.
[37] "DNV OS-F101: Submarine Pipeline Systems," 2012 ed: Det Norske Veritas, 2012.
[38] "Steel Pipelines and Associated Installations for High Pressure Gas Transmission, Institution of Gas Engineers and Managers Standard, IGEM/TD/1 Edition 5," 2008.
[39] API, "API RP 5L3: Recommended practice for conducting drop-weight tear tests on line pipe - 3rd edition," ed, 1996.
[40] K. A. Widenmaier and A. B. Rothwell, "The practical application of fracture control to natural gas pipelines," in *7th International Pipeline Conference*, Calgary, Alberta, Canada, September 29 - October 3, 2008, pp. 399-406, IPC2008-64557.
[41] T.Schmidt, A. Hasenhütl, M. Erdelen-Poppler, and A. Meißner, "Drop Weight Tear Testing on Seamless Pipe," presented at the 18th Joint Technical Meeting on Pipeline Research, San Francisco, CA, USA, 2011.
[42] A. B. Rothwell, "Fracture propagation control for gas pipelines - past, present and future," *Pipeline Technology*, vol. 1, pp. 387-405, 2000.
[43] W. A. Maxey, "Fracture Initiation, Propagation, and Arrest," in *5th AGA Symposium of Line Pipe Research, American Gas Association*, Houston, 1974, pp. J-1.
[44] A. Cosham, D. G. Jones, B. N. Leis, P. Hopkins, and J. Barnett, "Not another Chapry V-notch correction factor...?," in *6th International Pipeline Technology Conference*, Ostend, Belgium, 2013, pp. S03-03.
[45] X.-K. Zhu and B. N. Leis, "CVN and DWTT Energy Methods for Determining Fracture Arrest Toughness of High Strength Pipeline Steels," in *Proceedings of the 2012 9th International Pipeline Conference*, Calgary, Canada, September 24-28, 2012, pp. 565-573, IPC2012-90694.
[46] X.-K. Zhu and B. N. Leis, "Ductile Fracture Arrest Methods for Gas Transmission Pipelines Using Charpy Impact Energy or DWTT Energy," *Journal of Pipeline Engineering*, vol. 12, 2013.
[47] G. Wilkowski, D. Rudland, and Y. Y. Wang, "Recent Efforts on Characterizing Propagating Ductile Fracture Resistance of Linepipe Steels," in *Proceedings of the 3rd Pipeline Technology Conference*, Brugge, Belgium, 2000, pp. 359-386.
[48] J. Wolodko and M. Stephens, "Applicability of Existing Models for Predicting Ductile Fracture Arrest in High Pressure Pipelines," in *2006 International Pipeline Conference*, Calgary, Alberta, Canada, September 25–29, 2006, pp. 115-123, IPC2006-10110.
[49] N. Takahashi, H. Makino, R. Higuchi, and I. Takeuchi, "Toughness of high strength line pipe for fracture arrest assessment," in *Pipeline Technology Conference*, Ostend, Belgium, October 12-14, 2009, pp. Ostend2009-013.

[50] W. R. Corwin, R. L. Klueh, and J. M. Vitek, "Effect of specimen size and nickel content on the impact properties of 12 Cr-1 MoVW ferritic steel," *Journal of Nuclear Materials,* vol. 122, pp. 343-348, 1984.

[51] "ASTM E23: Standards Test Methods for Notched Bar Impact Testing of Metallic Materials," ed: American Society for Testing and Materials, 2007.

[52] A. Sladkowski and M. Sitarz, "Analysis of wheel–rail interaction using FE software," *Wear,* vol. 258, pp. 1217-1223, 2005.

[53] B. S. Louden, A. S. Kumar, F. A. Garner, M. L. Hamilton, and W. L. Hu, "The influence of specimen size on charpy impact testing of unirradiated HT-9," *Journal of Nuclear Materials,* vol. 155–157, Part 2, pp. 662-667, 1988.

[54] H. Kurishita, H. Kayano, M. Narui, and M. Yamazaki, "Current status of small specimen technology in Charpy impact testing," *Journal of Nuclear Materials,* vol. 212–215, Part B, pp. 1682-1687, 1994.

[55] F. Abe, T. Noda, H. Araki, M. Okada, M. Narui, and H. Kayano, "Effect of specimen size on the ductile-brittle transition behavior and the fracture sequence of 9Cr-W steels," *Journal of Nuclear Materials,* vol. 150, pp. 292-301, 1987.

[56] A. S. Kumar, L. E. Schubert, M. L. Hamilton, and N. S. Cannon, "Size effects on the upper shelf energy of a neutron irradiated pressure vessel weld metal," *Journal of Nuclear Materials,* vol. 225, pp. 238-244, 1995.

[57] L. E. Schubert, A. S. Kumar, S. T. Rosinki, and M. L. Hamilton, "Effect of specimen size on the impact properties of neutron irradiated A533B steel," *Journal of Nuclear Materials,* vol. 225, pp. 231-237, 1995.

[58] M. P. Manahan, "Miniaturized charpy test for reactor pressure vessel embrittlement characterization," in *Effects of Radiation on Materials: 18th International Symposium, ASTM STP 1325*, 1997.

[59] J. F. Grubb and M. P. Manahan Sr, "Effect of Temperature and Specimen Thickness on Toughness of Nickel Alloy 22," *Key Engineering Material* vol. 345-346 I, pp. 529-532, 2007.

[60] K. Wallin, "Upper shelf energy normalisation for sub-sized Charpy-V specimens," *International journal of pressure vessels and piping*, vol. 78, pp. 463-470, 2001.

[61] B. L. Ferguson, "The relationship between splitting phenomena and sample thickness in Charpy V-notcch impact testing," in *What does the Charpy test really tell us?*, 1978, pp. 90-107.

[62] B. Ferguson, "The Relationship Between Splitting Phenomena and Sample Thickness in Charpy V-notch Impact Testing," in *What Does the Charpy Test Really Tell Us?*, ed: American Society for Metals, 1978, pp. 90-107.

[63] W. Corwin, R. Klueh, and J. Vitek, "Effect of specimen size and nickel content on the impact properties of 12 Cr-1 MoVW ferritic steel," *Journal of Nuclear Materials,* vol. 122, pp. 343-348, 1984.

[64] B. S. Louden, A. S. Kumar, F. A. Garner, M. L. Hamilton, and W. Hu, "The influence of specimen size on Charpy impact testing of unirradiated HT-9," *Journal of Nuclear Materials,* vol. 155, pp. 662-667, 1988.

[65] A. Pineau, "Development of the local approach to fracture over the past 25 years: Theory and applications," *International Journal of Fracture,* vol. 138, pp. 139-166, 2006.

[66] F. M. Beremin, A. Pineau, F. Mudry, J. C. Devaux, Y. D'Escatha, and P. Ledermann, "A local criterion for cleavage fracture of a nuclear pressure vessel steel," *Metallurgical Transactions A,* vol. 14, pp. 2277-2287, 1983.

[67] A. Eberle , D. Klingbeil, W. Baer, P. Wossidlo, and R. Häcker, "The calculation of dynamic JR-curves from 2D and 3D finite element analysis of a Charpy test using a rate-dependent damage model," in *From Charpy To Present Impact Testing*. vol. 30, ed: Elsevier Science Ltd, 2002, pp. 403-410.

[68] M. Fumiyoshi, I. Masuo, T. Wataru, K. Noboru, and A. Kazushige, "Fracture mechanics analysis of Charpy test results based on the weibull stress criterion," in *From Charpy To Present Impact Testing*, ed: Elsevier Science Ltd, 2002, pp. 411-418.

[69] F. Mudry, "Improved charpy test evaluation for the toughness characterisation of high strength steels and their weldments," in *From Charpy To Present Impact Testing*, ed: Elsevier Science Ltd, 2002, pp. 427-435.

[70] V. Tvergaard and A. Needleman, "3D Charpy specimen analyses for welds," in *From Charpy To Present Impact Testing*, ed: Elsevier Science Ltd, 2002, pp. 437-444.

[71] A. Rossoll, C. Berdin, and C. Prioul, "Charpy impact test modelling and local approach to fracture," in *From Charpy To Present Impact Testing*, ed: Elsevier Science Ltd, 2002, pp. 445-452.

[72] B. Tanguy, J. Besson, R. Piques, and A. Pineau, "Numerical modeling of Charpy V—notch tests," in *From Charpy To Present Impact Testing*, ed: Elsevier Science Ltd, 2002, pp. 461-468.

[73] C. Poussard, C. Sainte Catherine, P. Galon, and Forget, "Finite element simulations of sub-size Charpy tests and associated transferability to toughness results," in *From Charpy To Present Impact Testing*, ed: Elsevier Science Ltd, 2002, pp. 469-478.

[74] C. K. Oh, Y. J. Kim, J. H. Baek, Y. P. Kim, and W. Kim, "A phenomenological model of ductile fracture for API X65 steel," *International Journal of Mechanical Sciences*, vol. 49, pp. 1399-1412, 2007.

[75] H. L. Yu and D. Y. Jeong, "Application of a stress triaxiality dependent fracture criterion in the finite element analysis of unnotched Charpy specimens," *Theoretical and Applied Fracture Mechanics*, vol. 54, pp. 54-62, 2010.

[76] L. C. A. Folch and F. M. Burdekin, "Application of coupled brittle-ductile model to study correlation between Charpy energy and fracture toughness values," *Engineering Fracture Mechanics*, vol. 63, pp. 57-80, 1999.

[77] K. C. Koppenhoefer and R. H. Dodds Jr, "Ductile crack growth in pre-cracked CVN specimens: Numerical studies," *Nuclear Engineering and Design*, vol. 180, pp. 221-241, 1998.

[78] B. Tanguy, J. Besson, R. Piques, and A. Pineau, "Ductile to brittle transition of an A508 steel characterized by Charpy impact test. Part II: Modeling of the Charpy transition curve," *Engineering Fracture Mechanics*, vol. 72, pp. 413-434, 2005.

[79] S. E. Sidener, A. S. Kumar, D. B. Oglesby, L. E. Schubert, M. L. Hamilton, and S. T. Rosinski, "Dynamic finite element modeling of the effects of size on the upper shelf energy of pressure vessel steels," *Journal of Nuclear Materials*, vol. 239, pp. 210-218, 1996.

[80] P. Thibaux, B. Tanguy, S. Muller, and F. Van Den Abeele, "Ductile fracture characterization of an X70 steel: Re-interpretation of classical tests using the finite element technique," Calgary, AB, 2009, pp. 179-186.

[81] K. C. Koppenhoefer and R. H. Dodds Jr, "Loading rate effects on cleavage fracture of pre-cracked CVN specimens: 3-D studies," *Engineering Fracture Mechanics,* vol. 58, pp. 249-270, 1997.

[82] B. Tanguy, T. T. Luu, G. Perrin, A. Pineau, and J. Besson, "Plastic and damage behaviour of a high strength X100 pipeline steel: Experiments and modelling," *International Journal of Pressure Vessels and Piping,* vol. 85, pp. 322-335, 2008.

[83] P. Haušild, I. Nedbal, C. Berdin, and C. Prioul, "The influence of ductile tearing on fracture energy in the ductile-to-brittle transition temperature range," *Materials Science and Engineering A,* vol. 335, pp. 164-174, 2002.

[84] P. Thibaux and F. Van Den Abeele, "Determination of crack initiation and propagation energy in instrumented Charpy V-notch impact tests by finite element simulations," in *Pipeline Technology Conference,* Ostend,, 2009, pp. Ostend2009-093.

[85] E. Marotta, M. Minotti, and P. Salvini, "Effect of fracture tunneling in DWT Tests," *Engineering Fracture Mechanics,* vol. 81, pp. 33-42, 2012.

[86] P. Salvini, A. Fonzo, and G. Mannucci, "Identification of CTOA and fracture process parameters by drop weight test and finite element simulation," *Engineering Fracture Mechanics,* vol. 70, pp. 553-566, 2003.

[87] P. E. O'Donoghue, M. F. Kanninen, C. P. Leung, G. Demofonti, and S. Venzi, "The development and validation of a dynamic fracture propagation model for gas transmission pipelines," *International Journal of Pressure Vessels and Piping,* vol. 70, pp. 11-25, 1997.

[88] D. J. Shim, G. Wilkowski, D. Rudland, A. B. Rothwell, and J. Merritt, "Numerical simulation of dynamic ductile fracture propagation using cohesive zone modelling," in *7th International Pipeline Conference*, Calgary, Alberta, Canada, 2008.

[89] K. Misawa, Y. Imai, and S. Aihara, "A New Model for Dynamic Crack Propagation and Arrest in Gas Pipelines," in *8th International Pipeline Conference* Calgary, Alberta, Canada 27 September - 1 October, 2010, pp. 685-694, IPC2010-31475.

[90] "ASTM A 370: Standard Test Methods and Definitions for Mechanical Testing of Steel Products," ed: American Society for Testing and Materials, 2012.

[91] A. L. Gurson, "Continuum theory of ductile rupture by void nucleation and growth: Part I—Yield criteria and flow rules for porous ductile media," *Journal of engineering materials and technology,* vol. 99, pp. 2-15, 1977.

[92] V. Tvergaard, "Influence of voids on shear band instabilities under plane strain conditions," *International Journal of Fracture,* vol. 17, pp. 384-407, 1981.

[93] ASTM, "E436: Standard Test Method for Drop-Weight Tear Tests of Ferritic Steels," ed, 2008.

[94] I. Satoshi, Y. Satoru, M. Masaki, S. Yuya, and T. Mikihiro, "Full gas burst test for HFW linepipe at low temperature " in *10th International Pipeline Conference* Calgary, Alberta, Canada, September 29–October 3, 2014, pp. V003T07A011, IPC2014-33326.

[95] JFE, "Drop-weight tear test (DWTT) for thin wll thickness pipe," in *Doc. JFE-ERW-TR-13-08*, ed, 2013.

[96] "ISO 148-1: Metallic materials - Charpy pendulum impact test - Test method," 2009 ed: International Organization for Standardization, 2009.

[97] F. Wang and X. Lian, "Selection of the mathematical model on ductile-brittle transition temperature curve of impact test," *Journal of Physical Testing and Chemical Analysis,* vol. 45, pp. 617-632, 2009.
[98] W. Oldfield, "Curve fitting impact test data: A statistical procedure," *Journal of ASTM standardization news,* vol. 3, pp. 24-29, 1975.
[99] B. Leis, X. Zhu, and T. Forte, "New approach to assess running fracture arrest in pipelines," in *Pipeline Technology Conference* Ostend, 2009, pp. Ostend2009-066.
[100] R. A. Grange, "Effect of microstructural banding in steel," *Metallurgical Transactions,* vol. 2, pp. 417-426, 1971.
[101] ANSI/API, "5L: Specification for Line Pipe," 44 ed, 2007.
[102] D. Stalheim, K. Barnes, and D. McCutcheon, "Alloy Designs for High Strength Oil and Gas Transmission Linepipe Steels," in *Proceedings of the International Symposium Microalloyed Steels for the Oil and Gas Industry*, 2006.
[103] J. M. Gary, "A guide for understanding and specifying chemical composition of high strength linepipe steels," ed: Companhia Brasileira de Metalurgia e Mineração, Ewi Microalloying, July, 2007.
[104] H. Yu, X. Liu, and X. Li, "FE analysis of inclusion deformation and crack generation during cold rolling with a transition layer," *Materials Letters,* vol. 62, pp. 1595-1598, 2008.
[105] H.-L. Yu, C. Lu, K. Tieu, and G.-Y. Deng, "A numerical model for simulation of crack initiation around inclusion under tensile load," *Journal of Computational and Theoretical Nanoscience,* vol. 9, pp. 1745-1749, 2012.
[106] A. Nonn and C. Kalwa, "Analysis of dynamic ductile fracture propagation in pipeline steels: A damage mechanics approach," in *6th International Pipeline Technology Conference*, Ostend, Belguim, 2013, pp. S34-01.
[107] F. Van den Abeele, J. Peirs, P. Verleysen, F. Oikonomides, and J. Van Wittenberghe, "Dynamic Behaviour of High Strength Pipeline Steel," in *9th International Pipeline Conference*, Calgary, Alberta, Canada, September 24–28, 2012, pp. 247-255, IPC2012-90224.
[108] E. B. Clark, B. N. Leis, and R. J. Eiber, "Final report on Integrity Characteristics of Vintage Pipelines," ed: Interstate Natural Gas Association of America, October 2004.
[109] W. A. Maxey, J. F. Kiefner, and R. J. Eiber, "Brittle fracture arrest in gas pipelines," vol. American Gas Association, NG-18 Report 135, Catalog No. L51436, ed, March 31, 1983.